Endothelial specific PER2 at the crossroads of light elicited circadian amplitude enhancement as novel cardioprotective strategy and transcriptional regulation of HIF1A-dependent metabolic adaptation to myocardial ischemia

Yoshimasa Oyama MD, PhD,[1*] Colleen M. Bartman PhD,[1,4*] Stephanie Bonney MS,[1,4] J. Scott Lee PhD,[1] Lori A. Walker PhD,[2] Jun Han PhD,[3] Christoph H. Borchers PhD,[3] Peter M. Buttrick MD,[2] Nathan Clendenen MD,[1] Sean P. Colgan PhD[1] and Tobias Eckle MD, PhD[1,2,4*]

[*]both authors contributed equally

[1]Mucosal Inflammation Program, Departments of Medicine and Anesthesiology, University of Colorado Anschutz Medical Campus, Aurora, CO, USA; [2]Division of Cardiology, Department of Medicine, University of Colorado Anschutz Medical Campus, Aurora, CO, USA, [3]Department of Biochemistry and Microbiology, Genome BC Proteomics Centre, University of Victoria, Victoria, BC, Canada; [4]Graduate Training Program in Cell Biology, Stem Cells, and Development, University of Colorado Anschutz Medical Campus, Aurora, CO, USA

[*]*Correspondence should be addressed to:*
Tobias Eckle, M.D., Ph.D.
Professor of Anesthesiology, Cardiology and Cell Biology
Department of Anesthesiology
University of Colorado Denver
12700 E 19th Avenue, Mailstop B112, RC 2, Room 7121
Aurora, CO 80045; Office: +1-303-724 -2932 or - 2947, Fax: +1-303-724-2852
Email: tobias.eckle@ucdenver.edu
;

Short title: Daylight as endothelium-targeting strategy in myocardial ischemia

ABSTRACT

Consistent daylight oscillations and abundant oxygen availability are fundamental to human health. While both are connected from an evolutionary and cellular perspective, only oxygen is an established therapy in cardiovascular medicine. Here, we probe the mechanistic intersection between light- (Period 2, PER2) and oxygen- (hypoxia inducible factor, HIF1A) sensing pathways in cellular adaptation to low oxygen conditions with respect to myocardial ischemia.

Using a whole genome array from daylight exposed wildtype or *Per2*$^{-/-}$ mice, an affinity purification-mass spectrometry-based proteomics screen for PER2 targets in hypoxic human endothelial cells, and targeted metabolomics from human healthy volunteers after daylight therapy, we investigated the intersection of light and hypoxia elicited pathways. Housing mice under daylight conditions prior to myocardial ischemia and reperfusion (IR)-injury, uncovered circadian PER2 amplitude enhancement as novel cardioprotective strategy, mimicking HIF1A metabolic adaptation to myocardial ischemia in a PER2 regulated manner. Whole genome array analysis from daylight exposed wildtype and *Per2*$^{-/-}$ mice or myocardial IR-injury in endothelial specific PER2 deficient mice (*Per2*$^{loxP/loxP}$-VE-Cadherin -Cre) revealed a critical role for light elicited PER2 in maintaining the endothelial barrier function during myocardial ischemia. Mechanistic studies in human endothelia pointed towards a master transcriptional regulatory role for endothelial PER2 in metabolic reprograming to hypoxia via HIF1A, which was mimicked during normoxic PER2 stabilization. Translational investigation of light elicited pathways in human healthy volunteers found similar increases of PER2 or mimicking of HIF1A dependent metabolism. These studies identify light elicited circadian amplitude enhancement of endothelial PER2 as a novel cardioprotective strategy. Furthermore, these studies identify PER2 as critical control point of endothelial metabolic reprograming to maintain vascular integrity during myocardial IR-injury and implicate the use of daylight

therapy to increase endothelial PER2 signaling as a strategy for the treatment of coronary artery disease.

INTRODUCTION

The appearance of sunlight and oxygen on earth were undoubtedly the most dramatic environmental changes during evolution [1]. As a result, almost all organisms on this planet are equipped with light- and oxygen- sensing pathways. Notably, light sensing and oxygen sensing pathways are linked on a cellular level in mammals [2-4]. Hypoxia inducible factor 1 (HIF1A), an evolutionarily conserved transcription factor enabling cellular adaptation to low oxygen availability [5], belongs to the same protein family as the light inducible circadian core protein Period 2 (PER2) [6]. Both belong to the *PAS* domain superfamily of signal sensors for oxygen, light, or metabolism [2, 7]. As such, *Hif1* mRNA levels cycle in a circadian manner in mouse cardiac tissue [8] and rhythmic oxygen levels reset the circadian clock through HIF1A [9]. This evolutionary conserved relationship between light (circadian)- and oxygen-sensing pathways suggest a role for light elicited circadian rhythm proteins in disease states of low oxygen availability, such as myocardial ischemia.

In the present studies, we sought to develop a cardioprotective strategy using light to target and manipulate PER2 function and uncover mechanisms of PER2 dependent adaptation to hypoxia or ischemia [8]. In a comprehensive and systems biology approach, we dissect light and hypoxia elicited pathways in mice and humans from a cellular level to the whole body. Our investigations reveal that circadian PER2 functions at the crossroads between light elicited circadian amplitude enhancement and transcriptional HIF1A-dependent adaptation to oxygen depletion in hypoxia or ischemia. Combined, we demonstrate a mechanistic understanding of cardioprotection with light therapy by targeting and manipulating hypoxic pathways to reduce infarct sizes after myocardial ischemia.

RESULTS

Daylight elicited cardiac PER2 amplitude enhancement as a novel cardioprotective mechanism

Daylight is the dominant regulator of human circadian rhythms and PER2 activity [10]. Here we investigated daylight exposure protocols and found that housing mice under "daylight conditions" (10,000 LUX, L:D 14:10h) robustly enhances cardioprotection, reflected as a time-dependent decrease in infarct size and circulating troponin-I levels **(Fig. 1A-C**). A following evaluation of locomotor activity, as determined by wheel running activity during daylight housing, excluded a phase shift of the circadian period as underlying mechanism, but identified increases of the total distance walked or the circadian amplitude (**Fig. 1D-F, Supplementary Fig. 1A, B**). Indeed, after housing PER2 reporter mice in daylight for one week, we found increases in the circadian peak and trough levels of cardiac PER2 protein levels (**Fig. 1G**). Further analysis of wheel running activity in *Per2*$^{-/-}$ mice revealed daylight elicited increases of the total distance walked or the circadian amplitude to be PER2 dependent (**Fig. 1H-J, Supplementary Fig. 2A, B**).

To confirm that visual light perception is required for cardiac circadian PER2 amplitude enhancement, we enucleated wildtype mice to remove any light sensing structures. Ocular enucleation induced a complete loss of PER2 stabilization in "blind" mice exposed to daylight conditions compared to "seeing" animals. **(Fig. 1K, L)**. Myocardial ischemia and reperfusion studies in blind mice under room light housing conditions found 'shifted' cardiac troponin kinetics (Troponin 'blind': 9AM<9PM vs Troponin 'seeing': 9AM>9PM) and slightly overall higher troponin levels in 'blind; mice ('blind' vs 'seeing' troponin: 168 vs 118

ng/ml, not significant), indicating a lack of circadian synchronization by light **(Fig. M, N, Supplementary Fig. 2C).**

Together, these data demonstrate that daylight elicited cardiac circadian amplitude enhancement via PER2 oscillatory overexpression is a cardioprotective strategy requiring visual light perception.

Daylight 'preconditions' the heart via adenosine and thereby establishes a HIF1A-similar signaling environment prior to ischemia

Next, we further deciphered the mechanism of daylight elicited cardiac circadian amplitude enhancement and cardioprotection. First, we evaluated the effect of daylight on infarct sizes or circulating troponin-I levels at 9PM, as one week of daylight housing had increased cardiac PER2 protein levels significantly more at 9PM compared to 9AM (**Fig. 1G**). However, we only found slightly smaller infarct sizes or troponin-I levels at 9PM compared to 9AM (**Fig. 2A**). Moreover, infarct sizes or troponin-I levels at 9PM after daylight 'pretreatment' were similar to recent findings at 9PM under standard housing conditions [8], indicating that we had achieved a maximum of cardioprotection elicited by daylight. Thus, all following studies focused on the robust cardioprotective effect observed at the 9AM time point.

Since daylight had increased the physical activity in mice (**Fig. 1E**), we investigated the influence of voluntary wheel running [11] on circadian amplitude and myocardial infarct sizes. In contrast to daylight exposure, however, two weeks of voluntary wheel running with a longer distance walked were necessary until we noted robust cardioprotection from myocardial ischemia **(Fig. 2B)** or a significant increase of the circadian amplitude **(Fig. 2C)**. Nevertheless, the total distance achieved on the wheel inversely correlated with infarct sizes **(Fig. 2D)**. We therefore evaluated two weeks of voluntary wheel running in *Per2*$^{-/-}$ mice, which revealed a decrease in total running distance, decreased circadian amplitude, increased infarct sizes and significant circadian disruption in *Per2*$^{-/-}$ mice compared to wildtype controls

(**Fig. 2E-H)**, demonstrating that the precise rhythmicity of PER2 is essential for driving cellular circadian oscillations [12].

Based on observations, that PER2 initiates a switch from energy-efficient lipid to oxygen-efficient glucose metabolism during myocardial ischemia which is pivotal to allow the myocardium to function [8, 13], we assessed the effect of daylight on glycolytic flux rates as possible underlying mechanism. Using liquid chromatography-tandem mass spectrometry studies following the infusion of labeled glucose ([U]^{13}C-glucose), we discovered that daylight significantly increased glycolytic flux in cardiac tissue prior to an ischemic event (**Fig. 2I**). We further found that daylight increased the activity of the key and rate limiting enzyme of glycolysis (phosphofructokinase) in heart tissue and plasma in a PER2 dependent manner (**Fig. 2J, K**). Considering glycolysis is HIF1A regulated under conditions of low oxygen availability [14], we investigated if daylight would also increase cardiac HIF1A stabilization under normoxic conditions. However, exposure of ODD-HIF1A reporter mice to one week of daylight indicated that daylight and PER2 mediated increases of glycolysis were at least not due to inhibition of prolyl hydroxylation and increased HIF1A stabilization [15] (**Fig. 2L**). On the other hand, studies have demonstrated that adenosine mediated increases of cAMP is a key regulator of PER2 expression and increased glycolysis [8, 16, 17]. We therefore evaluated if daylight potentially induces peripheral cAMP and PER2 via circulating adenosine [18]. Indeed, after one week of daylight, cardiac adenosine or cAMP levels were significantly increased, which was abolished in *Per2*$^{-/-}$ mice **(Fig. 2 M, N).** Finally, subsequent myocardial ischemia and reperfusion studies in *Per2*$^{-/-}$ mice confirmed that daylight elicited cardioprotection via circadian amplitude enhancement was PER2 dependent (**Fig. 2O, P**).

Taken together, these studies found that daylight does not work via increases of physical activity only but ‘preconditions’ cardiac tissue via increases of cardiac adenosine-cAMP signaling and activation of HIF1A regulated glycolysis in a PER2 dependent manner.

Furthermore, our data suggest daylight elicited adenosine as circulating signaling molecule [18] to enhance peripheral PER2 mediated cardioprotection.

Daylight elicited cardioprotection is abolished in mice with an endothelial specific deletion of PER2 and improves the endothelial barrier function

To further understand daylight elicited and PER2 dependent pathways, we performed a genome-wide array, profiling daylight dependent gene expression prior to an ischemic event. *In silico* analysis found dominant regulation of circadian and metabolic pathways (**Fig. 3A**) and identified the hypoxia/HIF1A-regulated Angiopoietin Like 4 (ANGPTL4) as the top light and PER2 dependent gene **(Fig. 3B)**, supporting our findings that daylight elicited PER2 activates certain HIF1A regulated pathways under normoxic conditions. As ANGPTL4 is an endothelial secreted protein which protects the endothelial barrier function during acute myocardial IR-injury [19], we next evaluated endothelial specific *Per2* deletion in myocardial IR-injury. Using a novel tissue specific mouse line with a 70% deletion of PER2 in the endothelium (**Fig. 3C,** $Per2^{loxP/loxP}$-VE-Cadherin-Cre), we found significantly increased infarct sizes and troponin-I serum levels in $Per2^{loxP/loxP}$-VE-Cadherin-Cre (**Fig. 3D-G)**. In fact, daylight elicited cardioprotection was abolished in $Per2^{loxP/loxP}$-VE-Cadherin-Cre mice. As these data implicated daylight in maintaining the vascular integrity during myocardial IR-injury, we determined the vascular leakage of Evans blue dye following 7 days of room light or daylight housing. As shown in **Figure 3H** and **I**, daylight 'pretreatment' significantly improved endothelial barrier function during myocardial IR-injury.

Taken together these data identify endothelial PER2 as a mechanism of daylight elicited cardioprotection and suggest daylight as a strategy to improve endothelial barrier function during conditions of low oxygen availability.

Endothelial PER2 is critical for the transcriptional control of HIF1A dependent glycolysis

Based on our findings for a critical role of endothelial specific PER2 in daylight mediated cardioprotection and endothelial barrier protection during myocardial IR-injury *in vivo*, we next evaluated endothelial PER2 signaling targets during hypoxia *in vitro*. For this purpose we generated a novel lentiviral mediated PER2 knockdown (KD) stable cell line in human microvascular endothelial cells (HMEC-1). Confirming oxygen as a regulator of the molecular circadian clock [9], the hypoxia induced increases of PER2 transcript and protein levels in control HMEC-1 were lost in PER2 KD cells **(Fig. 4A, B)**. As light elicited PER2 stabilization mimicked HIF1A regulated metabolism, we first evaluated the transcriptional regulation of glycolytic targets during hypoxia. Hypoxic PER2 KD HMEC-1 displayed abolished transcriptional induction of HIF1A dependent glycolytic enzymes (**Fig. 4C, D**). Functional studies revealed attenuated lactate production, reduced glycolytic capacity, and increased cytotoxicity in hypoxic PER2 KD cells (**Fig. 4E-H**). Based on observations in HMEC-1 that PER2 is significantly increased at zeitgeber time (ZT) 12 vs ZT0 [8], we determined whether oscillatory higher PER2 levels would affect metabolism under normoxic conditions and found a significant increase of glycolytic capacity at ZT12 in control HMEC-1 compared to PER2 KD cells **(Fig. 4I, J)**. Mechanistic studies, using a chromatin immunoprecipitation assay (ChIP,) uncovered hypoxia induced HIF1A binding to the lactate dehydrogenase promotor region, a response that was abolished in PER2 KD cells **(Figure 4K).**

Together with previous studies in PER2 gene-targeted mice [8], these findings highlight a critical role for endothelial PER2 in cellular metabolic adaption under normoxia or hypoxia and reveal endothelial PER2 as an essential co-factor of HIF1A mediated transcription of glycolytic genes, and thus a key regulator of glycolytic metabolism.

Identification of endothelial PER2 as a regulator of TCA cycle activity

As hypoxia increased PER2 protein like daylight, we next used an unbiased affinity purification-mass spectrometry-based proteomics screen for PER2 protein interactions under hypoxic conditions to gain a deeper mechanistic perspective of endothelial PER2 dependent mechanisms **(Fig. 5A, Supplementary Table 1, Supplementary Fig. 3**). Serendipitously, a high percentage of PER2-protein interactions hinted towards an important role for PER2 in controlling TCA cycle function (**Fig. 5B**). Subsequent Co-IP pull-downs on TCA cycle enzymes confirmed binding to PER2 during hypoxia (**Fig. 5C, D**). Following analyses of subcellular compartments found that hypoxia induced PER2 in the cytoplasm, nucleus and the mitochondria (**Fig. 5E**). Thus, PER2 protein interactions may facilitate the transport of mitochondrial proteins, which are almost exclusively synthesized in the cytosol. In fact, our proteomics screen indicated PER2 binding to the mitochondrial outer membrane translocase (Tom) complex (**Supplementary Table 1**) [20], which is the main protein entry gate of mitochondria [21]. Functional assays on TCA cycle enzyme activity confirmed regulation of TCA cycle function during hypoxia in a PER2 dependent manner (**Fig. 5F-H**) and hypoxic PER2 KD cells showed significantly less CO_2 production, a surrogate endpoint of TCA cycle function (**Fig. 5I**).

Considering TCA cycle enzyme activity is also known to be regulated by Sirtuin3 (SIRT3) mediated de-acetylation [22], which is under circadian control [23], we investigated whether hypoxia and HIF1A-PER2 dependent pathways would regulate SIRT3 expression. HMEC-1 transcriptional or translational analyses with a PER2 or HIF1A KD revealed a PER2-HIF1A dependent regulation of SIRT3 under hypoxic conditions (**Fig. 5J-L**, **Supplementary Fig. 4A and B)**. *In silico* analysis confirmed a hypoxia response element (HRE) in the human promoter region of SIRT3 **(Supplementary Fig. 4C)**.

Together, our proteomics screen, in conjunction with previous studies showing that the circadian clock drives oxidative metabolism in mice [23], uncovered a critical role for

endothelial PER2 in controlling oxidative TCA cycle metabolism during hypoxia by regulating transcriptional HIF1A-SIRT3-dependent pathways. Moreover, our data suggest a more complex function of PER2, possibly controlling TCA cycle function via post-translational mechanisms.

Endothelial PER2 regulates mitochondrial function via HIF1A-COX4.2

Additional analysis of our proteomics screen indicated binding of PER2 to mitochondrial complexes (**Supplementary Table 1**), supporting a role for PER2 in controlling mitochondrial function under hypoxia. Indeed, oxygen consumption rates (OCR; a measure of mitochondrial functionality), basal respiration, maximal respiration, ATP production, spare capacity, and maximal respiration were significantly reduced in PER2 KD cells during a mitochondrial stress test **(Fig. 6A-D, Supplementary Fig. 5A, B)**. Moreover, OCR levels were significantly increased in cells with higher PER2 levels at ZT12 when compared to ZT0,[8] confirming a role for oscillatory PER2 overexpression in metabolic adaptation under normoxia (**Supplementary Fig 5C, D).**

Considering HIF1A mediates a switch of complex 4 subunits (COX4.1 to COX4.2) in hypoxia to enhance oxygen efficiency, which conserves cellular ATP content [24], we next investigated the transcriptional regulation of COX4.2 in PER2 KD cells under hypoxia. Like other HIF1A dependent transcriptional regulations in PER2 deficient cells, we observed abolished increases of COX4.2 mRNA or complex 4 activity in hypoxic PER2 KD cells or ischemic hearts from *Per2*$^{-/-}$ mice, respectively (**Fig. 6E, F**).

To understand if compromised oxidative phosphorylation in PER2 deficiency would be associated with a reduced mitochondrial membrane potential, which is associated with compromised mitochondrial function [25], we next used MitoTracker deep red staining [26]. Studies in PER2 KD HMEC-1 indicated already reduced mitochondrial potential under normoxia (**Fig. 6G)**. Indeed, analysis of a cell energy phenotype assay revealed significantly

less aerobic metabolism in PER2KD cells at baseline (**Supplementary Fig. 6)**. Confirming these results, JC-1 assays showed a significant reduction in membrane potential in PER2 KD cells at both normoxia and under hypoxia (**Fig. 6H, Supplementary Fig. 7**).

To further explore PER2 dependent metabolism, we next used liquid chromatography-tandem mass spectrometry studies following the exposure of labeled glucose (^{13}C-glucose) or palmitic acid (^{13}C-palmitic acid) to assess metabolic flux rates in PER2 KD cells. Here we confirmed that PER2 is an essential regulator of glycolysis and oxidative metabolism under hypoxia (**Fig. 6I-J**). Moreover, we also found PER2 to be critical for the pentose phosphate pathway under normoxia or hypoxia, indicating that PER2 KD cells are compromised in generating the redox cofactor NADPH, which has a pivotal role for circadian timekeeping (**Fig. 6K**) [27]. As PER2 has been shown to inhibit lipid metabolism via PPARγ [28], we also found altered fatty acid metabolism in PER2KD cells under hypoxia (**Fig. 6L, M**).

Taken together, these data identify endothelial PER2 as transcriptional regulator of HIF1A dependent mitochondrial respiration and suggest PER2 as master regulator of endothelial metabolism, which is also supported by *in silico* analysis of our proteomics screen (**Supplementary Fig. 8).**

A light-sensing human endothelial cell line recapitulates *in vivo* light exposure

As proof of concept that PER2 mimics HIF1A pathways under normoxia, we recapitulated light sensing for PER2 overexpression on a cellular level by generating an HMEC-1 line, overexpressing the human light sensing photopigment melanopsin (OPN4), a retinal ganglion cell receptor responsible for circadian entrainment. Exposing the light sensing HMEC-1 cultures to light resulted in a significant increase of cAMP, phospho-CREB (cyclic AMP-responsive element binding protein), PER2 mRNA, glycolytic capacity and oxygen consumption rates (**Fig. 7A-H)**. Taken together, these studies demonstrate that normoxic

PER2 overexpression can optimize metabolism in a similar fashion as seen under hypoxic conditions.

In summary, our *in vivo* and *in vitro* studies on light-elicited pathways identified a light perception dependent circadian entrainment mechanism through adenosine-cAMP and HIF1A metabolic adaptation in a PER2 regulated manner. Furthermore, our studies suggest that light or hypoxia elicit PER2 as critical factor in maintaining endothelial barrier function during myocardial ischemia via metabolic reprogramming (**Fig. 7I**).

Daylight enhances the circadian amplitude of PER2 and mimics HIF1A dependent metabolism in humans

Next, we investigated if daylight would have similar effects on healthy human volunteers. Based on strategies using daylight therapy [10,000 LUX] to treat seasonal mood disorders or depression in humans [29], we adapted a similar protocol. We exposed human healthy volunteers to 30 min of daylight in the morning on 5 consecutive days and performed serial blood draws. Daylight therapy increased PER2 protein levels in human buccal or plasma samples in the morning (9AM) or evening (9PM), indicating enhancement of the circadian amplitude in different tissues at the same time via light therapy (**Fig. 8A-C, Supplementary Fig. 9)**. To test the efficacy of daylight therapy on the circadian system [30] we determined melatonin plasma levels, which were significantly suppressed upon light therapy (**Fig. 8D, E**). In addition, room light was less efficient than daylight therapy in suppressing melatonin (**Fig. 8D**). Further analyses revealed that daylight therapy increased plasma phosphofructokinase at 9AM and 9PM without increasing lactate dehydrogenase activity or plasma HIF1A levels (**Fig. 8F-I**). Moreover, plasma triglycerides, a surrogate for insulin sensitivity and carbohydrate metabolism [31], significantly decreased upon light therapy (**Fig. 8J**), indicating increased insulin sensitivity and glucose metabolism. Targeted metabolomics from human plasma samples confirmed a strong effect of light therapy on metabolic pathways such as

glycolysis or TCA cycle (**Fig. 8K, Supplementary Fig. 10**). In fact, we found significant decreases of pyruvate, lactate and succinate levels after 5 days of light therapy (**Fig. 8L-N**). Together with increased plasma phosphofructokinase activity, this finding indicates improved metabolic flux, possibly due to increased glycolysis, improved TCA cycle or mitochondrial function.

As sleep deprivation is directly associated with decreased insulin sensitivity and compromised glucose metabolism [32], we next determined how our light therapy protocol would impact human physiology in terms of sleep behavior. Using a validated accelerometer for actigraphy[33] (Actiwatch 2) we found less WASO (wake after sleep onset) episodes and overall improved sleep efficiency (**Fig. 8O-P, Supplementary Fig. 11**). In fact, visual actigraphy analysis following light therapy indicated improved circadian synchrony (**Fig. 8Q, Supplementary Fig. 11**) and thus enhanced circadian amplitude. Taken together, our data indicate that daylight therapy, a mechanism of circadian amplitude enhancement, targets similar PER2 dependent metabolic pathways in humans as seen in mice and may present a promising novel strategy for the treatment or prevention of low oxygen conditions such as myocardial ischemia.

DISCUSSION

In the present study, we demonstrated a potential role for daylight in cardioprotection from myocardial ischemia. *In vivo* murine studies using 14h-daylight exposure up to one week revealed a robust and time dependent cardioprotective effect. Following studies on daylight elicited cardioprotection uncovered circadian amplitude enhancement of cardiac PER2 as an underlying mechanism. Daylight was found to increase cardiac adenosine, cAMP and glycolysis prior to ischemia in a PER2 dependent manner, with targeted gene deletion of PER2 abolishing the daylight induced cardioprotective effects. A whole genome array on daylight and PER2 dependent pathways indicated that daylight activates hypoxia mediated pathways under normoxia and pointed towards a critical role for endothelial PER2 in regulating such pathways. In fact, studies on myocardial IR-injury using endothelial specific PER2 deficient mice revealed abolished cardioprotection by daylight. Moreover, daylight elicited cardioprotection was associated with improved endothelial barrier function during myocardial ischemia. In depth mechanistic studies on endothelial PER2 function revealed a prominent metabolic role for PER2 under hypoxia or normoxia, controlling glycolysis, TCA cycle or mitochondrial respiration. Translational studies in humans found that daylight

activated similar pathways as found in our murine studies. Together, these studies point towards PER2 as critical control point of endothelial metabolic reprograming to maintain vascular integrity during myocardial IR-injury and suggest daylight to increase PER2 signaling as therapeutic strategy for the treatment of coronary artery disease.

We found that daylight decreases infarct sizes, increases glycolysis, adenosine, cAMP and endothelial barrier function, changes gene transcription in murine cardiac tissues, and affects human metabolism which establishes a critical role for daylight in regulating important biological processes [34]. In fact, epidemiologic studies noting an increase in MIs during the darker winter months in *all* US states [35] provide strong evidence to support our conclusion that daylight elicits robust cardioprotection. The mechanism of how the entrainment signal gets to peripheral organs remains unclear but may incorporate neuro-hormonal factors, or autonomic innervation [36]. Studies on altered liver metabolism in constant darkness found adenosine as a possible circulating circadian factor [18], which suggests adenosine signaling as a mechanism for establishing circadian rhythmicity between peripheral organs and the SCN. Indeed, the importance of adenosine signaling via cAMP for PER2 stabilization and cardiac metabolic adaption to ischemia has been shown in recent studies investigating the mechanism of myocardial ischemic preconditioning [8]. In the current studies we found that light elicited cardiac circadian amplitude enhancement increased cardiac adenosine and cAMP levels, which was also PER2 dependent. While we did not determine plasma adenosine levels, we were able to detect adenosine increases in blood containing and flash frozen mouse hearts following one week of daylight housing. Since this response was abolished in whole body *Per2*$^{-/-}$ mice, and light perception was necessary to increase cardiac PER2 levels, adenosine signaling likely plays an important role in establishing circadian rhythmicity between peripheral organs and the SCN.

While cardiomyocytes are the major consumers of oxygen and account for approximately 75% of the myocardial volume, there is at least one capillary adjacent to every cardiomyocyte, and cardiomyocytes are outnumbered 3:1 by the endothelial cells [37]. Recent electron microscopic investigations during reperfusion after cardioplegia suggest that endothelial cells might be even more prone to damage during reperfusion than cardiomyocytes [38]. Mitochondrial metabolism in endothelia has been proposed as central oxygen sensor in the vasculature [39], and studies have suggested that human endothelial cells can regulate the activity of HIF1A, thus affecting key response pathways to hypoxia and metabolic stress [39]. Endothelial damage also accounts for the "no-reflow" phenomenon observed when regions of a de-occluded heart do not restore normal blood flow [40]. As such, endothelial dysfunction plays a significant role in myocardial IR-injury, rendering endothelial cells an attractive target for myocardial protection [41]. In the current studies, we uncovered a critical role for light elicited PER2 as regulator of endothelial metabolism. While PER2 has been implicated in controlling endothelial function in previous studies [42, 43], an endothelial specific role of PER2 during acute myocardial IR-injury, which can be targeted using daylight, has not yet been described. Moreover, our *in vivo* and *in vitro* studies suggest that light elicited reprograming of endothelial metabolism protects the endothelial barrier function during IR-injury. Together with previous studies on endothelia in IR-injury [41], these studies highlight the importance of cardiac endothelial metabolism in IR-injury and point towards unrecognized therapeutic strategies for cardiovascular disease using daylight or pharmacological compounds, such as the circadian rhythm enhancer nobiletin [44, 45], to increase endothelial PER2 amplitude.

The importance of HIF1A in cardioprotection has been shown in numerous studies [46] and the interaction between HIF1A and PER2 has been demonstrated on the protein [8, 47] and transcriptome level [48], In general, HIF1A requires hypoxic conditions to be

stabilized [46]. In the current studies we further established the dependence of HIF1A on PER2 as a transcription factor during hypoxia, supporting previous studies on PER2 function as an effector molecule for the recruitment of HIF1A to promoter regions of its downstream genes [47]. However, we also found that certain HIF1A pathways such as glycolysis or ANGPTL-4 signaling can also be activated via light elicited circadian overexpression of PER2 under normoxia. These findings would suggest that PER2 amplitude enhancement strategies are able to 'precondition' the myocardium by establishing a HIF1A-similar signaling environment prior to an ischemic event. While we did not see a daylight mediated HIF1A stabilization, we did not investigate HIF1A transactivation or binding activity, which has been found to be the mechanism of enhanced HIF1 transcription via PER2 overexpression under hypoxia [47].

Given a close association of circadian amplitude dampening and disease progression [49], 'clock'-enhancing strategies are promising novel approaches for disease treatment. Although it is well known that light regulates circadian rhythms [50] and that high intensities of light are more effective for circadian entrainment and amplitude enhancement [30], only a few reports exist on circadian entrainment and cardioprotection [51]. While previous studies suggested that short term intense light exposure could mediate cardioprotection in a PER2 dependent manner [8], no specific mechanisms were provided. In the current studies we uncovered that daylight elicited cardioprotection works via amplitude enhancement of endothelial specific PER2 and profiling of daylight elicited and PER2 dependent gene expression revealed daylight activation of circadian, metabolic or HIF1A regulated pathways. In fact, our *in vivo* and *in vitro* studies demonstrated that PER2 is not only an essential co-factor of HIF1A transcription in metabolic adaptation of the hypoxic endothelium, but also activates hypoxia dependent pathways under normoxic conditions, bypassing HIF1A stabilization, in mice and humans.

It is important to note the translation of our findings from mice as a model system to humans. Indeed, our light exposure strategy in humans showed similar kinetics as in mice. It is well known that circadian rhythms function independent of a diurnal or nocturnal behavior due to multiple yet parallel outputs from the SCN [52]. In fact, very fundamental features of the circadian system are the same in apparently diurnal and nocturnal animals, including the molecular oscillatory machinery and the mechanisms responsible for pacemaker entrainment by light [52]. In addition, PER2 is hypoxia regulated in mice and humans, which supports similar mechanisms in both species [8]. HIF1A regulation and function under hypoxia, which is strongly associated with PER2 [47], seems also to be independent of a nocturnal nature [46], despite HIF1A expression being under circadian control [48]. In fact, human and mouse studies on HIF1A find similar responses to cardiovascular ischemic events [46].

Supporting the importance of circadian rhythms in myocardial susceptibility to ischemia, recent studies found a diurnal pattern for troponin values in patients undergoing aortic valve replacement [53]. Here, troponin values following surgery were significantly higher in the morning when compared to the afternoon. While nothing can be done about a diurnal pattern, applying light therapy before high risk non-cardiac or cardiac surgery to enhance the circadian amplitude, however, might be able to provide robust cardioprotection and reduce mortality. Light elicited circadian amplitude enhancement suggests an overall increase in PER2 levels and concomitant cardioprotection even at the trough of the amplitude, indicating that this strategy could promote general cardioprotection and potentially decrease troponin levels in both the morning and evening times. Despite the fact we show that circadian amplitude enhancement is a reasonable strategy for adaptive protection from myocardial ischemia, its potential to also protect against the consequences of an ischemic event, however, will need further investigation in mechanistic research endeavors.

METHODS

Mouse experiments.

Experimental protocols were approved by the Institutional Review Board (Institutional Animal Care and Use Committee [IACUC]) at the University of Colorado Denver, USA. They were in accordance with the NIH guidelines for use of live animals. *All mice were housed in a 14 h (hours):10 h L(light):D(dark) cycle and we routinely used 12- to 16-week old male mice.* All mice had a C57BL/6J background. C57BL/6J, *Per2*$^{-/-}$ mice [Per2tm1Brd Tyrc-Brd/J[54]], PER2 [B6.129S6-*Per2*^{tm1Jt}/J] or HIF1A [FVB.129S6-Gt (ROSA) 26Sortm2 (HIF1A/luc) Kael/J] reporter mice were purchased from Jackson laboratories [15, 55]. HIF1A reporter mice were backcrossed for at least 6 generations to a C57BL/6J background. *Per2*$^{loxp/loxp}$ mice were generated by Ozgene (Pert, Australia). VE-Cadherin-Cre [B6.Cg-Tg(Cdh5-cre)7Mlia/J[56]] were purchased from Jackson laboratories. To obtain endothelial

tissue specific mice, we crossbred *Per2*$^{loxp/loxp}$ mice with the VE-Cadherin-Cre recombinase mouse. *We conducted all mouse experiments at same time points (9 AM) unless specified otherwise*.

Daylight exposure in mice

Mice were exposed to intense light (10,000 LUX, Lightbox simulating day light, Uplift Technologies DL930 Day-Light 10,000 Lux SAD, full spectrum) for 3, 5 or 7 days and compared to mice maintained at room light [200 LUX] for 7 days (***Note****: infarct sizes are always the same at 9AM regardless the length of being housed under normal housing conditions*) [17].

Murine model for cardiac MI and heart enzyme measurement

Murine *in situ* myocardial ischemia and reperfusion injury (*60-min ischemia/120 min reperfusion)* and troponin-I (cTnI) measurements were performed as described [57-59]. Infarct sizes were determined by calculating the percentage of infarcted myocardium to the area at risk (AAR) using a double staining technique with Evan's blue and triphenyltetrazolium chloride. AAR and the infarct size were determined via planimetry using the NIH software Image 1.0 (National Institutes of Health, Bethesda, MA). For cTnI measurements blood was collected by central venous puncture and cTnI was analyzed using a quantitative rapid cTnI assay (Life Diagnostics, Inc., West Chester, PA, USA). ***Note***: *cTnI is highly specific for myocardial ischemia and has a well-documented correlation with the infarct size in mice* [57, 59-61] *and humans* [62].

Wheel running

Mice were maintained individually in running-wheel cages (Starr Life Sciences, wheel diameter: 11.5 cm). Running-wheel activity was recorded every 5 minutes using the Vital View Data Acquisition System (Starr Life Sciences, Oakmont, PA). Data were analyzed using BioDare (Biological Data Repository) [63]. Amplitude of wheel running activity were

calculated using the fast fourier transform non-linear least squares (FFT-NLLS) method. The distance walked was calculated as the sum of a 7 day-recording.

Luciferase Assay

Expression of the PER2 or HIF1A protein using luciferase reporter mice was assayed as described [8]. Expression of the PER2 or HIF1A protein using luciferase reporter mice was determined using the tissue homogenates in T-per Tissue Protein Extraction Reagent (Pierce, Thermo Fisher Scientific, Waltham, MA). The homogenates were centrifuged for 30mins at 4900 x g at 4oC. The luciferase protein activity was measured by using the Dual-Luciferase Reporter Assay System from Promega according to the manufacturer's instructions using a Biotek Synergy 2 Multimode Microplate Reader (Winooski, VT).

Enucleation procedure in mice

Mice were pre-anesthetized with subcutaneous carprofen and buprenorphine injections and anesthetized with a ketamine/xylazine/ace cocktail. The periocular region was then clipped to remove surrounding hair. After a surgical scrub with betadine, the optic nerve and associated blood vessels were clamped with hemostats. After 2 minutes the entire globe of eye and the optic nerve were removed. For additional analgesia bupivacaine was dripped into the socket. Next, the complete upper and lower eyelid margin were removed with fine tip scissors and the eyelids were closed with 3-4 interrupted sutures. Mice were recovering in cages on warm water circulating blankets. Carprofen injections were repeated every 24 hours for 2 days post operatively. After a 2-week recovery period under standard housing conditions, mice underwent daylight housing or myocardial ischemia studies.

^{13}C-tracer studies *in vivo*

C57BL/6 wildtype mice were housed under daylight (10,000 LUX, L:D 14:10 h) or standard room light (200 LUX, L:D 14:10 h) for 7 days followed by infusion of 10 mg/kg/min U-^{13}C-glucose (Cambridge Isotope Laboratories, Tewksbury, MA) via an intra-arterial catheter over 90 minutes. Left ventricles of the hearts were flushed with ice cold KCl and the left ventricle

was shock frozen and analyzed by liquid chromatography–tandem mass spectrometry. Isotope-resolved metabolite analyses (^{13}C-Fructose-6-phosphate) were performed by LC-MS on a Waters Acquity ultrahigh-performance liquid chromatography (UPLC) system coupled to a Waters Synapt HDMS quadrupole time-of-flight mass spectrometer equipped with an atmospheric pressure electrospray ionization (ESI) source as described [8, 64-66].

PFK and cAMP-activity mouse tissue

To measure Phosphofructokinase activity from myocardium or plasma, C57BL/6J or *Per2*$^{-/-}$ mice were euthanized following light exposure. Blood was removed to obtain plasma further analysis, and the tissue was immediately flash frozen at -80°C. Enzyme activity from homogenized tissue or plasma was determined using a PFK Assay Kit from Biovison. To determine cAMP in cardiac tissue, a cyclic AMP Enzyme Immunoassay Kit (Mouse/Rat cAMP Parameter Assay Kit, R&D, Minneapolis, MN) was used according to the manufacturer's protocol.

Adenosine measurements

Whole murine hearts were collected in 1 mL of 80% MeOH and flash-frozen under liquid nitrogen and stored at -80°C. Adenosine was extracted and quantified on an Agilent Technologies 1260 Infinity HPLC using a phenomenex Luna C18(2) column (100 Å, 150 X 4.6 mm) as described [67].

Microarray analysis

Total RNA was isolated from heart tissue from daylight or room light 'pretreated' C57BL/6J or *Per2*$^{-/-}$ mice with the RNeasy micro kit (Qiagen, Valencia, CA) using Qiagen on-column DNase treatment to remove any contaminating genomic DNA. The integrity of RNA was assessed using a Tapestation 2200 (Agilent Technologies) and RNA concentration was determined using a NanoDrop ND-1000 spectrophotometer (NanoDrop, Rockland, DE). Hybridization cocktail was prepared starting with 100ng Total RNA using the GeneChip WT PLUS Reagent Kit. Samples were hybridized to the Arrays (Mouse Clariom D arrays) for 16

hours at 45 degrees C in a GeneChip Hybridization Oven 645. Arrays were then washed and stained in a GeneChip Fluidics Station 450 and scanned in a GeneChip Scanner 3000. Each array was subjected to visual inspection for gross abnormalities. Several other QC metrics were used to monitor hybridization efficiency and RNA integrity over the entire processing procedure. Raw image files were processed using Affymetrix GCOS 1.3 software to calculate individual probe cell intensity data and generate CEL data files. Using GCOS and the MAS 5.0 algorithm, intensity data was normalized per chip to a target intensity TGT value of 500 and expression data and present/absent calls for individual probe sets calculated. Gene symbols and names for data analyzed with the MAS 5.0 algorithm were from the Affymetrix NetAffx Mouse 430_2 annotations file. Quality control was performed by examining raw DAT image files for anomalies, confirming each GeneChip array had a background value less than 100, monitoring that the percentage present calls was appropriate for the cell type, and inspecting the poly (A) spike in controls, housekeeping genes, and hybridization controls to confirm labeling and hybridization consistency. According to our experimental setup the arrays were normalized, grouped and analyzed for differentially expressed transcripts based on different statistical tests. Different clustering algorithms allowed us to identify transcripts that show similar expression profiles. Using the TAC (Transcriptome Analysis Console, Affymetrix) software we were able to identify biological mechanisms, pathways and functions most relevant to our experimental dataset. Array data have been deposited in the Array Express database at EMBL-EBI (www.ebi.ac.uk/arrayexpress) under accession number E-MTAB-7196. *Username: Reviewer_E-MTAB-7196; Password: WWyjkjym.*

Modified Miles Assay

Extravasated Evans blue (ng) was determined from a standard curve and normalized to tissue weight (g). Evans blue dye content was determined from standard curve and normalized to heart tissue weight as published [19].

Cell culture

Human microvascular endothelial cells (HMEC-1) were cultured as described previously [68, 69]. PER2 KD and control cell lines (Scr) were selected using 2.5 μg/mL puromycin. HIF1A KD and control cell lines were selected using 350 μg/mL geneticin (G418). All experiments were conducted after serum starvation to reset circadian rhythmicity [8].

Hypoxia exposure. For hypoxia experiments cells were placed in a hypoxia chamber (Coy Laboratory Products Inc., Grass Lake, MI) in preequilibrated hypoxic medium at 1% O_2 for 24 hours.

Lentiviral-mediated generation of cells with knockdown of PER2 or HIF1A

Stable cell cultures with decreased PER2 and HIF1A expression were generated by lentiviral-mediated shRNA expression. pLKO.1 lentiviral vector targeting PER2 had shRNA sequence of CCG GGA CAC ACA CAA AGA ACT GAT ACT CGA GTA TCA GTT CTT TGT GTG TGT CTT TTT (TRCN0000018542) and HIF1A had shRNA sequence of CCG GCC AGT TAT GAT TGT GAA GTT ACT CGA GTA ACT TCA CAA TCA TAA CTG GTT TTT (TRCN 0000003809). For controls, nontargeting control shRNA (SHC002; Sigma) was used. HMEC-1 were co-transfected with pLK0.1 vectors and packaging plasmids to produce lentivirus. Filtered supernatants were used for infection of HMEC-1 and cells were selected with puromycin or geneticin until a knockdown was confirmed [64].

Transcriptional Analysis

Total RNA was isolated using Trizol Reagent (Invitrogen, Carlsbad, CA), phenol-chloroform extraction, and ethanol precipitation followed by purification in a modified protocol from RNeasy Mini Kit (Qiagen, Germantown, MD). RNA was quantified using either a Qubit 3.0 RNA BR Assay Kit (Thermo Fisher Scientific, Waltham, MA) or Nanodrop 2000. Quantification of transcript levels was determined by real-time RT-PCR (iCycler; Bio-Rad Laboratories, Inc, Hercules, CA). qPCR reactions contained 1x final primer concentration (Qiagen primers, Germantown, MD) or 1 μM sense and 1 μM antisense oligonucleotides (Invitrogen custom DNA oligos, Carlsbad, CA) with SYBR Green (Bio-Rad, Hercules, CA).

Primer sets used (Qiagen QuantiTect) were Hs_PER2_1_SG (QT0011207), Hs_PKM_1_SG (QT00028875), Hs_LDHA_1_SG (QT00001687), Hs_SIRT3_1_SG (QT00091490), Hs_ACTB_2_SG (QT01680476), and Hs_COX4|2_1_SG (QT00044933), Mm_Per2_1_SG (QT00198366), Mm_Angptl4_1_SG (QT00139748), Mm_Actb_2_SG (QT01136772). Primers for human OPN4 (Invitrogen, Carlsbad, CA, sense 5'-AGT CGC CCC TAC CCC AGC TA-3' and antisense 5'- CAC AGC TGC TGC CTC CAT GT-3') were custom designed. Each target sequence was amplified using the following protocol: 95°C for 3 min, 40 cycles of 95°C for 15 sec, 55°C for 0.5 min, 72°C for 10 sec, 72°C for 1 min and a melt curve protocol.

Immunoblotting experiments

Protein was isolated from HMEC-1 using M-Per following manufacturer's instructions (Thermo Fisher Scientific, Waltham, MA) and including a protease and phosphatase inhibitor cocktail (Thermo Fisher Scientific, Waltham, MA). Protein was quantified using a Qubit Fluorometer 3.0 and Qubit Protein Assay Kit (Thermo Fisher Scientific, Waltham, MA). 5 – 25 μg of protein was denatured at 95°C in Laemmli sample buffer for 5 min. Samples were resolved on a 4 – 10% polyacrylamide gel and transferred to nitrocellulose membranes, which were blocked for 1h at room temperature in either 5% BSA / TBST or 5% milk / TBST. The membranes were incubated in primary antibody at a concentration of 1:1000 overnight at 4°C. The primary antibodies used were rabbit polyclonal PER2 (Novus Biologicals, NB100-125, Littleton CO, or Abcam, ab64460, Cambridge, MA), rabbit polyclonal IDH2 (Novus Biologicals, NBP2-22166, Littleton CO), rabbit polyclonal SUCLG1 (Novus Biologicals, NBP1089489, Littleton CO), rabbit polyclonal ACO2 (Novus Biologicals, H00000050-D01P, Littleton CO), rabbit polyclonal SIRT3 (Abcam, ab86671, Cambridge, MA), anti-alpha Tubulin antibody (Abcam, ab7291, Cambridge, MA), Anti-VDAC1 / Porin antibody (Abcam, ab15895, Cambridge, MA), Anti-TATA binding protein (TBP) antibody (Abcam, ab51841, Cambridge, MA), mouse monoclonal β-ACTIN (Cell Signaling Technologies, 8H10D10,

Danvers, MA), and mouse monoclonal anti-DDK (FLAG) (OriGene Technologies, TA50011-100, Rockville, MD). The next day, blots were washed 3 – 4x with TBST and incubated with secondary antibody at a concentration of 1:5000 in the respective blocking buffer, washed an additional 3 times, and visualized using SuperSignal West Femto Maximum Sensitivity Substrate (Thermo Fisher Scientific, Waltham, MA). The secondary antibodies used were goat polyclonal IgG (Novus Biologicals, NB7487), goat anti-mouse IgM (Calbiochem, San Diego, CA), and goat anti-rabbit IgG (Thermo Fisher Scientific, Waltham, MA).

Lactate measurements

Lactate measurements were done using the L-Lactate Colorimetric Assay Kit following the manufacturer's protocol (Abcam, Cambridge, MA).

Cytotoxicity

Cytotoxicity was determined using the LDH-Cytotoxicity Assay Kit per manufacturer's protocol (Abcam, Cambridge, MA).

Seahorse stress tests

Glycolytic stress tests. The XF24 Seahorse Bioanalyzer was used in conjunction with glycolytic stress tests following manufacturer's specifications (Agilent, Santa Clara, CA). Cells were plated in the morning at a density of $1.2x10^5$ cells / well and serum starved in the evening one day prior to assaying. One hour prior to the stress test cells were incubated in XF Assay Medium (Agilent, Santa Clara, CA) at a pH of 7.4. Final concentration of glucose was 10 mM / well, oligomycin 1.0 μM / well, and 2-deoxyglucose 50 mM / well. *Mitochondrial stress tests.* The XF24 Seahorse Bioanalyzer was used for mitochondrial stress tests (Agilent, Santa Clara, CA). For all assays, pH and oxygen consumption rate (OCR) were measured. For TCA cycle readouts, an additional measurement of carbon dioxide evolution rate (CDER) was measured. Final concentrations were 1.0 μM oligomycin, 3.6 μM FCCP, and 1.125 μM Rotenone / Antimycin A. For fatty acid mitochondrial stress tests, cells were supplemented with palmitate:BSA (Agilent, 102720-100) prior to the run and half the plate received 800 μM

etomoxir as a control. *Cell energy phenotype assays*. Following manufacturer's instructions (Agilent, Santa Clara, CA), the Seahorse Bioanalyzer was used to assess cell energy phenotype at baseline.

Chromatin immunoprecipitation (ChIP) assay

ChIP assays were performed using the ChIP-IT™ Express Enzymatic Kit from Active Motif (Carlsbad, CA, USA). Briefly, Scr and PER2KD HMECs were grown to 90% confluence in phenol red-free Dulbecco's modified Eagle medium (DMEM) supplemented with 10% charcoal DEXTRAN-stripped FBS for at least 3 days. After hypoxia exposure at 1% O_2 for 24h, ChIP assays were performed according to manufacturer's protocol. Briefly, chromatin was cross-linked in 1% formaldehyde in minimal cell culture medium (Invitrogen, Carlsbad, CA), and nuclei were extracted. Chromatin was enzymatically digested for 11mins to yield 200- to 1,500-bp DNA fragments and the supernatant containing precleared chromatin was then incubated at 4°C overnight with mouse monoclonal HIF1A antibody (H1alpha67, ChIP Grade, Abcam, Cambridge, MA) or rabbit IgG control (Cell Signaling, Danvers, MA). After reverse cross-linking by heating the samples at 65°C overnight and treating with Proteinase K, DNA was purified using phenol-chloroform extraction. Quantitative analyses of DNA products obtained from ChIP assay were performed by RT-PCR with primers specific for the human LDHA promoter. RT-PCRs conducted on DNA derived from input chromatin templates served as positive controls whereas reactions conducted on IgG-precipitated templates served as negative controls. The RT-PCR signal was barely detectable for these controls. The signal for these samples and IgG-precipitated templates was negligible on gels. Primers used were: sense ATT ACG TGC CAG AAG CTG TT and antisense TTT CCT CAT CCA TGA AAC CT for the human LDHa promoter. Conventional PCR signals were stained with ethidium bromide in 1% agarose gels.

Affinity purification-mass spectrometry-based proteomics

HMEC-1 were placed in a hypoxia chamber (Coy Laboratory Products Inc.) in preequilibrated hypoxic medium at 1% O2. Following 24 h of hypoxia or normoxia, the samples were isolated for cytoplasmic and nuclear protein fractions according to the NE-PER kit specifications (Thermo Scientific, 78833). To identify interacting proteins with PER2, co-immunoprecipitation (Co-IP) for PER2 was performed using the Pierce Co-IP Kit (Thermo Scientific, 26149). Specifically, 10 µg of rabbit anti-PER2 antibody (Novus, NB100-125) was immobilized to the amine-reactive resin. 100 µg of sample was incubated overnight at 4 ^{o}C with the anti-PER2 coupled resin. Samples were washed and then eluted. Samples were loaded onto a 1.5mm NuPAGE Bis Tris 4-12% gradient gel and proteins were separated as previously described[70]. The gel was stained using SimplyBlue™ SafeStain (Invitrogen, Carlsbad, CA) and de-stained with water. Each lane of the gel was divided into 9 equal-sized bands, gels were destained, disulfide bonds were reduced, and cysteine residues were alkylated as previously described [70]. Gel pieces were subsequently washed with 100 µL of distilled water followed by addition of 100 mL of acetonitrile and dried on SpeedVac (Savant Thermo Scientific). Then 100 ng of trypsin was added to each sample and allowed to rehydrate the gel plugs at 4 °C for 45 min and then incubated at 37 °C overnight. The tryptic mixtures were acidified with formic acid up to a final concentration of 1%. Peptides were extracted two times from the gel plugs using 1% formic acid in 50% acetonitrile. The collected extractions were pooled with the initial digestion supernatant and dried on SpeedVac (Savant ThermoFisher). Samples were desalted on Thermo Scientific Pierce C18 Tip. Similar to previously described studies [71], samples were analyzed on an LTQ Orbitrap Velos mass spectrometer (Thermo Scientific) coupled to an Eksigent nanoLC-2D system through a nanoelectrospray LC-MS interface. Specific to these experiments and following desalting, the peptides from each sample were separated over a 90-min linear gradient of 2-40% ACN with 0.1% formic acid. LC mobile phase solvents and sample dilutions used 0.1% formic acid in water and 0.1% formic acid in acetonitrile (Optima^{TM} LC/MS, Fisher

Scientific). Data acquisition and mass spectrometer was operated in positive ion mode as previously described [71]. Full MS scans were acquired in the Orbitrap mass analyzer as in previous studies [72]. For database searching and protein identification, MS/MS spectra were extracted from raw data files and converted into mgf files using MassMatrix (Cleveland, OH). These .mgf files were then independently searched against mouse SwissProt database using an in-house Mascot™ server (Version 2.2, Matrix Science). Mass tolerances were +/- 15 ppm for MS peaks, and +/- 0.6 Da for MS/MS fragment ions. Trypsin specificity was used allowing for 1 missed cleavage. Met oxidation, protein N-terminal acetylation, peptide N-terminal pyroglutamic acid formation were allowed for variable modifications while carbamidomethyl of Cys was set as a fixed modification. Scaffold Software (version 4.4.6, Proteome Software), peptide, and protein identification probability parameters were used as previously described [71]. Following identification of potential PER2 interacting proteins in normoxia, hypoxia, and normoxia vs. hypoxia, lists obtained from Scaffold were analyzed by Ingenuity Pathway Analysis (Qiagen), Panther Classification System, and Reactome Analysis to detect pathways PER2 regulates in normoxia and hypoxia.

Co-immunoprecipitations (Co-IPs)

Co-IPs were done using the Pierce Co-Immunoprecipitation (Co-IP) Kit (Thermo Fisher Scientific, Waltham, MA). 10 µg of antibody was immobilized to columns. Pulled-down protein was quantified using a Qubit Fluorometer 3.0 and resolved by immunoblotting as described.

Subcellular compartment analysis

HMEC-1 were placed in hypoxia (1% O2) or normoxia for 24 h. After normoxia or hypoxia exposure, samples were isolated for cytoplasmic and nuclear protein fractions according to the NE-PER kit specifications (Thermo Fisher Scientific, Waltham, MA). Mitochondria protein fraction was isolated with the Dounce homogenization method according to the Mitochondria Isolation Kit for Cultured Cells specifications (Thermo Fisher Scientific, Waltham, MA).

Enzyme activities IDH, ACO, SUCLG, Complex IV, PFK, LDH

Human isocitrate dehydrogenase (IDH, Biovision, Milpitas, CA), aconitase (ACO, Abcam, Cambridge, MA), succinyl-CoA synthetase (SUCLG, Abcam, Cambridge, MA), phosphofructokinase (PFK, Biovision, Milpitas, CA) and lactate dehydrogenase (LDH, Biovision, Milpitas, CA) activity or mouse complex 4 activity (Abcam, Cambridge, MA) were measure colorimetric assay kits adhering to manufacturer's instructions.

Mitochondrial membrane potential dyes

MitoTracker Red CMXRos (Invitrogen Molecular Probes, Carlsbad, CA) and JC-1 Mitochondrial Membrane Potential Assay (Abcam, Cambridge, MA) were used per manufacturer's specifications using 5 µM of JC-1 for 30 minutes at 37C. JC-1 quantification was done by calculating mean intensity.

13C-tracers *in vitro*. HMEC-1s were serum starved in either MCDB131 (low glucose) or glucose-free DMEM for 24 h prior to assay. Respective mediums were supplemented with either 12 mM U-^{13}C-glucose (Cambridge Isotope Laboratories, Tewksbury, MA) or 166.67 µM 1,2-$^{13}C_2$-palmitic acid (Cambridge Isotope Laboratories, Tewksbury, MA) in hypoxia or normoxia for 24 h. Frozen cell pellets were extracted at $2e^6$ cells/mL in ice cold lysis/ extraction buffer (methanol:acetonitrile:water 5:3:2). Samples were agitated at 4 °C for 30 min followed by centrifugation at 10,000 g for 10 min at 4 °C. Protein and lipid pellets were discarded, and supernatants were stored at -80 °C prior to metabolomics analysis. Ten µL of extracts were injected into a UHPLC system (Vanquish, Thermo, San Jose, CA, USA) and run on a Kinetex C18 column (150 x 2.1 mm, 1.7 µm - Phenomenex, Torrance, CA, USA). Solvents were Optima H2O (Phase A) and Optima acetonitrile (Phase B) supplemented with 0.1% formic acid for positive mode runs and 1 mM NH4OAc for negative mode runs. For [U-^{13}C]-glucose flux analysis [73], samples were run on a 3 min isocratic (95% A, 5% B) run at 250 µL/min [74, 75]. For [1,2-$^{13}C_2$]-palmitate flux analysis, samples were analyzed using a 9 min gradient from 5-95% acetonitrile organic phase at 400 µL/min. The autosampler was held

at 7 °C for all runs; the column compartment was held at 25 °C for the 3 min method and 45 °C for the 9 min method [76]. The UHPLC system was coupled online with a Q Exactive mass spectrometer (Thermo, Bremen, Germany), scanning in Full MS mode (2 μscans) at 70,000 resolution in the 60-900 m/z range in negative and then positive ion mode (separate runs). Eluate was subjected to electrospray ionization (ESI) with 4 kV spray voltage. Nitrogen gas settings were 15 sheath gas and 5 auxiliary gas for the 3 min runs; 45 sheath gas and 15 auxiliary gas for the 9 min runs. Metabolite assignments and isotopologue distributions were determined using Maven (Princeton, NJ, USA), upon conversion of '*.raw*' files to '*.mzXML*' format through MassMatrix (Cleveland, OH, USA). Chromatographic and MS technical stability were assessed by determining CVs for heavy and light isotopologues in a technical mixture of extract run every 10 injections.

Light sensing cells

HMEC-1 WT cells were transfected with pCMV6-Entry (C-terminal Myc and DDK Tagged, OriGene Technologies, Rockville, MD) or OPN4 (Myc-DDK-Tagged)-pCMV6-Entry transcript variant 1 (TrueORF Gold Expression-Validated cDNA Clones from OriGene Technologies, Rockville, MD) using FuGene HD Transfection Reagent (Promega, Madison, WI). After transfection, cells were kept in complete darkness until room light (~200 LUX) or daylight (~10,000 LUX) exposures for 30 minutes. Melanopsin protein expression validation was done by isolating protein using RIPA buffer (Thermo Fisher Scientific, Waltham, MA) supplemented with protease and phosphatase inhibitor cocktail (Thermo Fisher Scientific, Waltham, MA). Immunoblotting for anti-DDK (OriGene Technologies, Rockville, MD) was used to detect DDK-tagged melanopsin in transfected cells. Light-sensing cells subjected to glycolytic or mitochondrial stress tests on the Seahorse Bioanalyzer were exposed to light 30 min prior to Seahorse analyses.

cAMP ELISA and phospho-CREB assays

Phospho-CREB (S133) Immunoassay (R&D Systems, Minneapolis, MN) or cAMP Parameter Assay Kit for human (R&D Systems, Minneapolis, MN) were used according to the manufacturer's protocol.

Human light exposure

Healthy human volunteers were exposed to daylight exposure (10,000 LUX) for 30 min every morning for five days from 8:30 AM – 9:00 AM. 5 mL blood was drawn on day one at 8:30 AM and 9:00 AM (before and after light exposure). While light exposure was repeated every morning for the five days, the next blood draws were on day two, three and five at 9:00 AM as indicated. In subset of experiments blood draws were also performed at 9 PM after 5 days of daylight therapy. For experiments involving actigraphy watches, the same volunteers wore the watch for one week without bright light exposure and maintained wearing the watches during the second week when light exposure was included. Actigraphy data were obtained by using a validated accelerometer (Actiwatch 2). We obtained approval from the Institutional Review Board (COMIRB #13-1607) for our human studies prior to written informed consent from everyone. A total of 20 healthy volunteers were enrolled (11 female and 6 male, age range between 21-44 yrs.).

Human plasma melatonin, HIF1A and triglyceride levels

Melatonin levels were measured using the MT Elisa Kit for humans (My BioSource, San Diego, CA). HIF1A levels from human plasma samples were measured using the human HIF1A ELISA Kit from Invitrogen (Carlsbad, CA). Triglycerides were determined using a human Triglyceride Quantification Assay kit (Abcam, Cambridge, MA).

Targeted metabolomics - mass spectrometry

Targeted metabolomics of human plasma following light exposure was performed as previously reported (A three-minute method for high-throughput quantitative metabolomics and quantitative tracing experiments of central carbon and nitrogen pathways [75]. In brief, plasma samples were diluted at 1:25 in ice cold extraction solution (methanol, acetonitrile,

water at a ratio of 5:3:2) and vortexed for 30 minutes at 4° C followed by removal of insoluble proteins and lipids by centrifugation at 10,000 RCF for 10 minutes at 4° C. The supernatants were collected and stored at -80° C until analysis. Analyses were performed using a Vanquish UHPLC system coupled to a Q Exactive mass spectrometer (Thermo Fisher Scientific, San Jose, CA, USA). Samples were resolved by a Kinetex C18 column (2.1 × 150 mm, 1.7 μm particle size; Phenomenex, Torrance, CA, USA) with a guard column at 25°C with an isocratic condition of 5% acetonitrile, 95% water, and 0.1% formic acid with a flow rate of 250 μL/min. The mass spectrometer was operated independently in positive or negative ion mode, scanning in Full MS mode from 60 to 900 m/z at 70,000 resolutions, with 4 kV spray voltage, 15 sheath gas, 5 auxiliary gas. Calibration was performed prior to analysis. Acquired data was converted from. raw to. mzXML file format using Mass Matrix (Cleveland, OH, USA). Metabolite assignments, isotopologue distributions, and correction for expected natural abundances of deuterium, 13C, and 15N isotopes were performed using MAVEN (Princeton, NJ, USA). Metabolite assignments were referenced to experimental retention times for over 400 analytical standards (MSMLS, IROATech, Bolton, MA, USA) and were determined over a 3-minute isocratic method with 20 μL of standards and samples injected for UHPLC/MS analysis.

Data analysis

For comparison of two groups the unpaired student t-test was performed. For multiple group comparisons a one-way analysis of variance with a Tukey's post hoc test was performed. Values are expressed as mean±SD. $P<0.05$ was considered statistically significant. For all statistical analysis, GraphPad Prism 5.0 software was used. The authors had full access to and take full responsibility for the integrity of the data. All authors have read and agree to the manuscript as written.

Acknowledgement

The authors wish to acknowledge Melissa Card, the University of Colorado Molecular and Cellular Analytical Core of the Colorado Nutrition and Obesity Research Center for use of the Seahorse Bioanalyzer, and the University of Colorado School of Medicine Biological Mass Spectrometry Core Facility for technical assistance.

Funding:

The present research work is supported by National Heart, Lung, and Blood Institute Grant (NIH-NHLBI) 5R01HL122472 to T.E., Colorado Clinical and Translational Sciences Institute (CCTSI) TL1 TR001081 and American Heart Association (AHA) Predoctoral Fellowship 16PRE30510006 Grant to C.M.B and AHA Postdoctoral Fellowship 19POST34380105 Grant to O.Y.

Competing interests: The authors declare there are no conflicts of interest.

REFERENCES

1. Zerkle AL, Poulton SW, Newton RJ, Mettam C, Claire MW, Bekker A, et al. Onset of the aerobic nitrogen cycle during the Great Oxidation Event. Nature. 2017;542(7642):465-7. doi: 10.1038/nature20826. PubMed PMID: 28166535.

2. Hogenesch JB, Gu YZ, Jain S, Bradfield CA. The basic-helix-loop-helix-PAS orphan MOP3 forms transcriptionally active complexes with circadian and hypoxia factors. Proc Natl Acad Sci U S A. 1998;95(10):5474-9. Epub 1998/05/20. PubMed PMID: 9576906; PubMed Central PMCID: PMCPMC20401.

3. Gu YZ, Hogenesch JB, Bradfield CA. The PAS superfamily: sensors of environmental and developmental signals. Annu Rev Pharmacol Toxicol. 2000;40:519-61. Epub 2000/06/03. doi: 10.1146/annurev.pharmtox.40.1.519. PubMed PMID: 10836146.
4. McIntosh BE, Hogenesch JB, Bradfield CA. Mammalian Per-Arnt-Sim proteins in environmental adaptation. Annu Rev Physiol. 2010;72:625-45. Epub 2010/02/13. doi: 10.1146/annurev-physiol-021909-135922. PubMed PMID: 20148691.
5. Semenza GL. Hypoxia. Cross talk between oxygen sensing and the cell cycle machinery. Am J Physiol Cell Physiol. 2011;301(3):C550-2. doi: 10.1152/ajpcell.00176.2011. PubMed PMID: 21677261; PubMed Central PMCID: PMC3174572.
6. Liu W, Shen SM, Zhao XY, Chen GQ. Targeted genes and interacting proteins of hypoxia inducible factor-1. Int J Biochem Mol Biol. 2012;3(2):165-78. Epub 2012/07/10. PubMed PMID: 22773957; PubMed Central PMCID: PMCPMC3388736.
7. Taylor BL, Zhulin IB. PAS domains: internal sensors of oxygen, redox potential, and light. Microbiol Mol Biol Rev. 1999;63(2):479-506. PubMed PMID: 10357859; PubMed Central PMCID: PMC98974.
8. Eckle T, Hartmann K, Bonney S, Reithel S, Mittelbronn M, Walker LA, et al. Adora2b-elicited Per2 stabilization promotes a HIF-dependent metabolic switch crucial for myocardial adaptation to ischemia. Nat Med. 2012;18(5):774-82. doi: 10.1038/nm.2728. PubMed PMID: 22504483; PubMed Central PMCID: PMC3378044.
9. Adamovich Y, Ladeuix B, Golik M, Koeners MP, Asher G. Rhythmic Oxygen Levels Reset Circadian Clocks through HIF1alpha. Cell metabolism. 2017;25(1):93-101. doi: 10.1016/j.cmet.2016.09.014. PubMed PMID: 27773695.
10. Bonney S, Hughes K, Harter PN, Mittelbronn M, Walker L, Eckle T. Cardiac period 2 in myocardial ischemia: clinical implications of a light dependent protein. Int J Biochem Cell Biol. 2013;45(3):667-71. doi: 10.1016/j.biocel.2012.12.022. PubMed PMID: 23291353; PubMed Central PMCID: PMC3761885.
11. Schroeder AM, Truong D, Loh DH, Jordan MC, Roos KP, Colwell CS. Voluntary scheduled exercise alters diurnal rhythms of behaviour, physiology and gene expression in wild-type and vasoactive intestinal peptide-deficient mice. J Physiol. 2012;590(23):6213-26. Epub 2012/09/19. doi: 10.1113/jphysiol.2012.233676. PubMed PMID: 22988135; PubMed Central PMCID: PMCPMC3530127.
12. Hallows WC, Ptacek LJ, Fu YH. Solving the mystery of human sleep schedules one mutation at a time. Crit Rev Biochem Mol Biol. 2013;48(5):465-75. doi: 10.3109/10409238.2013.831395. PubMed PMID: 24001255; PubMed Central PMCID: PMC4089902.
13. Aragones J, Fraisl P, Baes M, Carmeliet P. Oxygen Sensors at the Crossroad of Metabolism. Cell metabolism. 2009;9(1):11-22. Epub 2009/01/02. doi: S1550-4131(08)00318-5 [pii]
10.1016/j.cmet.2008.10.001. PubMed PMID: 19117543.
14. Krishnan J, Suter M, Windak R, Krebs T, Felley A, Montessuit C, et al. Activation of a HIF1alpha-PPARgamma axis underlies the integration of glycolytic and lipid anabolic pathways in pathologic cardiac hypertrophy. Cell metabolism. 2009;9(6):512-24. Epub 2009/06/06. doi: 10.1016/j.cmet.2009.05.005. PubMed PMID: 19490906.
15. Safran M, Kim WY, O'Connell F, Flippin L, Gunzler V, Horner JW, et al. Mouse model for noninvasive imaging of HIF prolyl hydroxylase activity: assessment of an oral agent that stimulates erythropoietin production. Proc Natl Acad Sci U S A. 2006;103(1):105-10. Epub 2005/12/24. doi: 10.1073/pnas.0509459103. PubMed PMID: 16373502; PubMed Central PMCID: PMCPMC1324998.
16. O'Neill JS, Maywood ES, Chesham JE, Takahashi JS, Hastings MH. cAMP-dependent signaling as a core component of the mammalian circadian pacemaker. Science.

2008;320(5878):949-53. Epub 2008/05/20. doi: 10.1126/science.1152506. PubMed PMID: 18487196; PubMed Central PMCID: PMCPMC2735813.
17. Bartman CM, Oyama Y, Brodsky K, Khailova L, Walker L, Koeppen M, et al. Intense light-elicited upregulation of miR-21 facilitates glycolysis and cardioprotection through Per2-dependent mechanisms. PLoS One. 2017;12(4):e0176243. Epub 2017/04/28. doi: 10.1371/journal.pone.0176243. PubMed PMID: 28448534.
18. Zhang J, Kaasik K, Blackburn MR, Lee CC. Constant darkness is a circadian metabolic signal in mammals. Nature. 2006;439(7074):340-3. Epub 2006/01/20. doi: 10.1038/nature04368. PubMed PMID: 16421573.
19. Galaup A, Gomez E, Souktani R, Durand M, Cazes A, Monnot C, et al. Protection against myocardial infarction and no-reflow through preservation of vascular integrity by angiopoietin-like 4. Circulation. 2012;125(1):140-9. Epub 2011/11/17. doi: 10.1161/circulationaha.111.049072. PubMed PMID: 22086875.
20. Faou P, Hoogenraad NJ. Tom34: a cytosolic cochaperone of the Hsp90/Hsp70 protein complex involved in mitochondrial protein import. Biochim Biophys Acta. 2012;1823(2):348-57. Epub 2011/12/20. doi: 10.1016/j.bbamcr.2011.12.001. PubMed PMID: 22178133.
21. Boengler K, Heusch G, Schulz R. Nuclear-encoded mitochondrial proteins and their role in cardioprotection. Biochim Biophys Acta. 2011;1813(7):1286-94. Epub 2011/01/25. doi: 10.1016/j.bbamcr.2011.01.009. PubMed PMID: 21255616.
22. Yu W, Dittenhafer-Reed KE, Denu JM. SIRT3 protein deacetylates isocitrate dehydrogenase 2 (IDH2) and regulates mitochondrial redox status. J Biol Chem. 2012;287(17):14078-86. Epub 2012/03/15. doi: 10.1074/jbc.M112.355206. PubMed PMID: 22416140; PubMed Central PMCID: PMCPMC3340192.
23. Peek CB, Affinati AH, Ramsey KM, Kuo HY, Yu W, Sena LA, et al. Circadian clock NAD+ cycle drives mitochondrial oxidative metabolism in mice. Science. 2013;342(6158):1243417. Epub 2013/09/21. doi: 10.1126/science.1243417. PubMed PMID: 24051248; PubMed Central PMCID: PMCPMC3963134.
24. Fukuda R, Zhang H, Kim JW, Shimoda L, Dang CV, Semenza GL. HIF-1 regulates cytochrome oxidase subunits to optimize efficiency of respiration in hypoxic cells. Cell. 2007;129(1):111-22. Epub 2007/04/10. doi: 10.1016/j.cell.2007.01.047. PubMed PMID: 17418790.
25. Solaini G, Baracca A, Lenaz G, Sgarbi G. Hypoxia and mitochondrial oxidative metabolism. Biochim Biophys Acta. 2010;1797(6-7):1171-7. Epub 2010/02/16. doi: 10.1016/j.bbabio.2010.02.011. PubMed PMID: 20153717.
26. Zhou R, Yazdi AS, Menu P, Tschopp J. A role for mitochondria in NLRP3 inflammasome activation. Nature. 2011;469(7329):221-5. Epub 2010/12/03. doi: 10.1038/nature09663. PubMed PMID: 21124315.
27. Rey G, Valekunja UK, Feeney KA, Wulund L, Milev NB, Stangherlin A, et al. The Pentose Phosphate Pathway Regulates the Circadian Clock. Cell metabolism. 2016;24(3):462-73. Epub 2016/08/23. doi: 10.1016/j.cmet.2016.07.024. PubMed PMID: 27546460; PubMed Central PMCID: PMCPMC5031559.
28. Grimaldi B, Bellet MM, Katada S, Astarita G, Hirayama J, Amin RH, et al. PER2 controls lipid metabolism by direct regulation of PPARgamma. Cell metabolism. 2010;12(5):509-20. Epub 2010/11/03. doi: 10.1016/j.cmet.2010.10.005. PubMed PMID: 21035761; PubMed Central PMCID: PMCPMC4103168.
29. Yorguner Kupeli N, Bulut NS, Carkaxhiu Bulut G, Kurt E, Kora K. Efficacy of bright light therapy in bipolar depression. Psychiatry Res. 2017;260:432-8. Epub 2017/12/22. doi: 10.1016/j.psychres.2017.12.020. PubMed PMID: 29268206.

30. Lewy AJ, Wehr TA, Goodwin FK, Newsome DA, Markey SP. Light suppresses melatonin secretion in humans. Science. 1980;210(4475):1267-9. Epub 1980/12/12. PubMed PMID: 7434030.
31. Ginsberg HN, Zhang YL, Hernandez-Ono A. Regulation of plasma triglycerides in insulin resistance and diabetes. Arch Med Res. 2005;36(3):232-40. Epub 2005/06/01. doi: 10.1016/j.arcmed.2005.01.005. PubMed PMID: 15925013.
32. Depner CM, Stothard ER, Wright KP, Jr. Metabolic consequences of sleep and circadian disorders. Curr Diab Rep. 2014;14(7):507. doi: 10.1007/s11892-014-0507-z. PubMed PMID: 24816752.
33. Lee PH, Suen LK. The convergent validity of Actiwatch 2 and ActiGraph Link accelerometers in measuring total sleeping period, wake after sleep onset, and sleep efficiency in free-living condition. Sleep & breathing = Schlaf & Atmung. 2017;21(1):209-15. Epub 2016/09/12. doi: 10.1007/s11325-016-1406-0. PubMed PMID: 27614441.
34. Zadeh RS, Shepley MM, Williams G, Chung SS. The impact of windows and daylight on acute-care nurses' physiological, psychological, and behavioral health. Herd. 2014;7(4):35-61. Epub 2014/10/11. PubMed PMID: 25303426.
35. Spencer FA, Goldberg RJ, Becker RC, Gore JM. Seasonal distribution of acute myocardial infarction in the second National Registry of Myocardial Infarction. J Am Coll Cardiol. 1998;31(6):1226-33. PubMed PMID: 9581712.
36. Takahashi JS. Transcriptional architecture of the mammalian circadian clock. Nat Rev Genet. 2017;18(3):164-79. doi: 10.1038/nrg.2016.150. PubMed PMID: 27990019.
37. Brutsaert DL. Cardiac endothelial-myocardial signaling: its role in cardiac growth, contractile performance, and rhythmicity. Physiol Rev. 2003;83(1):59-115. Epub 2002/12/31. doi: 10.1152/physrev.00017.2002. PubMed PMID: 12506127.
38. Schmiedl A, Richter J, Schnabel PA. Different preservation of myocardial capillary endothelial cells and cardiomyocytes during and after cardioplegic ischemia (25 degrees C) of canine hearts. Pathol Res Pract. 2002;198(4):281-90. Epub 2002/06/07. PubMed PMID: 12049337.
39. Davidson SM, Duchen MR. Endothelial mitochondria: contributing to vascular function and disease. Circ Res. 2007;100(8):1128-41. Epub 2007/04/28. doi: 10.1161/01.RES.0000261970.18328.1d. PubMed PMID: 17463328.
40. Reffelmann T, Kloner RA. The no-reflow phenomenon: A basic mechanism of myocardial ischemia and reperfusion. Basic Res Cardiol. 2006;101(5):359-72. Epub 2006/08/18. doi: 10.1007/s00395-006-0615-2. PubMed PMID: 16915531.
41. Yang Q, He GW, Underwood MJ, Yu CM. Cellular and molecular mechanisms of endothelial ischemia/reperfusion injury: perspectives and implications for postischemic myocardial protection. Am J Transl Res. 2016;8(2):765-77. Epub 2016/05/10. PubMed PMID: 27158368; PubMed Central PMCID: PMCPMC4846925.
42. Viswambharan H, Carvas JM, Antic V, Marecic A, Jud C, Zaugg CE, et al. Mutation of the circadian clock gene Per2 alters vascular endothelial function. Circulation. 2007;115(16):2188-95. Epub 2007/04/04. doi: 10.1161/circulationaha.106.653303. PubMed PMID: 17404161.
43. Wang CY, Wen MS, Wang HW, Hsieh IC, Li Y, Liu PY, et al. Increased vascular senescence and impaired endothelial progenitor cell function mediated by mutation of circadian gene Per2. Circulation. 2008;118(21):2166-73. Epub 2008/11/05. doi: 10.1161/circulationaha.108.790469. PubMed PMID: 18981300; PubMed Central PMCID: PMCPMC2656770.
44. Gile J, Scott B, Eckle T. The Period 2 Enhancer Nobiletin as Novel Therapy in Murine Models of Circadian Disruption Resembling Delirium. Crit Care Med. 2018. Epub 2018/03/01. doi: 10.1097/CCM.0000000000003077. PubMed PMID: 29489460.

45. Oyama Y, Bartman CM, Gile J, Sehrt D, Eckle T. The circadian PER2 enhancer Nobiletin reverses the deleterious effects of midazolam in myocardial ischemia and reperfusion injury. Curr Pharm Des. 2018. Epub 2018/09/25. doi: 10.2174/1381612824666180924102530. PubMed PMID: 30246635.
46. Semenza GL. Hypoxia-inducible factor 1 and cardiovascular disease. Annu Rev Physiol. 2014;76:39-56. Epub 2013/08/31. doi: 10.1146/annurev-physiol-021113-170322. PubMed PMID: 23988176; PubMed Central PMCID: PMCPMC4696033.
47. Kobayashi M, Morinibu A, Koyasu S, Goto Y, Hiraoka M, Harada H. A circadian clock gene, PER2, activates HIF-1 as an effector molecule for recruitment of HIF-1alpha to promoter regions of its downstream genes. The FEBS journal. 2017;284(22):3804-16. Epub 2017/10/01. doi: 10.1111/febs.14280. PubMed PMID: 28963769.
48. Wu Y, Tang D, Liu N, Xiong W, Huang H, Li Y, et al. Reciprocal Regulation between the Circadian Clock and Hypoxia Signaling at the Genome Level in Mammals. Cell metabolism. 2017;25(1):73-85. doi: 10.1016/j.cmet.2016.09.009. PubMed PMID: 27773697.
49. Gloston GF, Yoo SH, Chen ZJ. Clock-Enhancing Small Molecules and Potential Applications in Chronic Diseases and Aging. Front Neurol. 2017;8:100. Epub 2017/04/01. doi: 10.3389/fneur.2017.00100. PubMed PMID: 28360884; PubMed Central PMCID: PMCPMC5350099.
50. Czeisler CA, Johnson MP, Duffy JF, Brown EN, Ronda JM, Kronauer RE. Exposure to bright light and darkness to treat physiologic maladaptation to night work. N Engl J Med. 1990;322(18):1253-9. Epub 1990/05/03. doi: 10.1056/nejm199005033221801. PubMed PMID: 2325721.
51. Martino TA, Tata N, Belsham DD, Chalmers J, Straume M, Lee P, et al. Disturbed diurnal rhythm alters gene expression and exacerbates cardiovascular disease with rescue by resynchronization. Hypertension. 2007;49(5):1104-13. Epub 2007/03/07. doi: 10.1161/hypertensionaha.106.083568. PubMed PMID: 17339537.
52. Kronfeld-Schor N, Bloch G, Schwartz WJ. Animal clocks: when science meets nature. Proc Biol Sci. 2013;280(1765):20131354. Epub 2013/07/05. doi: 10.1098/rspb.2013.1354. PubMed PMID: 23825215; PubMed Central PMCID: PMCPMC3712458.
53. Montaigne D, Marechal X, Modine T, Coisne A, Mouton S, Fayad G, et al. Daytime variation of perioperative myocardial injury in cardiac surgery and its prevention by Rev-Erbalpha antagonism: a single-centre propensity-matched cohort study and a randomised study. Lancet. 2018;391(10115):59-69. Epub 2017/11/07. doi: 10.1016/s0140-6736(17)32132-3. PubMed PMID: 29107324.
54. Zheng B, Larkin DW, Albrecht U, Sun ZS, Sage M, Eichele G, et al. The mPer2 gene encodes a functional component of the mammalian circadian clock. Nature. 1999;400(6740):169-73. Epub 1999/07/17. doi: 10.1038/22118. PubMed PMID: 10408444.
55. Yoo SH, Yamazaki S, Lowrey PL, Shimomura K, Ko CH, Buhr ED, et al. PERIOD2::LUCIFERASE real-time reporting of circadian dynamics reveals persistent circadian oscillations in mouse peripheral tissues. Proc Natl Acad Sci U S A. 2004;101(15):5339-46. Epub 2004/02/14. doi: 10.1073/pnas.0308709101 0308709101 [pii]. PubMed PMID: 14963227; PubMed Central PMCID: PMC397382.
56. Alva JA, Zovein AC, Monvoisin A, Murphy T, Salazar A, Harvey NL, et al. VE-Cadherin-Cre-recombinase transgenic mouse: a tool for lineage analysis and gene deletion in endothelial cells. Dev Dyn. 2006;235(3):759-67. Epub 2006/02/02. doi: 10.1002/dvdy.20643. PubMed PMID: 16450386.
57. Eckle T, Grenz A, Kohler D, Redel A, Falk M, Rolauffs B, et al. Systematic evaluation of a novel model for cardiac ischemic preconditioning in mice. Am J Physiol Heart Circ Physiol. 2006;291(5):H2533-40. doi: 10.1152/ajpheart.00472.2006. PubMed PMID: 16766632.

58. Eckle T, Koeppen M, Eltzschig H. Use of a hanging weight system for coronary artery occlusion in mice. J Vis Exp. 2011;(50). doi: 10.3791/2526. PubMed PMID: 21540816; PubMed Central PMCID: PMC3169250.
59. Eckle T, Krahn T, Grenz A, Kohler D, Mittelbronn M, Ledent C, et al. Cardioprotection by ecto-5'-nucleotidase (CD73) and A2B adenosine receptors. Circulation. 2007;115(12):1581-90. doi: 10.1161/CIRCULATIONAHA.106.669697. PubMed PMID: 17353435.
60. Eckle T, Kohler D, Lehmann R, El Kasmi K, Eltzschig HK. Hypoxia-inducible factor-1 is central to cardioprotection: a new paradigm for ischemic preconditioning. Circulation. 2008;118(2):166-75. doi: 10.1161/CIRCULATIONAHA.107.758516. PubMed PMID: 18591435.
61. Kohler D, Eckle T, Faigle M, Grenz A, Mittelbronn M, Laucher S, et al. CD39/ectonucleoside triphosphate diphosphohydrolase 1 provides myocardial protection during cardiac ischemia/reperfusion injury. Circulation. 2007;116(16):1784-94. doi: 10.1161/CIRCULATIONAHA.107.690180. PubMed PMID: 17909107.
62. Vasile VC, Babuin L, Giannitsis E, Katus HA, Jaffe AS. Relationship of MRI-determined infarct size and cTnI measurements in patients with ST-elevation myocardial infarction. Clin Chem. 2008;54(3):617-9. Epub 2008/03/04. doi: 54/3/617 [pii] 10.1373/clinchem.2007.095604. PubMed PMID: 18310155.
63. Moore A, Zielinski T, Millar AJ. Online period estimation and determination of rhythmicity in circadian data, using the BioDare data infrastructure. Methods Mol Biol. 2014;1158:13-44. Epub 2014/05/06. doi: 10.1007/978-1-4939-0700-7_2. PubMed PMID: 24792042.
64. Eckle T, Brodsky K, Bonney M, Packard T, Han J, Borchers CH, et al. HIF1A reduces acute lung injury by optimizing carbohydrate metabolism in the alveolar epithelium. PLoS Biol. 2013;11(9):e1001665. doi: 10.1371/journal.pbio.1001665. PubMed PMID: 24086109; PubMed Central PMCID: PMC3782424.
65. Han J, Gagnon S, Eckle T, Borchers CH. Metabolomic analysis of key central carbon metabolism carboxylic acids as their 3-nitrophenylhydrazones by UPLC/ESI-MS. Electrophoresis. 2013;34(19):2891-900. doi: 10.1002/elps.201200601. PubMed PMID: 23580203; PubMed Central PMCID: PMC4033578.
66. Han J, Tschernutter V, Yang J, Eckle T, Borchers CH. Analysis of selected sugars and sugar phosphates in mouse heart tissue by reductive amination and liquid chromatography-electrospray ionization mass spectrometry. Anal Chem. 2013;85(12):5965-73. doi: 10.1021/ac400769g. PubMed PMID: 23682691; PubMed Central PMCID: PMC3989532.
67. Lee JS, Wang RX, Alexeev EE, Lanis JM, Battista KD, Glover LE, et al. Hypoxanthine is a checkpoint stress metabolite in colonic epithelial energy modulation and barrier function. J Biol Chem. 2018;293(16):6039-51. Epub 2018/03/01. doi: 10.1074/jbc.RA117.000269. PubMed PMID: 29487135; PubMed Central PMCID: PMCPMC5912467.
68. Eltzschig HK, Abdulla P, Hoffman E, Hamilton KE, Daniels D, Schonfeld C, et al. HIF-1-dependent repression of equilibrative nucleoside transporter (ENT) in hypoxia. J Exp Med. 2005;202(11):1493-505.
69. Eltzschig HK, Ibla JC, Furuta GT, Leonard MO, Jacobson KA, Enjyoji K, et al. Coordinated adenine nucleotide phosphohydrolysis and nucleoside signaling in posthypoxic endothelium: role of ectonucleotidases and adenosine A2B receptors. J Exp Med. 2003;198(5):783-96. Epub 2003/08/27. doi: 10.1084/jem.20030891 jem.20030891 [pii]. PubMed PMID: 12939345; PubMed Central PMCID: PMC2194189.
70. Silliman CC, Dzieciatkowska M, Moore EE, Kelher MR, Banerjee A, Liang X, et al. Proteomic analyses of human plasma: Venus versus Mars. Transfusion. 2012;52(2):417-24.

Epub 2011/09/02. doi: 10.1111/j.1537-2995.2011.03316.x. PubMed PMID: 21880043; PubMed Central PMCID: PMCPMC3235251.
71. Barrett AS, Wither MJ, Hill RC, Dzieciatkowska M, D'Alessandro A, Reisz JA, et al. Hydroxylamine Chemical Digestion for Insoluble Extracellular Matrix Characterization. J Proteome Res. 2017;16(11):4177-84. Epub 2017/10/04. doi: 10.1021/acs.jproteome.7b00527. PubMed PMID: 28971683; PubMed Central PMCID: PMCPMC5802359.
72. Sun L, Zhu G, Dovichi NJ. Comparison of the LTQ-Orbitrap Velos and the Q-Exactive for proteomic analysis of 1-1000 ng RAW 264.7 cell lysate digests. Rapid Commun Mass Spectrom. 2013;27(1):157-62. Epub 2012/12/15. doi: 10.1002/rcm.6437. PubMed PMID: 23239329; PubMed Central PMCID: PMCPMC3673017.
73. Thwe PM, Pelgrom L, Cooper R, Beauchamp S, Reisz JA, D'Alessandro A, et al. Cell-Intrinsic Glycogen Metabolism Supports Early Glycolytic Reprogramming Required for Dendritic Cell Immune Responses. Cell metabolism. 2017;26(3):558-67.e5. Epub 2017/09/07. doi: 10.1016/j.cmet.2017.08.012. PubMed PMID: 28877459; PubMed Central PMCID: PMCPMC5657596.
74. Nemkov T, D'Alessandro A, Hansen KC. Three-minute method for amino acid analysis by UHPLC and high-resolution quadrupole orbitrap mass spectrometry. Amino Acids. 2015;47(11):2345-57. Epub 2015/06/11. doi: 10.1007/s00726-015-2019-9. PubMed PMID: 26058356; PubMed Central PMCID: PMCPMC4624008.
75. Nemkov T, Hansen KC, D'Alessandro A. A three-minute method for high-throughput quantitative metabolomics and quantitative tracing experiments of central carbon and nitrogen pathways. Rapid Commun Mass Spectrom. 2017;31(8):663-73. Epub 2017/02/15. doi: 10.1002/rcm.7834. PubMed PMID: 28195377; PubMed Central PMCID: PMCPMC5364945.
76. McCurdy CE, Schenk S, Hetrick B, Houck J, Drew BG, Kaye S, et al. Maternal obesity reduces oxidative capacity in fetal skeletal muscle of Japanese macaques. JCI insight. 2016;1(16):e86612. Epub 2016/10/14. doi: 10.1172/jci.insight.86612. PubMed PMID: 27734025; PubMed Central PMCID: PMCPMC5053156.

Figure Legends

Figure 1. Daylight elicited circadian PER2 amplitude enhancement is cardioprotective. **(A-C)** C57BL/6 mice housed under daylight conditions (10,000 LUX, L:D 14:10 h) for 3, 5, or 7 days were subjected to 60 min of *in situ* myocardial ischemia followed by 2h reperfusion at 9AM and compared to mice housed under standard room light (200 LUX, L:D 14:10 h, 7 days). Infarct sizes are expressed as the percent of the area at risk that was exposed to myocardial ischemia (double staining with Evan's blue and triphenyltetrazolium chloride; mean±SD; n=6). **(B)** Parallel measurements of serum troponin-I by ELISA (mean±SD; n=6). **(c)** Representative images of infarcts. **(D-F)** Wheel running measurements during 7 days of room light or daylight housing conditions in C57BL/6 mice (n=6, see also **Supplementary Fig. 1** for individual recordings). **(G)** Cardiac PER2 luciferase activity in mice after daylight or standard room light for 7 days (mean±SD; n=4). **(H-J)** Wheel running during 7 days of room light or daylight housing in C57BL/6 and *Per2*$^{-/-}$ mice (n=5-6, see also **Supplementary Fig. 2** for individual recordings). (**K, L**) Immunoblot and quantification for PER2 protein in seeing or enucleated (blind) C57BL/6 mice after 7 days of room light or daylight at 9AM (mean±SD; n=5). **(M**) Troponin-I serum levels in seeing or blind C57BL/6 mice housed under roomlight conditions followed by 60 min ischemia and 2 h reperfusion at 9AM or 9PM (mean±SD; n=4, see also **Supplementary Fig. 2**). **(N)** Representative infarct staining from blind and seeing C57BL/6 mice at 9PM.

Figure 2. Daylight increases cardiac adenosine-cAMP and glycolytic flux via PER2. **(A)** Infarct sizes in C57BL/6 mice that were housed under daylight (10,000 LUX, L:D 14:10 h) for 7 days and subjected to 60 min of *in situ* myocardial ischemia followed by 2h reperfusion at 9AM or 9PM (mean±SD; n=6). **(B-D)** C57BL/6 mice exposed to voluntary wheel running for 1 versus 2 weeks. Shown are infarct sizes after 60 min of myocardial ischemia and 2h reperfusion at 9AM or circadian amplitude and distance walked measurements (mean±SD; n=6). (**E-H**) Wheel running measurements during or infarct size studies after 2 weeks of

wheel running at 9AM in C57BL/6 or *Per2*$^{-/-}$ mice (mean±SD; n=5). One representative infarct size staining and one wheel running activity recording is shown. **(I)** C57BL/6 mice were housed under daylight or standard room light (200 LUX, L:D 14:10 h) for 7 days followed by the infusion of 10 mg/kg/min U-^{13}C-glucose via an intra-arterial catheter over 90 minutes. Hearts were flushed with ice cold KCl and the left ventricle was shock frozen at 9 AM and analyzed by liquid chromatography–tandem mass spectrometry (mean±SD; n=4). **(J, K)** Phosphofructokinase (PFK) activity in both heart tissue and plasma samples from C57BL/6 or *Per2*$^{-/-}$ mice at 9AM after 7d of room- or daylight housing (mean±SD; n=4-5). (**L**) Cardiac HIF1A protein levels were determined at 9AM after 7d of room- or daylight housing using HIF1A luciferase mice (mean±SD; n=4). **(M, N)** Adenosine measured by HPLC or cAMP determined by ELISA in heart tissue from C57BL/6 or *Per2*$^{-/-}$ mice at 9AM after 7d of room- or daylight housing (mean±SD; n=5). **(O)** C57BL/6 or *Per2*$^{-/-}$ mice housed under room- or daylight for 7 d prior to 60 min myocardial ischemia and 2 h reperfusion at 9 AM. Infarct sizes are expressed as the percent of the area at risk that was exposed to myocardial ischemia (mean±SD; n=5). (**P**) Representative infarct staining.

Figure 3. Daylight elicited cardioprotection is endothelial PER2 specific. (A) Whole genome array from C57BL/6 or *Per2*$^{-/-}$ heart tissue after 7d of daylight (10,000 LUX, L:D 14:10 h) or standard room light (200 LUX, L:D 14:10 h) housing at 9AM (n=3 per group, total of 12 arrays). (**B**) Validation of transcript levels of the top light and PER2 dependent gene (ANGPTL-4) identified by whole genome array (mean±SD; n=4-5). (**C**) RT-PCR data showing *Per2* mRNA transcript levels from endothelial cells isolated from endothelial specific PER2 deficient (*Per2*$^{loxP/loxP}$-VE-Cadherin-Cre) or control (VE-Cadherin-Cre) hearts (mean±SD; n=3). (**D, E**) Infarct sizes or serum troponin-I in *Per2*$^{loxP/loxP}$-VE-Cadherin-Cre or VE-Cadherin-Cre mice housed under room- or daylight conditions for 7d followed by 60 min of *in situ* myocardial ischemia and 2h reperfusion at 9AM (mean±SD; n=5). (**F, G**)

Representative infarct staining. (**H, I**) Vascular leakage of Evans blue dye in C57BL/6 after 60 min of *in situ* myocardial ischemia and 2h reperfusion at 9AM following 7 days of room- or daylight housing (mean±SD; n=5).

Figure 4. Endothelial PER2 is critical for the transcriptional control of HIF1A dependent glycolysis. HMEC-1 controls (Scr; treated with lentiviral scrambled shRNA) or HMEC-1 PER2 knockdown (KD; treated with lentiviral PER2 shRNA) were synchronized via serum starvation and exposed to 24 h of normoxia (Nx) or 1% hypoxia (Hx). **(A, B)** PER2 transcript or protein levels from stable lentiviral mediated PER2KD or Scr control HMEC-1 were determined by real-time RT-PCR relative to housekeeping gene beta-actin or immunoblot analysis of PER2 protein, respectively (mean±SD, n = 3). **(C, D)** Transcript expression of pyruvate kinase (PKM) or lactate dehydrogenase (LDHa) in stable lentiviral mediated PER2KD HMEC-1 or controls (Scr, mean±SD, n=3). **(E)** Lactate levels in supernatants obtained from HMEC-1 with a lentiviral-mediated PER2KD HMEC-1 or controls (Scr; mean±SD, n=3). **(F, G)** Glucose metabolism from stable lentiviral mediated PER2KD or Scr control HMEC-1 after 24h at 1% hypoxia. Glycolysis assay was performed using a glycolytic stress test kit on a Seahorse Biosciences XF24 analyzer. The extracellular acidification rate (ECAR) in response to glucose, oligomycin or 2-deoxy-D-glucose (2-DG) was measured (mean±SD, n=3). **(H)** LDH-Cytotoxicity assay from HMEC-1 with a lentiviral-mediated PER2KD or controls (Scr, mean±SD, n=10). (**I, J**) Glycolytic stress tests using a Seahorse Bioanalyzer at Zeitgeber (ZT) 0 or ZT12 (mean±SD, n=10) under normoxic conditions. **(K)** Chromatin immunoprecipitation analysis to detect HIF1A protein binding to the human LDHa promoter using lentiviral-mediated PER2KD HMEC-1 or controls (Scr). qRT-PCR for the human LDHa promoter was performed for quantification. PCR end-products (after 35 cycles) analyzed on a 2% agarose gel (top) or CT values form the qRT-PCR are shown (bottom, n=3).

Figure 5. Identification of endothelial PER2 as a regulator of TCA cycle activity. HMEC-1 or stable lentiviral mediated PER2KD and Scr control HMEC-1 were synchronized and exposed to 24h of normoxia (Nx) or 1% hypoxia (Hx). In a subset of experiments synchronized stable lentiviral mediated HIF1AKD and Scr HMEC-1 were exposed to Nx or Hx. **(A-B)** Affinity purification-mass spectrometry-based proteomics screen for PER2 protein interactions in normoxic and hypoxic HMEC-1 (see also **Supplementary Fig. 3**). (**C, D**) Co-immunoprecipitation for PER2 in hypoxic or normoxic HMEC-1 against isocitrate dehydrogenase 2 (IDH2), succinyl Co-A ligase (SUCLG1) and aconitase (ACO2) and vice versa. One representative blot of three is displayed. (**E**) Subcellular compartment analysis of PER2 during normoxia or hypoxia (C= cytoplasm, N=nucleus, M=mitochondria; compartment specific loading controls: Tubulin Alpha 1a (TUBA1A) for cytoplasm, TATA-Box Binding Protein (TBP) for nucleus and Voltage Dependent Anion Channel 1 (VDAC1) for mitochondria). **(F-H)** TCA cycle enzyme activities of IDH, SUCLG and ACO from stable lentiviral mediated PER2KD and Scr control HMEC-1 during hypoxia (mean±SD, n=3). **(I)** Carbon dioxide evolution rates (CDER), as a surrogate for TCA cycle function, in PER2 KD or Scr HMEC-1 measured by a mitochondrial stress test using a Seahorse XF24 FluxPak assay (mean±SD, n=5). (**J-L**) SIRT3 transcript or protein levels from stable lentiviral mediated PER2KD and Scr or stable lentiviral mediated HIF1AKD and Scr control HMEC-1 (mean±SD, n = 3, see also **Supplementary Fig. 4**).

Figure 6. Endothelial PER2 regulates mitochondrial function via HIF1A-COX4.2. (A-D) Oxygen consumption rates (OCR) measured by a mitochondrial stress test kit on a Seahorse Biosciences XF24 analyzer in PER2KD or Scr HMEC-1 with or without the irreversible carnitine palmitoyltransferase-1 inhibitor etomoxir (Eto). Quantification of basal respiration, maximum achievable respiration, and maximal respiration due to endogenous fatty acid are

shown (mean±SD, n=5, see also **Supplementary Fig. 5**). **(E**) Cox4.2 transcript levels in PER2 KD or Scr HMEC-1 after 24h of Nx or 1% Hx treatment (mean±SD, n=6). **(F)** Complex IV enzyme activity in *Per2*$^{-/-}$ or C57BL/6 mouse hearts subjected to 45 min of ischemia (mean±SD, n=4). **(G)** MitoTracker Red CMXRos staining of PER2 KD or Scr HMEC-1 at baseline. One representative image of 5 is shown (see also **Supplementary Fig. 6** for a corresponding cell energy phenotype assay). **(h)** Quantification of the mitochondrial membrane potential probe JC-1(mean±SD, n=6; see also **Supplementary Fig. 7**). **(I-K)** U-^{13}C-glucose was added to the supernatant of PER2 KD or Scr HMEC-1. Following 24h of Nx or 1% Hx treatment cells were harvested and analyzed for ^{13}C-metabolites using liquid chromatography–tandem mass spectrometry. Data are presented as percentage of total metabolite present (mean±SD, n=3,). **(L, M)** 1,2-^{13}C-palmitic acid tracers in PER2 KD or Scr HMEC-1 in 24 h Nx or 1% Hx (mean±SD, n=3).

Figure 7. Light-sensing human cell line recapitulates *in vivo* light exposure. (**A**) Study design and verification of melanopsin overexpression by immunoblot. pCMV6 is the empty vector control and OPN4-pCMV6 is the plasmid containing the gene encoding melanopsin (n=3). (**B-H**) cAMP, pCREB levels, PER2 transcript, glycolytic capacity and maximum achievable respiration after light sensing cells were exposed to daylight (mean±SD, n=6-10). (**I**) Schematic model.

Figure 8. Daylight enhances the circadian amplitude of PER2 and mimics HIF1A dependent metabolism in humans. **(A)** Protocol for daylight exposure experiments in healthy human volunteers. 20 healthy volunteers (11 female and 6 male, age range between 21-44 yrs.) were exposed to daylight (10,000 LUX) from 8.30-9.00 AM on 5 consecutive days. **(B, C**) PER2 protein levels from buccal tissue or plasma samples at 9AM during 5d of daylight exposure assessed by immunoblot or ELISA, respectively (mean±SD; n=6, see also

Supplementary Fig. 9). **(D)** Effect of room light versus daylight on human plasma melatonin levels (mean±SD; n=3-6). (**e**) Longitudinal monitoring of human plasma melatonin levels during 5d of daylight exposure at 9AM (mean±SD; n=3-6). **(F)** Human plasma phosphofructokinase (PFK) activity during 5d of daylight exposure at 9AM (mean±SD; n=3-6). (**G**) Human plasma PFK activity after 5d of daylight exposure at 9PM (mean±SD; n=3). **(H**) Human plasma lactate dehydrogenase (LDH) activity during 5d of daylight exposure (mean±SD; n=8). **(I)** HIF1A human plasma levels during 5d of daylight exposure at 9AM (mean±SD; n=6). **(J)** Human plasma triglyceride levels during 5 d of daylight exposure at 9 AM (mean±SD; n=8). **(K-N)** Targeted metabolomics using mass-spectrometry on human plasma samples from healthy volunteers exposed to daylight therapy for 5 days. Key metabolites of glycolysis (pyruvate, lactate) or TCA cycle (succinate) are shown for day 3 and day 5 of daylight therapy (mean±SD; n=3, see also **Supplementary Fig. 10**). **(O-Q)** Actigraphy data using a validated accelerometer (Actiwatch 2). Shown are the wake-up episodes after the sleep onset (WASO, **O**), the sleep efficiency (**P**, mean±SD; n=6) and one representative actigraphy recording from one healthy volunteer before and during daylight therapy (**Q**, **Note**: synchronized sleep phases [turquoise bar] during daylight exposure [red square]; see also **Supplementary Figure 11**).

Supp. Table 1.	*Affinity purification-mass spectrometry-based proteomics screen for PER2 protein interactions under hypoxic conditions*

Accession No.	PER2 protein interactions in hypoxia 1% **(bold highlights investigated/discussed pathways)**
P54577	Tyrosine--tRNA ligase, cytoplasmic OS=Homo sapiens GN=YARS PE=1 SV=4
O60684	Importin subunit alpha-7 OS=Homo sapiens GN=KPNA6 PE=1 SV=1
Q7KZ85	Transcription elongation factor SPT6 OS=Homo sapiens GN=SUPT6H PE=1 SV=2
Q9NTK5	Obg-like ATPase 1 OS=Homo sapiens GN=OLA1 PE=1 SV=2
P53618	Coatomer subunit beta OS=Homo sapiens GN=COPB1 PE=1 SV=3
P13667	Protein disulfide-isomerase A4 OS=Homo sapiens GN=PDIA4 PE=1 SV=2
P56192	Methionine--tRNA ligase, cytoplasmic OS=Homo sapiens GN=MARS PE=1 SV=2
P31327	Carbamoyl-phosphate synthase [ammonia], mitochondrial OS=Homo sapiens GN=CPS1 PE=1 SV=2
P39687	Acidic leucine-rich nuclear phosphoprotein 32 family member A OS=Homo sapiens GN=ANP32A PE=1 SV=1
Q00796	Sorbitol dehydrogenase OS=Homo sapiens GN=SORD PE=1 SV=4
P41252	Isoleucine--tRNA ligase, cytoplasmic OS=Homo sapiens GN=IARS PE=1 SV=2
P11498	Pyruvate carboxylase, mitochondrial OS=Homo sapiens GN=PC PE=1 SV=2
P29401	Transketolase OS=Homo sapiens GN=TKT PE=1 SV=3
P27694	Replication protein A 70 kDa DNA-binding subunit OS=Homo sapiens GN=RPA1 PE=1 SV=2
P07195	**L-lactate dehydrogenase B chain OS=Homo sapiens GN=LDHB PE=1 SV=2**
P78386	Keratin, type II cuticular Hb5 OS=Homo sapiens GN=KRT85 PE=1 SV=1
Q9BY44	Eukaryotic translation initiation factor 2A OS=Homo sapiens GN=EIF2A PE=1 SV=3
P48444	Coatomer subunit delta OS=Homo sapiens GN=ARCN1 PE=1 SV=1
P61626	Lysozyme C OS=Homo sapiens GN=LYZ PE=1 SV=1
Q9BRJ2	39S ribosomal protein L45, mitochondrial OS=Homo sapiens GN=MRPL45 PE=1 SV=2
Q9NSE4	Isoleucine--tRNA ligase, mitochondrial OS=Homo sapiens GN=IARS2 PE=1 SV=2
Q9Y3A5	Ribosome maturation protein SBDS OS=Homo sapiens GN=SBDS PE=1 SV=4
P02788	Lactotransferrin OS=Homo sapiens GN=LTF PE=1 SV=6
P04062	Glucosylceramidase OS=Homo sapiens GN=GBA PE=1 SV=3

Q9HCC0	Methylcrotonoyl-CoA carboxylase beta chain, mitochondrial OS=Homo sapiens GN=MCCC2 PE=1 SV=1
P37268	Squalene synthase OS=Homo sapiens GN=FDFT1 PE=1 SV=1
P12081	Histidine--tRNA ligase, cytoplasmic OS=Homo sapiens GN=HARS PE=1 SV=2
P61011	Signal recognition particle 54 kDa protein OS=Homo sapiens GN=SRP54 PE=1 SV=1
Q9NYK5	39S ribosomal protein L39, mitochondrial OS=Homo sapiens GN=MRPL39 PE=1 SV=3
P55060	Exportin-2 OS=Homo sapiens GN=CSE1L PE=1 SV=3
Q16777	Histone H2A type 2-C OS=Homo sapiens GN=HIST2H2AC PE=1 SV=4
P82932	28S ribosomal protein S6, mitochondrial OS=Homo sapiens GN=MRPS6 PE=1 SV=3
Q96I59	Probable asparagine--tRNA ligase, mitochondrial OS=Homo sapiens GN=NARS2 PE=1 SV=3
P30101	Protein disulfide-isomerase A3 OS=Homo sapiens GN=PDIA3 PE=1 SV=4
O15355	Protein phosphatase 1G OS=Homo sapiens GN=PPM1G PE=1 SV=1
P51398	28S ribosomal protein S29, mitochondrial OS=Homo sapiens GN=DAP3 PE=1 SV=1
Q9GZZ8	Extracellular glycoprotein lacritin OS=Homo sapiens GN=LACRT PE=1 SV=1
P50336	Protoporphyrinogen oxidase OS=Homo sapiens GN=PPOX PE=1 SV=1
O60313	Dynamin-like 120 kDa protein, mitochondrial OS=Homo sapiens GN=OPA1 PE=1 SV=3
P31025	Lipocalin-1 OS=Homo sapiens GN=LCN1 PE=1 SV=1
Q6L8Q7	2',5'-phosphodiesterase 12 OS=Homo sapiens GN=PDE12 PE=1 SV=2
O00629	Importin subunit alpha-3 OS=Homo sapiens GN=KPNA4 PE=1 SV=1
P10768	S-formylglutathione hydrolase OS=Homo sapiens GN=ESD PE=1 SV=2
Q9BYD6	39S ribosomal protein L1, mitochondrial OS=Homo sapiens GN=MRPL1 PE=1 SV=2
Q92665	28S ribosomal protein S31, mitochondrial OS=Homo sapiens GN=MRPS31 PE=1 SV=3
P43490	Nicotinamide phosphoribosyltransferase OS=Homo sapiens GN=NAMPT PE=1 SV=1
Q8N5N7	39S ribosomal protein L50, mitochondrial OS=Homo sapiens GN=MRPL50 PE=1 SV=2
Q16555	Dihydropyrimidinase-related protein 2 OS=Homo sapiens GN=DPYSL2 PE=1 SV=1
O95573	Long-chain-fatty-acid--CoA ligase 3 OS=Homo sapiens GN=ACSL3 PE=1 SV=3

O94903	Proline synthase co-transcribed bacterial homolog protein OS=Homo sapiens GN=PROSC PE=1 SV=1
Q15785	**Mitochondrial import receptor subunit TOM34 OS=Homo sapiens GN=TOMM34 PE=1 SV=2**
O95218	Zinc finger Ran-binding domain-containing protein 2 OS=Homo sapiens GN=ZRANB2 PE=1 SV=2
P09622	Dihydrolipoyl dehydrogenase, mitochondrial OS=Homo sapiens GN=DLD PE=1 SV=2
P47813	Eukaryotic translation initiation factor 1A, X-chromosomal OS=Homo sapiens GN=EIF1AX PE=1 SV=2
Q9BV79	Trans-2-enoyl-CoA reductase, mitochondrial OS=Homo sapiens GN=MECR PE=1 SV=2
O00410	Importin-5 OS=Homo sapiens GN=IPO5 PE=1 SV=4
Q8NBN7	Retinol dehydrogenase 13 OS=Homo sapiens GN=RDH13 PE=1 SV=2
Q92688	Acidic leucine-rich nuclear phosphoprotein 32 family member B OS=Homo sapiens GN=ANP32B PE=1 SV=1
O75821	Eukaryotic translation initiation factor 3 subunit G OS=Homo sapiens GN=EIF3G PE=1 SV=2
Q7Z4V5	Hepatoma-derived growth factor-related protein 2 OS=Homo sapiens GN=HDGFRP2 PE=1 SV=1
P82664	28S ribosomal protein S10, mitochondrial OS=Homo sapiens GN=MRPS10 PE=1 SV=2
P53597	**Succinyl-CoA ligase [ADP/GDP-forming] subunit alpha, mitochondrial OS=Homo sapiens GN=SUCLG1 PE=1 SV=4**
Q9NXG2	THUMP domain-containing protein 1 OS=Homo sapiens GN=THUMPD1 PE=1 SV=2
P08195	4F2 cell-surface antigen heavy chain OS=Homo sapiens GN=SLC3A2 PE=1 SV=3
Q9NPJ3	Acyl-coenzyme A thioesterase 13 OS=Homo sapiens GN=ACOT13 PE=1 SV=1
Q8TCC3	39S ribosomal protein L30, mitochondrial OS=Homo sapiens GN=MRPL30 PE=1 SV=1
P51553	**Isocitrate dehydrogenase [NAD] subunit gamma, mitochondrial OS=Homo sapiens GN=IDH3G PE=1 SV=1**
Q01813	ATP-dependent 6-phosphofructokinase, platelet type OS=Homo sapiens GN=PFKP PE=1 SV=2
P09429	High mobility group protein B1 OS=Homo sapiens GN=HMGB1 PE=1 SV=3
Q9BYD3	39S ribosomal protein L4, mitochondrial OS=Homo sapiens GN=MRPL4 PE=1 SV=1
P10909	Clusterin OS=Homo sapiens GN=CLU PE=1 SV=1
O00203	AP-3 complex subunit beta-1 OS=Homo sapiens GN=AP3B1 PE=1 SV=3

Q96A33	Coiled-coil domain-containing protein 47 OS=Homo sapiens GN=CCDC47 PE=1 SV=1
P01833	Polymeric immunoglobulin receptor OS=Homo sapiens GN=PIGR PE=1 SV=4
Q9Y3D3	28S ribosomal protein S16, mitochondrial OS=Homo sapiens GN=MRPS16 PE=1 SV=1
Q9NVS2	28S ribosomal protein S18a, mitochondrial OS=Homo sapiens GN=MRPS18A PE=1 SV=1
Q9BWD1	Acetyl-CoA acetyltransferase, cytosolic OS=Homo sapiens GN=ACAT2 PE=1 SV=2
Q15323	Keratin, type I cuticular Ha1 OS=Homo sapiens GN=KRT31 PE=2 SV=3
Q7Z7F7	39S ribosomal protein L55, mitochondrial OS=Homo sapiens GN=MRPL55 PE=1 SV=1
Q13509	Tubulin beta-3 chain OS=Homo sapiens GN=TUBB3 PE=1 SV=2
Q9Y676	28S ribosomal protein S18b, mitochondrial OS=Homo sapiens GN=MRPS18B PE=1 SV=1
Q9H2U2	Inorganic pyrophosphatase 2, mitochondrial OS=Homo sapiens GN=PPA2 PE=1 SV=2
Q9Y3D7	Mitochondrial import inner membrane translocase subunit TIM16 OS=Homo sapiens GN=PAM16 PE=1 SV=2
Q9BWM7	Sideroflexin-3 OS=Homo sapiens GN=SFXN3 PE=1 SV=2
Q16378	Proline-rich protein 4 OS=Homo sapiens GN=PRR4 PE=1 SV=3
Q3ZCQ8	Mitochondrial import inner membrane translocase subunit TIM50 OS=Homo sapiens GN=TIMM50 PE=1 SV=2
P16615	Sarcoplasmic/endoplasmic reticulum calcium ATPase 2 OS=Homo sapiens GN=ATP2A2 PE=1 SV=1
P32119	Peroxiredoxin-2 OS=Homo sapiens GN=PRDX2 PE=1 SV=5
Q9H4M9	EH domain-containing protein 1 OS=Homo sapiens GN=EHD1 PE=1 SV=2
O43583	Density-regulated protein OS=Homo sapiens GN=DENR PE=1 SV=2
Q14197	Peptidyl-tRNA hydrolase ICT1, mitochondrial OS=Homo sapiens GN=ICT1 PE=1 SV=1
Q9UGP8	Translocation protein SEC63 homolog OS=Homo sapiens GN=SEC63 PE=1 SV=2
P10599	Thioredoxin OS=Homo sapiens GN=TXN PE=1 SV=3
P11310	Medium-chain specific acyl-CoA dehydrogenase, mitochondrial OS=Homo sapiens GN=ACADM PE=1 SV=1
Q7Z2W9	39S ribosomal protein L21, mitochondrial OS=Homo sapiens GN=MRPL21 PE=1 SV=2
O94979	Protein transport protein Sec31A OS=Homo sapiens GN=SEC31A PE=1 SV=3

Q99536	Synaptic vesicle membrane protein VAT-1 homolog OS=Homo sapiens GN=VAT1 PE=1 SV=2
P04350	Tubulin beta-4A chain OS=Homo sapiens GN=TUBB4A PE=1 SV=2
P01876	Ig alpha-1 chain C region OS=Homo sapiens GN=IGHA1 PE=1 SV=2
P41250	Glycine--tRNA ligase OS=Homo sapiens GN=GARS PE=1 SV=3
Q8TCS8	Polyribonucleotide nucleotidyltransferase 1, mitochondrial OS=Homo sapiens GN=PNPT1 PE=1 SV=2
Q9BYN8	28S ribosomal protein S26, mitochondrial OS=Homo sapiens GN=MRPS26 PE=1 SV=1
P00505	Aspartate aminotransferase, mitochondrial OS=Homo sapiens GN=GOT2 PE=1 SV=3
P61769	Beta-2-microglobulin OS=Homo sapiens GN=B2M PE=1 SV=1
Q8TEA8	D-tyrosyl-tRNA(Tyr) deacylase 1 OS=Homo sapiens GN=DTD1 PE=1 SV=2
Q7Z794	Keratin, type II cytoskeletal 1b OS=Homo sapiens GN=KRT77 PE=2 SV=3
P78385	Keratin, type II cuticular Hb3 OS=Homo sapiens GN=KRT83 PE=1 SV=2
Q6IN85	Serine/threonine-protein phosphatase 4 regulatory subunit 3A OS=Homo sapiens GN=SMEK1 PE=1 SV=1
P08727	Keratin, type I cytoskeletal 19 OS=Homo sapiens GN=KRT19 PE=1 SV=4
P12273	Prolactin-inducible protein OS=Homo sapiens GN=PIP PE=1 SV=1
O75323	Protein NipSnap homolog 2 OS=Homo sapiens GN=GBAS PE=1 SV=1
Q8N983	39S ribosomal protein L43, mitochondrial OS=Homo sapiens GN=MRPL43 PE=1 SV=1
P62917	60S ribosomal protein L8 OS=Homo sapiens GN=RPL8 PE=1 SV=2
P20290	Transcription factor BTF3 OS=Homo sapiens GN=BTF3 PE=1 SV=1
Q9UBM7	7-dehydrocholesterol reductase OS=Homo sapiens GN=DHCR7 PE=1 SV=1
P05023	Sodium/potassium-transporting ATPase subunit alpha-1 OS=Homo sapiens GN=ATP1A1 PE=1 SV=1
Q9BXW7	Cat eye syndrome critical region protein 5 OS=Homo sapiens GN=CECR5 PE=1 SV=1
P23921	Ribonucleoside-diphosphate reductase large subunit OS=Homo sapiens GN=RRM1 PE=1 SV=1
Q9BVJ7	Dual specificity protein phosphatase 23 OS=Homo sapiens GN=DUSP23 PE=1 SV=1
Q9P2J5	Leucine--tRNA ligase, cytoplasmic OS=Homo sapiens GN=LARS PE=1 SV=2

P50213	**Isocitrate dehydrogenase [NAD] subunit alpha, mitochondrial OS=Homo sapiens GN=IDH3A PE=1 SV=1**
P01024	Complement C3 OS=Homo sapiens GN=C3 PE=1 SV=2
Q9NVJ2	ADP-ribosylation factor-like protein 8B OS=Homo sapiens GN=ARL8B PE=1 SV=1
Q9NWU5	39S ribosomal protein L22, mitochondrial OS=Homo sapiens GN=MRPL22 PE=1 SV=1
Q99935	Proline-rich protein 1 OS=Homo sapiens GN=PROL1 PE=1 SV=2
Q96MG8	Protein-L-isoaspartate O-methyltransferase domain-containing protein 1 OS=Homo sapiens GN=PCMTD1 PE=2 SV=2
P14854	**Cytochrome c oxidase subunit 6B1 OS=Homo sapiens GN=COX6B1 PE=1 SV=2**
P00387	**NADH-cytochrome b5 reductase 3 OS=Homo sapiens GN=CYB5R3 PE=1 SV=3**
P22830	Ferrochelatase, mitochondrial OS=Homo sapiens GN=FECH PE=1 SV=2
Q6UX04	Peptidyl-prolyl cis-trans isomerase CWC27 homolog OS=Homo sapiens GN=CWC27 PE=1 SV=1
Q92947	Glutaryl-CoA dehydrogenase, mitochondrial OS=Homo sapiens GN=GCDH PE=1 SV=1
Q9BRP8	Partner of Y14 and mago OS=Homo sapiens GN=WIBG PE=1 SV=1
Q12768	WASH complex subunit strumpellin OS=Homo sapiens GN=KIAA0196 PE=1 SV=1
Q9BUF5	Tubulin beta-6 chain OS=Homo sapiens GN=TUBB6 PE=1 SV=1
Q9NVA1	**Ubiquinol-cytochrome-c reductase complex assembly factor 1 OS=Homo sapiens GN=UQCC1 PE=1 SV=3**
Q9Y3C4	EKC/KEOPS complex subunit TPRKB OS=Homo sapiens GN=TPRKB PE=1 SV=1
P61020	Ras-related protein Rab-5B OS=Homo sapiens GN=RAB5B PE=1 SV=1
Q9P032	NADH dehydrogenase [ubiquinone] 1 alpha subcomplex assembly factor 4 OS=Homo sapiens GN=NDUFAF4 PE=1 SV=1
P49915	GMP synthase [glutamine-hydrolyzing] OS=Homo sapiens GN=GMPS PE=1 SV=1
Q9UBP6	tRNA (guanine-N(7)-)-methyltransferase OS=Homo sapiens GN=METTL1 PE=1 SV=1
O75964	**ATP synthase subunit g, mitochondrial OS=Homo sapiens GN=ATP5L PE=1 SV=3**
Q9HDC9	Adipocyte plasma membrane-associated protein OS=Homo sapiens GN=APMAP PE=1 SV=2
P82663	28S ribosomal protein S25, mitochondrial OS=Homo sapiens GN=MRPS25 PE=1 SV=1

Q02338	D-beta-hydroxybutyrate dehydrogenase, mitochondrial OS=Homo sapiens GN=BDH1 PE=1 SV=3
O75556	Mammaglobin-B OS=Homo sapiens GN=SCGB2A1 PE=1 SV=1
P01834	Ig kappa chain C region OS=Homo sapiens GN=IGKC PE=1 SV=1
Q9Y3D6	Mitochondrial fission 1 protein OS=Homo sapiens GN=FIS1 PE=1 SV=2
O95881	Thioredoxin domain-containing protein 12 OS=Homo sapiens GN=TXNDC12 PE=1 SV=1
Q8N1N4	Keratin, type II cytoskeletal 78 OS=Homo sapiens GN=KRT78 PE=2 SV=2
Q6UW78	UPF0723 protein C11orf83 OS=Homo sapiens GN=C11orf83 PE=1 SV=2
Q15067	Peroxisomal acyl-coenzyme A oxidase 1 OS=Homo sapiens GN=ACOX1 PE=1 SV=3
P50443	Sulfate transporter OS=Homo sapiens GN=SLC26A2 PE=1 SV=2
P25789	Proteasome subunit alpha type-4 OS=Homo sapiens GN=PSMA4 PE=1 SV=1
P52294	Importin subunit alpha-5 OS=Homo sapiens GN=KPNA1 PE=1 SV=3
Q5T653	39S ribosomal protein L2, mitochondrial OS=Homo sapiens GN=MRPL2 PE=1 SV=2
Q4U2R6	39S ribosomal protein L51, mitochondrial OS=Homo sapiens GN=MRPL51 PE=1 SV=1
P68366	Tubulin alpha-4A chain OS=Homo sapiens GN=TUBA4A PE=1 SV=1
P22102	Trifunctional purine biosynthetic protein adenosine-3 OS=Homo sapiens GN=GART PE=1 SV=1
Q9Y3D5	28S ribosomal protein S18c, mitochondrial OS=Homo sapiens GN=MRPS18C PE=1 SV=1
Q15691	Microtubule-associated protein RP/EB family member 1 OS=Homo sapiens GN=MAPRE1 PE=1 SV=3
Q13451	Peptidyl-prolyl cis-trans isomerase FKBP5 OS=Homo sapiens GN=FKBP5 PE=1 SV=2
P11908	Ribose-phosphate pyrophosphokinase 2 OS=Homo sapiens GN=PRPS2 PE=1 SV=2
O43837	Isocitrate dehydrogenase [NAD] subunit beta, mitochondrial OS=Homo sapiens GN=IDH3B PE=1 SV=2
Q96DA0	Zymogen granule protein 16 homolog B OS=Homo sapiens GN=ZG16B PE=1 SV=3
Q7Z7K0	COX assembly mitochondrial protein homolog OS=Homo sapiens GN=CMC1 PE=1 SV=1
Q8N5M4	Tetratricopeptide repeat protein 9C OS=Homo sapiens GN=TTC9C PE=1 SV=1
O43776	Asparagine--tRNA ligase, cytoplasmic OS=Homo sapiens GN=NARS PE=1 SV=1

Q9Y4B6	Protein VPRBP OS=Homo sapiens GN=VPRBP PE=1 SV=3
P04818	Thymidylate synthase OS=Homo sapiens GN=TYMS PE=1 SV=3
O00743	Serine/threonine-protein phosphatase 6 catalytic subunit OS=Homo sapiens GN=PPP6C PE=1 SV=1
P46459	Vesicle-fusing ATPase OS=Homo sapiens GN=NSF PE=1 SV=3
Q9BYC8	39S ribosomal protein L32, mitochondrial OS=Homo sapiens GN=MRPL32 PE=1 SV=1
P06702	Protein S100-A9 OS=Homo sapiens GN=S100A9 PE=1 SV=1
O75348	V-type proton ATPase subunit G 1 OS=Homo sapiens GN=ATP6V1G1 PE=1 SV=3
Q9BSJ8	Extended synaptotagmin-1 OS=Homo sapiens GN=ESYT1 PE=1 SV=1
P26640	Valine--tRNA ligase OS=Homo sapiens GN=VARS PE=1 SV=4
Q9UK45	U6 snRNA-associated Sm-like protein LSm7 OS=Homo sapiens GN=LSM7 PE=1 SV=1
Q16540	39S ribosomal protein L23, mitochondrial OS=Homo sapiens GN=MRPL23 PE=1 SV=1
P27816	Microtubule-associated protein 4 OS=Homo sapiens GN=MAP4 PE=1 SV=3
Q15738	Sterol-4-alpha-carboxylate 3-dehydrogenase, decarboxylating OS=Homo sapiens GN=NSDHL PE=1 SV=2
P60520	Gamma-aminobutyric acid receptor-associated protein-like 2 OS=Homo sapiens GN=GABARAPL2 PE=1 SV=1
Q9H061	Transmembrane protein 126A OS=Homo sapiens GN=TMEM126A PE=1 SV=1
P09001	39S ribosomal protein L3, mitochondrial OS=Homo sapiens GN=MRPL3 PE=1 SV=1
P48735	Isocitrate dehydrogenase [NADP], mitochondrial OS=Homo sapiens GN=IDH2 PE=1 SV=2
Q7Z7H8	39S ribosomal protein L10, mitochondrial OS=Homo sapiens GN=MRPL10 PE=1 SV=3
P60900	Proteasome subunit alpha type-6 OS=Homo sapiens GN=PSMA6 PE=1 SV=1
Q9BRQ8	Apoptosis-inducing factor 2 OS=Homo sapiens GN=AIFM2 PE=1 SV=1
P30084	Enoyl-CoA hydratase, mitochondrial OS=Homo sapiens GN=ECHS1 PE=1 SV=4
Q9HAV7	GrpE protein homolog 1, mitochondrial OS=Homo sapiens GN=GRPEL1 PE=1 SV=2
Q8N5K1	CDGSH iron-sulfur domain-containing protein 2 OS=Homo sapiens GN=CISD2 PE=1 SV=1
P49721	Proteasome subunit beta type-2 OS=Homo sapiens GN=PSMB2 PE=1 SV=1

Q96EY7	Pentatricopeptide repeat domain-containing protein 3, mitochondrial OS=Homo sapiens GN=PTCD3 PE=1 SV=3
P06744	Glucose-6-phosphate isomerase OS=Homo sapiens GN=GPI PE=1 SV=4
P35244	Replication protein A 14 kDa subunit OS=Homo sapiens GN=RPA3 PE=1 SV=1
P41567	Eukaryotic translation initiation factor 1 OS=Homo sapiens GN=EIF1 PE=1 SV=1
Q08257	Quinone oxidoreductase OS=Homo sapiens GN=CRYZ PE=1 SV=1
P22307	Non-specific lipid-transfer protein OS=Homo sapiens GN=SCP2 PE=1 SV=2
O00442	RNA 3'-terminal phosphate cyclase OS=Homo sapiens GN=RTCA PE=1 SV=1
Q92900	Regulator of nonsense transcripts 1 OS=Homo sapiens GN=UPF1 PE=1 SV=2
O75394	39S ribosomal protein L33, mitochondrial OS=Homo sapiens GN=MRPL33 PE=1 SV=1
Q96EL2	28S ribosomal protein S24, mitochondrial OS=Homo sapiens GN=MRPS24 PE=1 SV=1
Q96KG9	N-terminal kinase-like protein OS=Homo sapiens GN=SCYL1 PE=1 SV=1
Q8WWY3	U4/U6 small nuclear ribonucleoprotein Prp31 OS=Homo sapiens GN=PRPF31 PE=1 SV=2
P09132	Signal recognition particle 19 kDa protein OS=Homo sapiens GN=SRP19 PE=1 SV=3
Q9UHR5	SAP30-binding protein OS=Homo sapiens GN=SAP30BP PE=1 SV=1
Q16850	Lanosterol 14-alpha demethylase OS=Homo sapiens GN=CYP51A1 PE=1 SV=3
O95433	Activator of 90 kDa heat shock protein ATPase homolog 1 OS=Homo sapiens GN=AHSA1 PE=1 SV=1
Q14232	Translation initiation factor eIF-2B subunit alpha OS=Homo sapiens GN=EIF2B1 PE=1 SV=1
P34897	Serine hydroxymethyltransferase, mitochondrial OS=Homo sapiens GN=SHMT2 PE=1 SV=3
Q30201	Hereditary hemochromatosis protein OS=Homo sapiens GN=HFE PE=1 SV=1
Q9Y606	tRNA pseudouridine synthase A, mitochondrial OS=Homo sapiens GN=PUS1 PE=1 SV=3
B9A064	Immunoglobulin lambda-like polypeptide 5 OS=Homo sapiens GN=IGLL5 PE=2 SV=2
Q9Y446	Plakophilin-3 OS=Homo sapiens GN=PKP3 PE=1 SV=1
P06396	Gelsolin OS=Homo sapiens GN=GSN PE=1 SV=1
P31947	14-3-3 protein sigma OS=Homo sapiens GN=SFN PE=1 SV=1
O15427	Monocarboxylate transporter 4 OS=Homo sapiens GN=SLC16A3 PE=1 SV=1

Q9UDW1	**Cytochrome b-c1 complex subunit 9 OS=Homo sapiens GN=UQCR10 PE=1 SV=3**
O75351	Vacuolar protein sorting-associated protein 4B OS=Homo sapiens GN=VPS4B PE=1 SV=2
P30837	Aldehyde dehydrogenase X, mitochondrial OS=Homo sapiens GN=ALDH1B1 PE=1 SV=3
Q96DB5	Regulator of microtubule dynamics protein 1 OS=Homo sapiens GN=RMDN1 PE=1 SV=1
O60613	15 kDa selenoprotein OS=Homo sapiens GN=SEP15 PE=1 SV=3
Q9Y2Z4	Tyrosine--tRNA ligase, mitochondrial OS=Homo sapiens GN=YARS2 PE=1 SV=2
Q96GC5	39S ribosomal protein L48, mitochondrial OS=Homo sapiens GN=MRPL48 PE=1 SV=2
O00267	Transcription elongation factor SPT5 OS=Homo sapiens GN=SUPT5H PE=1 SV=1
P30046	D-dopachrome decarboxylase OS=Homo sapiens GN=DDT PE=1 SV=3
Q10713	Mitochondrial-processing peptidase subunit alpha OS=Homo sapiens GN=PMPCA PE=1 SV=2
Q96IJ6	Mannose-1-phosphate guanyltransferase alpha OS=Homo sapiens GN=GMPPA PE=1 SV=1
Q13835	Plakophilin-1 OS=Homo sapiens GN=PKP1 PE=1 SV=2
P55058	Phospholipid transfer protein OS=Homo sapiens GN=PLTP PE=1 SV=1
P27348	14-3-3 protein theta OS=Homo sapiens GN=YWHAQ PE=1 SV=1
P25311	Zinc-alpha-2-glycoprotein OS=Homo sapiens GN=AZGP1 PE=1 SV=2
Q9BQA1	Methylosome protein 50 OS=Homo sapiens GN=WDR77 PE=1 SV=1
P11172	Uridine 5'-monophosphate synthase OS=Homo sapiens GN=UMPS PE=1 SV=1
P10515	Dihydrolipoyllysine-residue acetyltransferase component of pyruvate dehydrogenase complex, mitochondrial OS=Homo sapiens GN=DLAT PE=1 SV=3
P42765	3-ketoacyl-CoA thiolase, mitochondrial OS=Homo sapiens GN=ACAA2 PE=1 SV=2
Q8NFV4	Alpha/beta hydrolase domain-containing protein 11 OS=Homo sapiens GN=ABHD11 PE=2 SV=1
Q10567	AP-1 complex subunit beta-1 OS=Homo sapiens GN=AP1B1 PE=1 SV=2
P17812	CTP synthase 1 OS=Homo sapiens GN=CTPS1 PE=1 SV=2
P16152	Carbonyl reductase [NADPH] 1 OS=Homo sapiens GN=CBR1 PE=1 SV=3
Q9H875	PRKR-interacting protein 1 OS=Homo sapiens GN=PRKRIP1 PE=1 SV=1
Q9BYC9	39S ribosomal protein L20, mitochondrial

	OS=Homo sapiens GN=MRPL20 PE=1 SV=1
P63172	Dynein light chain Tctex-type 1 OS=Homo sapiens GN=DYNLT1 PE=1 SV=1
P23527	Histone H2B type 1-O OS=Homo sapiens GN=HIST1H2BO PE=1 SV=3
Q96A35	39S ribosomal protein L24, mitochondrial OS=Homo sapiens GN=MRPL24 PE=1 SV=1
Q9NYL4	Peptidyl-prolyl cis-trans isomerase FKBP11 OS=Homo sapiens GN=FKBP11 PE=1 SV=1
O00303	Eukaryotic translation initiation factor 3 subunit F OS=Homo sapiens GN=EIF3F PE=1 SV=1
P31153	S-adenosylmethionine synthase isoform type-2 OS=Homo sapiens GN=MAT2A PE=1 SV=1
Q53H12	Acylglycerol kinase, mitochondrial OS=Homo sapiens GN=AGK PE=1 SV=2
P27824	Calnexin OS=Homo sapiens GN=CANX PE=1 SV=2
P38606	V-type proton ATPase catalytic subunit A OS=Homo sapiens GN=ATP6V1A PE=1 SV=2
P49770	Translation initiation factor eIF-2B subunit beta OS=Homo sapiens GN=EIF2B2 PE=1 SV=3
Q02952	A-kinase anchor protein 12 OS=Homo sapiens GN=AKAP12 PE=1 SV=4
P25787	Proteasome subunit alpha type-2 OS=Homo sapiens GN=PSMA2 PE=1 SV=2
P26440	Isovaleryl-CoA dehydrogenase, mitochondrial OS=Homo sapiens GN=IVD PE=1 SV=1
Q15382	GTP-binding protein Rheb OS=Homo sapiens GN=RHEB PE=1 SV=1
Q9BTT0	Acidic leucine-rich nuclear phosphoprotein 32 family member E OS=Homo sapiens GN=ANP32E PE=1 SV=1
Q96CT7	Coiled-coil domain-containing protein 124 OS=Homo sapiens GN=CCDC124 PE=1 SV=1
P00450	Ceruloplasmin OS=Homo sapiens GN=CP PE=1 SV=1
Q8TF66	Leucine-rich repeat-containing protein 15 OS=Homo sapiens GN=LRRC15 PE=1 SV=2
Q9UHG3	Prenylcysteine oxidase 1 OS=Homo sapiens GN=PCYOX1 PE=1 SV=3
Q9Y2S6	Translation machinery-associated protein 7 OS=Homo sapiens GN=TMA7 PE=1 SV=1
Q9BZL1	Ubiquitin-like protein 5 OS=Homo sapiens GN=UBL5 PE=1 SV=1
P84085	ADP-ribosylation factor 5 OS=Homo sapiens GN=ARF5 PE=1 SV=2
O43504	Ragulator complex protein LAMTOR5 OS=Homo sapiens GN=LAMTOR5 PE=1 SV=1
O00487	26S proteasome non-ATPase regulatory subunit 14 OS=Homo sapiens GN=PSMD14 PE=1 SV=1
Q15165	Serum paraoxonase/arylesterase 2 OS=Homo sapiens GN=PON2 PE=1 SV=3

Q12974	Protein tyrosine phosphatase type IVA 2 OS=Homo sapiens GN=PTP4A2 PE=1 SV=1
Q9UL25	Ras-related protein Rab-21 OS=Homo sapiens GN=RAB21 PE=1 SV=3
P61009	Signal peptidase complex subunit 3 OS=Homo sapiens GN=SPCS3 PE=1 SV=1
Q9NQH7	Probable Xaa-Pro aminopeptidase 3 OS=Homo sapiens GN=XPNPEP3 PE=1 SV=1
O76031	ATP-dependent Clp protease ATP-binding subunit clpX-like, mitochondrial OS=Homo sapiens GN=CLPX PE=1 SV=2
P31949	Protein S100-A11 OS=Homo sapiens GN=S100A11 PE=1 SV=2
Q86YS7	C2 domain-containing protein 5 OS=Homo sapiens GN=C2CD5 PE=1 SV=1
Q5T749	Keratinocyte proline-rich protein OS=Homo sapiens GN=KPRP PE=1 SV=1
Q9HA64	Ketosamine-3-kinase OS=Homo sapiens GN=FN3KRP PE=1 SV=2
Q9Y5J6	Mitochondrial import inner membrane translocase subunit Tim10 B OS=Homo sapiens GN=TIMM10B PE=1 SV=1
P55081	Microfibrillar-associated protein 1 OS=Homo sapiens GN=MFAP1 PE=1 SV=2
Q9UGM3	Deleted in malignant brain tumors 1 protein OS=Homo sapiens GN=DMBT1 PE=1 SV=2
Q15758	Neutral amino acid transporter B(0) OS=Homo sapiens GN=SLC1A5 PE=1 SV=2
P57088	Transmembrane protein 33 OS=Homo sapiens GN=TMEM33 PE=1 SV=2
Q15369	Transcription elongation factor B polypeptide 1 OS=Homo sapiens GN=TCEB1 PE=1 SV=1
P62333	26S protease regulatory subunit 10B OS=Homo sapiens GN=PSMC6 PE=1 SV=1
P60468	Protein transport protein Sec61 subunit beta OS=Homo sapiens GN=SEC61B PE=1 SV=2
Q9H9B4	Sideroflexin-1 OS=Homo sapiens GN=SFXN1 PE=1 SV=4
O95757	Heat shock 70 kDa protein 4L OS=Homo sapiens GN=HSPA4L PE=1 SV=3
Q08380	Galectin-3-binding protein OS=Homo sapiens GN=LGALS3BP PE=1 SV=1
Q92764	Keratin, type I cuticular Ha5 OS=Homo sapiens GN=KRT35 PE=2 SV=5
Q7L592	NADH dehydrogenase [ubiquinone] complex I, assembly factor 7 OS=Homo sapiens GN=NDUFAF7 PE=1 SV=1
Q2M389	WASH complex subunit 7 OS=Homo sapiens GN=KIAA1033 PE=1 SV=2
O75600	2-amino-3-ketobutyrate coenzyme A ligase, mitochondrial OS=Homo sapiens GN=GCAT PE=1 SV=1

Q9H3H3	UPF0696 protein C11orf68 OS=Homo sapiens GN=C11orf68 PE=1 SV=2
Q9H936	Mitochondrial glutamate carrier 1 OS=Homo sapiens GN=SLC25A22 PE=1 SV=1
Q13795	ADP-ribosylation factor-related protein 1 OS=Homo sapiens GN=ARFRP1 PE=1 SV=1
O75352	Mannose-P-dolichol utilization defect 1 protein OS=Homo sapiens GN=MPDU1 PE=1 SV=2
Q6P161	39S ribosomal protein L54, mitochondrial OS=Homo sapiens GN=MRPL54 PE=1 SV=1
P26447	Protein S100-A4 OS=Homo sapiens GN=S100A4 PE=1 SV=1
Q9H0U4	Ras-related protein Rab-1B OS=Homo sapiens GN=RAB1B PE=1 SV=1
Q13885	Tubulin beta-2A chain OS=Homo sapiens GN=TUBB2A PE=1 SV=1
P61026	Ras-related protein Rab-10 OS=Homo sapiens GN=RAB10 PE=1 SV=1
Q9NSB4	Keratin, type II cuticular Hb2 OS=Homo sapiens GN=KRT82 PE=1 SV=3
P54619	5'-AMP-activated protein kinase subunit gamma-1 OS=Homo sapiens GN=PRKAG1 PE=1 SV=1
Q6P587	Acylpyruvase FAHD1, mitochondrial OS=Homo sapiens GN=FAHD1 PE=1 SV=2
Q9Y4L1	Hypoxia up-regulated protein 1 OS=Homo sapiens GN=HYOU1 PE=1 SV=1
P11802	Cyclin-dependent kinase 4 OS=Homo sapiens GN=CDK4 PE=1 SV=2
P20340	Ras-related protein Rab-6A OS=Homo sapiens GN=RAB6A PE=1 SV=3
Q13085	Acetyl-CoA carboxylase 1 OS=Homo sapiens GN=ACACA PE=1 SV=2
P82912	28S ribosomal protein S11, mitochondrial OS=Homo sapiens GN=MRPS11 PE=1 SV=2
P49366	Deoxyhypusine synthase OS=Homo sapiens GN=DHPS PE=1 SV=1
A6NDG6	Phosphoglycolate phosphatase OS=Homo sapiens GN=PGP PE=1 SV=1
P17858	**ATP-dependent 6-phosphofructokinase, liver type OS=Homo sapiens GN=PFKL PE=1 SV=6**
P54920	Alpha-soluble NSF attachment protein OS=Homo sapiens GN=NAPA PE=1 SV=3
P08237	ATP-dependent 6-phosphofructokinase, muscle type OS=Homo sapiens GN=PFKM PE=1 SV=2
Q9P0S2	**Cytochrome c oxidase assembly protein COX16 homolog, mitochondrial OS=Homo sapiens GN=COX16 PE=1 SV=1**
Q96S44	TP53-regulating kinase OS=Homo sapiens GN=TP53RK PE=1 SV=2
O95777	U6 snRNA-associated Sm-like protein LSm8 OS=Homo sapiens GN=LSM8 PE=1 SV=3

O75822	Eukaryotic translation initiation factor 3 subunit J OS=Homo sapiens GN=EIF3J PE=1 SV=2
O95968	Secretoglobin family 1D member 1 OS=Homo sapiens GN=SCGB1D1 PE=1 SV=1
P49247	Ribose-5-phosphate isomerase OS=Homo sapiens GN=RPIA PE=1 SV=3
P82675	28S ribosomal protein S5, mitochondrial OS=Homo sapiens GN=MRPS5 PE=1 SV=2
P62310	U6 snRNA-associated Sm-like protein LSm3 OS=Homo sapiens GN=LSM3 PE=1 SV=2
Q15286	Ras-related protein Rab-35 OS=Homo sapiens GN=RAB35 PE=1 SV=1
P02452	Collagen alpha-1(I) chain OS=Homo sapiens GN=COL1A1 PE=1 SV=5
O76071	Probable cytosolic iron-sulfur protein assembly protein CIAO1 OS=Homo sapiens GN=CIAO1 PE=1 SV=1
P30048	Thioredoxin-dependent peroxide reductase, mitochondrial OS=Homo sapiens GN=PRDX3 PE=1 SV=3
P20962	Parathymosin OS=Homo sapiens GN=PTMS PE=1 SV=2
Q5JTJ3	**Cytochrome c oxidase assembly factor 6 homolog OS=Homo sapiens GN=COA6 PE=1 SV=1**
Q15527	Surfeit locus protein 2 OS=Homo sapiens GN=SURF2 PE=1 SV=3
Q6MZM0	Hephaestin-like protein 1 OS=Homo sapiens GN=HEPHL1 PE=2 SV=2
Q92541	RNA polymerase-associated protein RTF1 homolog OS=Homo sapiens GN=RTF1 PE=1 SV=4
P24928	DNA-directed RNA polymerase II subunit RPB1 OS=Homo sapiens GN=POLR2A PE=1 SV=2
P01037	Cystatin-SN OS=Homo sapiens GN=CST1 PE=1 SV=3
Q13228	Selenium-binding protein 1 OS=Homo sapiens GN=SELENBP1 PE=1 SV=2
O14548	**Cytochrome c oxidase subunit 7A-related protein, mitochondrial OS=Homo sapiens GN=COX7A2L PE=1 SV=2**
P24844	Myosin regulatory light polypeptide 9 OS=Homo sapiens GN=MYL9 PE=1 SV=4
Q92626	Peroxidasin homolog OS=Homo sapiens GN=PXDN PE=1 SV=2
P21281	V-type proton ATPase subunit B, brain isoform OS=Homo sapiens GN=ATP6V1B2 PE=1 SV=3
Q03426	Mevalonate kinase OS=Homo sapiens GN=MVK PE=1 SV=1
P23786	Carnitine O-palmitoyltransferase 2, mitochondrial OS=Homo sapiens GN=CPT2 PE=1 SV=2

P61619	Protein transport protein Sec61 subunit alpha isoform 1 OS=Homo sapiens GN=SEC61A1 PE=1 SV=2
Q99439	Calponin-2 OS=Homo sapiens GN=CNN2 PE=1 SV=4
P27144	Adenylate kinase 4, mitochondrial OS=Homo sapiens GN=AK4 PE=1 SV=1
Q969X5	Endoplasmic reticulum-Golgi intermediate compartment protein 1 OS=Homo sapiens GN=ERGIC1 PE=1 SV=1
O43592	Exportin-T OS=Homo sapiens GN=XPOT PE=1 SV=2
Q02252	Methylmalonate-semialdehyde dehydrogenase [acylating], mitochondrial OS=Homo sapiens GN=ALDH6A1 PE=1 SV=2
Q15645	Pachytene checkpoint protein 2 homolog OS=Homo sapiens GN=TRIP13 PE=1 SV=2
Q16706	Alpha-mannosidase 2 OS=Homo sapiens GN=MAN2A1 PE=1 SV=2
Q96EK6	Glucosamine 6-phosphate N-acetyltransferase OS=Homo sapiens GN=GNPNAT1 PE=1 SV=1
P33121	Long-chain-fatty-acid--CoA ligase 1 OS=Homo sapiens GN=ACSL1 PE=1 SV=1
Q9BY32	Inosine triphosphate pyrophosphatase OS=Homo sapiens GN=ITPA PE=1 SV=2
Q92572	AP-3 complex subunit sigma-1 OS=Homo sapiens GN=AP3S1 PE=1 SV=1
P23919	Thymidylate kinase OS=Homo sapiens GN=DTYMK PE=1 SV=4
O14561	Acyl carrier protein, mitochondrial OS=Homo sapiens GN=NDUFAB1 PE=1 SV=3
P49590	Probable histidine--tRNA ligase, mitochondrial OS=Homo sapiens GN=HARS2 PE=1 SV=1
P20061	Transcobalamin-1 OS=Homo sapiens GN=TCN1 PE=1 SV=2
P0CG05	Ig lambda-2 chain C regions OS=Homo sapiens GN=IGLC2 PE=1 SV=1
O00233	26S proteasome non-ATPase regulatory subunit 9 OS=Homo sapiens GN=PSMD9 PE=1 SV=3
Q92973	Transportin-1 OS=Homo sapiens GN=TNPO1 PE=1 SV=2
Q8TAT6	Nuclear protein localization protein 4 homolog OS=Homo sapiens GN=NPLOC4 PE=1 SV=3
P04080	Cystatin-B OS=Homo sapiens GN=CSTB PE=1 SV=2
Q16891	MICOS complex subunit MIC60 OS=Homo sapiens GN=IMMT PE=1 SV=1
P36969	Phospholipid hydroperoxide glutathione peroxidase, mitochondrial OS=Homo sapiens GN=GPX4 PE=1 SV=3
P49720	Proteasome subunit beta type-3 OS=Homo sapiens GN=PSMB3 PE=1 SV=2

Q13405	39S ribosomal protein L49, mitochondrial OS=Homo sapiens GN=MRPL49 PE=1 SV=1
Q86X55	Histone-arginine methyltransferase CARM1 OS=Homo sapiens GN=CARM1 PE=1 SV=3
Q15155	Nodal modulator 1 OS=Homo sapiens GN=NOMO1 PE=1 SV=5
Q8NF37	Lysophosphatidylcholine acyltransferase 1 OS=Homo sapiens GN=LPCAT1 PE=1 SV=2
P60510	Serine/threonine-protein phosphatase 4 catalytic subunit OS=Homo sapiens GN=PPP4C PE=1 SV=1
P61019	Ras-related protein Rab-2A OS=Homo sapiens GN=RAB2A PE=1 SV=1
Q9UI10	Translation initiation factor eIF-2B subunit delta OS=Homo sapiens GN=EIF2B4 PE=1 SV=2
Q08188	Protein-glutamine gamma-glutamyltransferase E OS=Homo sapiens GN=TGM3 PE=1 SV=4
Q13162	Peroxiredoxin-4 OS=Homo sapiens GN=PRDX4 PE=1 SV=1
P55786	Puromycin-sensitive aminopeptidase OS=Homo sapiens GN=NPEPPS PE=1 SV=2
P19474	E3 ubiquitin-protein ligase TRIM21 OS=Homo sapiens GN=TRIM21 PE=1 SV=1
Q9UJ83	2-hydroxyacyl-CoA lyase 1 OS=Homo sapiens GN=HACL1 PE=1 SV=2
Q9BUP3	Oxidoreductase HTATIP2 OS=Homo sapiens GN=HTATIP2 PE=1 SV=2
Q96IU4	Alpha/beta hydrolase domain-containing protein 14B OS=Homo sapiens GN=ABHD14B PE=1 SV=1
O95487	Protein transport protein Sec24B OS=Homo sapiens GN=SEC24B PE=1 SV=2
P84101	Small EDRK-rich factor 2 OS=Homo sapiens GN=SERF2 PE=1 SV=1
P48960	CD97 antigen OS=Homo sapiens GN=CD97 PE=1 SV=4
Q9H9P8	L-2-hydroxyglutarate dehydrogenase, mitochondrial OS=Homo sapiens GN=L2HGDH PE=1 SV=3
Q9BW61	DET1- and DDB1-associated protein 1 OS=Homo sapiens GN=DDA1 PE=1 SV=1
P20930	Filaggrin OS=Homo sapiens GN=FLG PE=1 SV=3
Q86SJ6	Desmoglein-4 OS=Homo sapiens GN=DSG4 PE=1 SV=1
P09110	3-ketoacyl-CoA thiolase, peroxisomal OS=Homo sapiens GN=ACAA1 PE=1 SV=2
P50552	Vasodilator-stimulated phosphoprotein OS=Homo sapiens GN=VASP PE=1 SV=3
P28072	Proteasome subunit beta type-6 OS=Homo sapiens GN=PSMB6 PE=1 SV=4
Q9NZT1	Calmodulin-like protein 5 OS=Homo sapiens GN=CALML5 PE=1 SV=2

P04259	Keratin, type II cytoskeletal 6B OS=Homo sapiens GN=KRT6B PE=1 SV=5
Q13685	Angio-associated migratory cell protein OS=Homo sapiens GN=AAMP PE=1 SV=2
Q15437	Protein transport protein Sec23B OS=Homo sapiens GN=SEC23B PE=1 SV=2
Q9UK41	Vacuolar protein sorting-associated protein 28 homolog OS=Homo sapiens GN=VPS28 PE=1 SV=1
P04632	Calpain small subunit 1 OS=Homo sapiens GN=CAPNS1 PE=1 SV=1
Q04941	Proteolipid protein 2 OS=Homo sapiens GN=PLP2 PE=1 SV=1
Q9Y296	Trafficking protein particle complex subunit 4 OS=Homo sapiens GN=TRAPPC4 PE=1 SV=1
Q9Y587	AP-4 complex subunit sigma-1 OS=Homo sapiens GN=AP4S1 PE=2 SV=1
O14972	Down syndrome critical region protein 3 OS=Homo sapiens GN=DSCR3 PE=2 SV=1
Q5VYK3	Proteasome-associated protein ECM29 homolog OS=Homo sapiens GN=ECM29 PE=1 SV=2
O15228	Dihydroxyacetone phosphate acyltransferase OS=Homo sapiens GN=GNPAT PE=1 SV=1
Q13442	28 kDa heat- and acid-stable phosphoprotein OS=Homo sapiens GN=PDAP1 PE=1 SV=1
Q9Y315	Deoxyribose-phosphate aldolase OS=Homo sapiens GN=DERA PE=1 SV=2
Q9ULA0	Aspartyl aminopeptidase OS=Homo sapiens GN=DNPEP PE=1 SV=1
P19623	Spermidine synthase OS=Homo sapiens GN=SRM PE=1 SV=1
Q7Z4G1	COMM domain-containing protein 6 OS=Homo sapiens GN=COMMD6 PE=1 SV=1
Q6DKJ4	Nucleoredoxin OS=Homo sapiens GN=NXN PE=1 SV=2
Q9UBE0	SUMO-activating enzyme subunit 1 OS=Homo sapiens GN=SAE1 PE=1 SV=1
Q96AB3	Isochorismatase domain-containing protein 2, mitochondrial OS=Homo sapiens GN=ISOC2 PE=1 SV=1
Q5U5X0	Complex III assembly factor LYRM7 OS=Homo sapiens GN=LYRM7 PE=1 SV=1
Q96QA5	Gasdermin-A OS=Homo sapiens GN=GSDMA PE=1 SV=4
Q8IVF2	Protein AHNAK2 OS=Homo sapiens GN=AHNAK2 PE=1 SV=2
P98160	Basement membrane-specific heparan sulfate proteoglycan core protein OS=Homo sapiens GN=HSPG2 PE=1 SV=4
Q9H6E5	Speckle targeted PIP5K1A-regulated poly(A) polymerase OS=Homo sapiens GN=TUT1 PE=1

	SV=2
P01620	Ig kappa chain V-III region SIE OS=Homo sapiens PE=1 SV=1
Q96RQ3	Methylcrotonoyl-CoA carboxylase subunit alpha, mitochondrial OS=Homo sapiens GN=MCCC1 PE=1 SV=3
Q9UBW8	COP9 signalosome complex subunit 7a OS=Homo sapiens GN=COPS7A PE=1 SV=1
Q08209	Serine/threonine-protein phosphatase 2B catalytic subunit alpha isoform OS=Homo sapiens GN=PPP3CA PE=1 SV=1
Q9BUP0	EF-hand domain-containing protein D1 OS=Homo sapiens GN=EFHD1 PE=1 SV=1
O75439	Mitochondrial-processing peptidase subunit beta OS=Homo sapiens GN=PMPCB PE=1 SV=2
Q86YQ8	Copine-8 OS=Homo sapiens GN=CPNE8 PE=1 SV=2
Q8IV08	Phospholipase D3 OS=Homo sapiens GN=PLD3 PE=1 SV=1
P00367	Glutamate dehydrogenase 1, mitochondrial OS=Homo sapiens GN=GLUD1 PE=1 SV=2
P52565	Rho GDP-dissociation inhibitor 1 OS=Homo sapiens GN=ARHGDIA PE=1 SV=3
P35613	Basigin OS=Homo sapiens GN=BSG PE=1 SV=2
P29144	Tripeptidyl-peptidase 2 OS=Homo sapiens GN=TPP2 PE=1 SV=4
P61923	Coatomer subunit zeta-1 OS=Homo sapiens GN=COPZ1 PE=1 SV=1
Q9GZY4	**Cytochrome c oxidase assembly factor 1 homolog OS=Homo sapiens GN=COA1 PE=1 SV=1**
Q9Y266	Nuclear migration protein nudC OS=Homo sapiens GN=NUDC PE=1 SV=1
P40616	ADP-ribosylation factor-like protein 1 OS=Homo sapiens GN=ARL1 PE=1 SV=1
P53701	**Cytochrome c-type heme lyase OS=Homo sapiens GN=HCCS PE=1 SV=1**
Q15125	3-beta-hydroxysteroid-Delta(8),Delta(7)-isomerase OS=Homo sapiens GN=EBP PE=1 SV=3
Q8NC60	Nitric oxide-associated protein 1 OS=Homo sapiens GN=NOA1 PE=1 SV=2
Q9H6V9	UPF0554 protein C2orf43 OS=Homo sapiens GN=C2orf43 PE=1 SV=1
P36543	V-type proton ATPase subunit E 1 OS=Homo sapiens GN=ATP6V1E1 PE=1 SV=1
Q16186	Proteasomal ubiquitin receptor ADRM1 OS=Homo sapiens GN=ADRM1 PE=1 SV=2
Q01650	Large neutral amino acids transporter small subunit 1 OS=Homo sapiens GN=SLC7A5 PE=1 SV=2

Q9C0C9	E2/E3 hybrid ubiquitin-protein ligase UBE2O OS=Homo sapiens GN=UBE2O PE=1 SV=3
Q12849	G-rich sequence factor 1 OS=Homo sapiens GN=GRSF1 PE=1 SV=3
Q99798	**Aconitate hydratase, mitochondrial OS=Homo sapiens GN=ACO2 PE=1 SV=2**
O14617	AP-3 complex subunit delta-1 OS=Homo sapiens GN=AP3D1 PE=1 SV=1
P01871	Ig mu chain C region OS=Homo sapiens GN=IGHM PE=1 SV=3
Q9Y262	Eukaryotic translation initiation factor 3 subunit L OS=Homo sapiens GN=EIF3L PE=1 SV=1
Q9UBC9	Small proline-rich protein 3 OS=Homo sapiens GN=SPRR3 PE=1 SV=2
P01591	Immunoglobulin J chain OS=Homo sapiens GN=IGJ PE=1 SV=4
P30419	Glycylpeptide N-tetradecanoyltransferase 1 OS=Homo sapiens GN=NMT1 PE=1 SV=2
Q9NWS0	PIH1 domain-containing protein 1 OS=Homo sapiens GN=PIH1D1 PE=1 SV=1
Q5TAQ9	DDB1- and CUL4-associated factor 8 OS=Homo sapiens GN=DCAF8 PE=1 SV=1
P39748	Flap endonuclease 1 OS=Homo sapiens GN=FEN1 PE=1 SV=1
Q9Y241	HIG1 domain family member 1A, mitochondrial OS=Homo sapiens GN=HIGD1A PE=1 SV=1
Q15054	DNA polymerase delta subunit 3 OS=Homo sapiens GN=POLD3 PE=1 SV=2
Q969U7	Proteasome assembly chaperone 2 OS=Homo sapiens GN=PSMG2 PE=1 SV=1
Q13217	DnaJ homolog subfamily C member 3 OS=Homo sapiens GN=DNAJC3 PE=1 SV=1
P45880	Voltage-dependent anion-selective channel protein 2 OS=Homo sapiens GN=VDAC2 PE=1 SV=2
P20839	Inosine-5'-monophosphate dehydrogenase 1 OS=Homo sapiens GN=IMPDH1 PE=1 SV=2
O43709	Probable 18S rRNA (guanine-N(7))-methyltransferase OS=Homo sapiens GN=WBSCR22 PE=1 SV=2
P54802	Alpha-N-acetylglucosaminidase OS=Homo sapiens GN=NAGLU PE=1 SV=2
Q9UBV2	Protein sel-1 homolog 1 OS=Homo sapiens GN=SEL1L PE=1 SV=3
Q9Y248	DNA replication complex GINS protein PSF2 OS=Homo sapiens GN=GINS2 PE=1 SV=1
P23368	NAD-dependent malic enzyme, mitochondrial OS=Homo sapiens GN=ME2 PE=1 SV=1
O00232	26S proteasome non-ATPase regulatory subunit 12 OS=Homo sapiens GN=PSMD12 PE=1 SV=3
A1L0T0	Acetolactate synthase-like protein OS=Homo sapiens GN=ILVBL PE=1 SV=2

Q14847	LIM and SH3 domain protein 1 OS=Homo sapiens GN=LASP1 PE=1 SV=2
Q14558	Phosphoribosyl pyrophosphate synthase-associated protein 1 OS=Homo sapiens GN=PRPSAP1 PE=1 SV=2
O95202	LETM1 and EF-hand domain-containing protein 1, mitochondrial OS=Homo sapiens GN=LETM1 PE=1 SV=1
P30566	Adenylosuccinate lyase OS=Homo sapiens GN=ADSL PE=1 SV=2
P17655	Calpain-2 catalytic subunit OS=Homo sapiens GN=CAPN2 PE=1 SV=6
O94925	Glutaminase kidney isoform, mitochondrial OS=Homo sapiens GN=GLS PE=1 SV=1
Q02790	Peptidyl-prolyl cis-trans isomerase FKBP4 OS=Homo sapiens GN=FKBP4 PE=1 SV=3
P80303	Nucleobindin-2 OS=Homo sapiens GN=NUCB2 PE=1 SV=2
Q99497	Protein DJ-1 OS=Homo sapiens GN=PARK7 PE=1 SV=2
Q9UBX3	Mitochondrial dicarboxylate carrier OS=Homo sapiens GN=SLC25A10 PE=1 SV=2
Q9Y6C9	Mitochondrial carrier homolog 2 OS=Homo sapiens GN=MTCH2 PE=1 SV=1
O43464	Serine protease HTRA2, mitochondrial OS=Homo sapiens GN=HTRA2 PE=1 SV=2
Q92615	La-related protein 4B OS=Homo sapiens GN=LARP4B PE=1 SV=3
P67812	Signal peptidase complex catalytic subunit SEC11A OS=Homo sapiens GN=SEC11A PE=1 SV=1
P22314	Ubiquitin-like modifier-activating enzyme 1 OS=Homo sapiens GN=UBA1 PE=1 SV=3
P04183	Thymidine kinase, cytosolic OS=Homo sapiens GN=TK1 PE=1 SV=2
O96011	Peroxisomal membrane protein 11B OS=Homo sapiens GN=PEX11B PE=1 SV=1
Q9P000	COMM domain-containing protein 9 OS=Homo sapiens GN=COMMD9 PE=1 SV=2
P43897	Elongation factor Ts, mitochondrial OS=Homo sapiens GN=TSFM PE=1 SV=2
P04179	Superoxide dismutase [Mn], mitochondrial OS=Homo sapiens GN=SOD2 PE=1 SV=2
Q13423	NAD(P) transhydrogenase, mitochondrial OS=Homo sapiens GN=NNT PE=1 SV=3
O43719	HIV Tat-specific factor 1 OS=Homo sapiens GN=HTATSF1 PE=1 SV=1
Q9GZQ3	COMM domain-containing protein 5 OS=Homo sapiens GN=COMMD5 PE=1 SV=1
P58546	Myotrophin OS=Homo sapiens GN=MTPN PE=1 SV=2
Q96ND0	Protein FAM210A OS=Homo sapiens

	GN=FAM210A PE=1 SV=2
O43854	EGF-like repeat and discoidin I-like domain-containing protein 3 OS=Homo sapiens GN=EDIL3 PE=1 SV=1
Q9H173	Nucleotide exchange factor SIL1 OS=Homo sapiens GN=SIL1 PE=1 SV=1
Q9H814	Phosphorylated adapter RNA export protein OS=Homo sapiens GN=PHAX PE=1 SV=1
A0FGR8	Extended synaptotagmin-2 OS=Homo sapiens GN=ESYT2 PE=1 SV=1
O95071	E3 ubiquitin-protein ligase UBR5 OS=Homo sapiens GN=UBR5 PE=1 SV=2
Q6GMV3	Putative peptidyl-tRNA hydrolase PTRHD1 OS=Homo sapiens GN=PTRHD1 PE=1 SV=1
Q00688	Peptidyl-prolyl cis-trans isomerase FKBP3 OS=Homo sapiens GN=FKBP3 PE=1 SV=1
Q7Z4H8	KDEL motif-containing protein 2 OS=Homo sapiens GN=KDELC2 PE=1 SV=2
P51570	Galactokinase OS=Homo sapiens GN=GALK1 PE=1 SV=1
O75436	Vacuolar protein sorting-associated protein 26A OS=Homo sapiens GN=VPS26A PE=1 SV=2
P11217	Glycogen phosphorylase, muscle form OS=Homo sapiens GN=PYGM PE=1 SV=6
O75367	Core histone macro-H2A.1 OS=Homo sapiens GN=H2AFY PE=1 SV=4
P13693	Translationally-controlled tumor protein OS=Homo sapiens GN=TPT1 PE=1 SV=1
Q08554	Desmocollin-1 OS=Homo sapiens GN=DSC1 PE=1 SV=2
O95302	Peptidyl-prolyl cis-trans isomerase FKBP9 OS=Homo sapiens GN=FKBP9 PE=1 SV=2
Q86WW8	**Cytochrome c oxidase assembly factor 5 OS=Homo sapiens GN=COA5 PE=1 SV=1**
P08473	Neprilysin OS=Homo sapiens GN=MME PE=1 SV=2
Q15181	Inorganic pyrophosphatase OS=Homo sapiens GN=PPA1 PE=1 SV=2
Q9BSE5	Agmatinase, mitochondrial OS=Homo sapiens GN=AGMAT PE=1 SV=2
O94952	F-box only protein 21 OS=Homo sapiens GN=FBXO21 PE=2 SV=2
P05114	Non-histone chromosomal protein HMG-14 OS=Homo sapiens GN=HMGN1 PE=1 SV=3
P00491	Purine nucleoside phosphorylase OS=Homo sapiens GN=PNP PE=1 SV=2
P53611	Geranylgeranyl transferase type-2 subunit beta OS=Homo sapiens GN=RABGGTB PE=1 SV=2
P49006	MARCKS-related protein OS=Homo sapiens GN=MARCKSL1 PE=1 SV=2
Q06210	Glutamine--fructose-6-phosphate aminotransferase [isomerizing] 1 OS=Homo

	sapiens GN=GFPT1 PE=1 SV=3
P46379	Large proline-rich protein BAG6 OS=Homo sapiens GN=BAG6 PE=1 SV=2
Q02218	2-oxoglutarate dehydrogenase, mitochondrial OS=Homo sapiens GN=OGDH PE=1 SV=3
P30626	Sorcin OS=Homo sapiens GN=SRI PE=1 SV=1
Q99436	Proteasome subunit beta type-7 OS=Homo sapiens GN=PSMB7 PE=1 SV=1
Q8WUF5	RelA-associated inhibitor OS=Homo sapiens GN=PPP1R13L PE=1 SV=4
Q6KB66	Keratin, type II cytoskeletal 80 OS=Homo sapiens GN=KRT80 PE=1 SV=2
Q9Y3D0	Mitotic spindle-associated MMXD complex subunit MIP18 OS=Homo sapiens GN=FAM96B PE=1 SV=1
P20020	Plasma membrane calcium-transporting ATPase 1 OS=Homo sapiens GN=ATP2B1 PE=1 SV=3
Q05639	Elongation factor 1-alpha 2 OS=Homo sapiens GN=EEF1A2 PE=1 SV=1
P10586	Receptor-type tyrosine-protein phosphatase F OS=Homo sapiens GN=PTPRF PE=1 SV=2
O75616	GTPase Era, mitochondrial OS=Homo sapiens GN=ERAL1 PE=1 SV=2
P30740	Leukocyte elastase inhibitor OS=Homo sapiens GN=SERPINB1 PE=1 SV=1
Q8TAE8	Growth arrest and DNA damage-inducible proteins-interacting protein 1 OS=Homo sapiens GN=GADD45GIP1 PE=1 SV=1
Q9UBQ7	Glyoxylate reductase/hydroxypyruvate reductase OS=Homo sapiens GN=GRHPR PE=1 SV=1
O43847	Nardilysin OS=Homo sapiens GN=NRD1 PE=1 SV=2
P08236	Beta-glucuronidase OS=Homo sapiens GN=GUSB PE=1 SV=2
P57081	tRNA (guanine-N(7)-)-methyltransferase non-catalytic subunit WDR4 OS=Homo sapiens GN=WDR4 PE=1 SV=2
P01781	Ig heavy chain V-III region GAL OS=Homo sapiens PE=1 SV=1
P62328	Thymosin beta-4 OS=Homo sapiens GN=TMSB4X PE=1 SV=2
Q9Y5J7	Mitochondrial import inner membrane translocase subunit Tim9 OS=Homo sapiens GN=TIMM9 PE=1 SV=1
Q96K17	Transcription factor BTF3 homolog 4 OS=Homo sapiens GN=BTF3L4 PE=1 SV=1
P48507	Glutamate--cysteine ligase regulatory subunit OS=Homo sapiens GN=GCLM PE=1 SV=1
Q969Z0	Protein TBRG4 OS=Homo sapiens GN=TBRG4 PE=1 SV=1

Q96SW2	Protein cereblon OS=Homo sapiens GN=CRBN PE=1 SV=1
O15439	Multidrug resistance-associated protein 4 OS=Homo sapiens GN=ABCC4 PE=1 SV=3
O00186	Syntaxin-binding protein 3 OS=Homo sapiens GN=STXBP3 PE=1 SV=2
Q8WWC4	Uncharacterized protein C2orf47, mitochondrial OS=Homo sapiens GN=C2orf47 PE=1 SV=1
O43865	Putative adenosylhomocysteinase 2 OS=Homo sapiens GN=AHCYL1 PE=1 SV=2
Q4G0J3	La-related protein 7 OS=Homo sapiens GN=LARP7 PE=1 SV=1
Q96GD0	Pyridoxal phosphate phosphatase OS=Homo sapiens GN=PDXP PE=1 SV=2
Q8N4Q0	Zinc-binding alcohol dehydrogenase domain-containing protein 2 OS=Homo sapiens GN=ZADH2 PE=1 SV=1
O75569	Interferon-inducible double-stranded RNA-dependent protein kinase activator A OS=Homo sapiens GN=PRKRA PE=1 SV=1
O95817	BAG family molecular chaperone regulator 3 OS=Homo sapiens GN=BAG3 PE=1 SV=3
P47929	Galectin-7 OS=Homo sapiens GN=LGALS7 PE=1 SV=2
P82914	28S ribosomal protein S15, mitochondrial OS=Homo sapiens GN=MRPS15 PE=1 SV=1
Q14764	Major vault protein OS=Homo sapiens GN=MVP PE=1 SV=4
P80748	Ig lambda chain V-III region LOI OS=Homo sapiens PE=1 SV=1
Q13144	Translation initiation factor eIF-2B subunit epsilon OS=Homo sapiens GN=EIF2B5 PE=1 SV=3
O60869	Endothelial differentiation-related factor 1 OS=Homo sapiens GN=EDF1 PE=1 SV=1
P30043	Flavin reductase (NADPH) OS=Homo sapiens GN=BLVRB PE=1 SV=3
Q13610	Periodic tryptophan protein 1 homolog OS=Homo sapiens GN=PWP1 PE=1 SV=1
Q9HCN4	GPN-loop GTPase 1 OS=Homo sapiens GN=GPN1 PE=1 SV=1
Q13561	Dynactin subunit 2 OS=Homo sapiens GN=DCTN2 PE=1 SV=4
Q96PZ0	Pseudouridylate synthase 7 homolog OS=Homo sapiens GN=PUS7 PE=1 SV=2
P04207	Ig kappa chain V-III region CLL OS=Homo sapiens PE=1 SV=2
Q9H9T3	Elongator complex protein 3 OS=Homo sapiens GN=ELP3 PE=1 SV=2

Figure 1

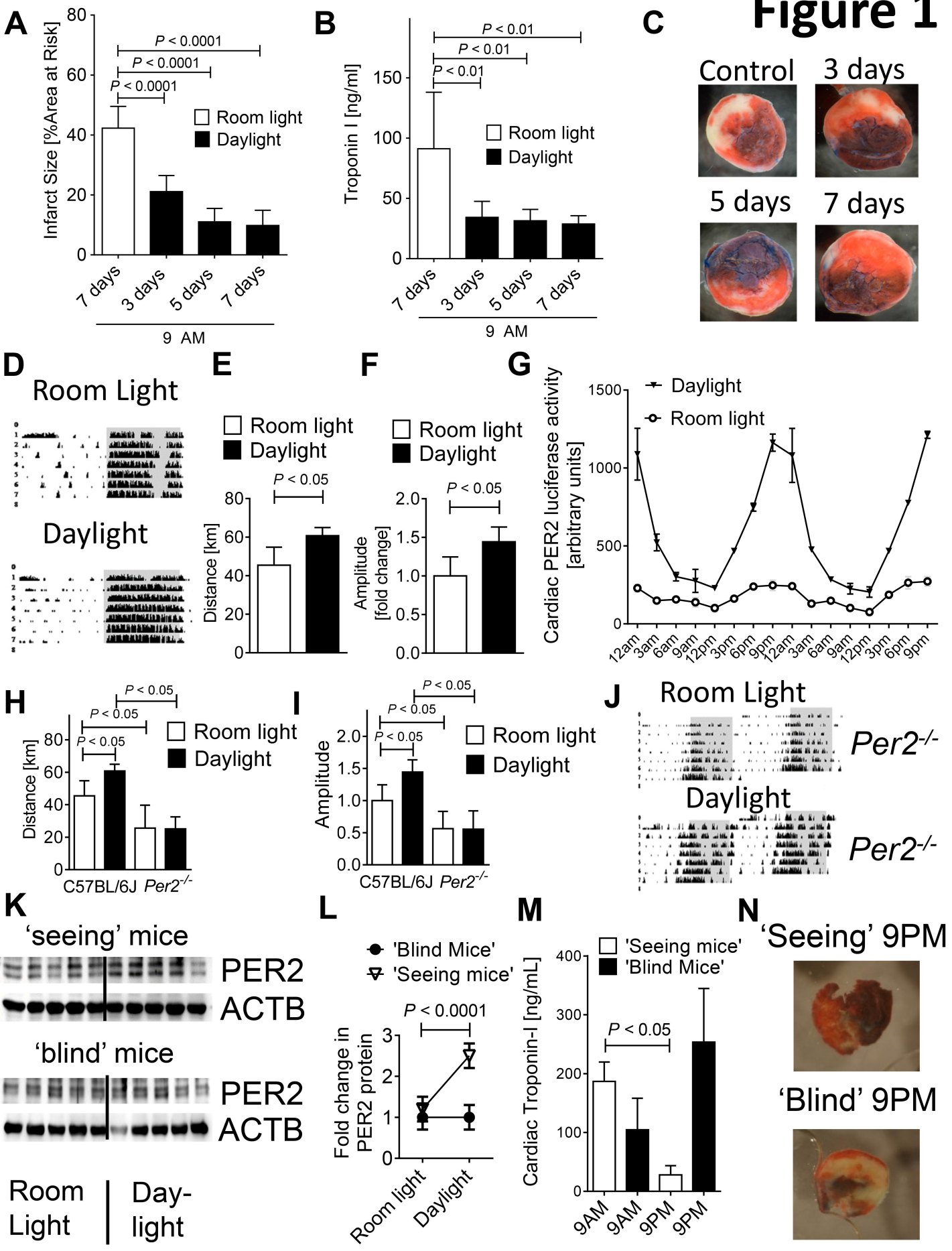
A
Infarct Size [%Area at Risk]
P < 0.0001
P < 0.0001
P < 0.0001
Room light
Daylight
7 days
3 days
5 days
7 days
9 AM
B
Troponin I [ng/ml]
P < 0.01
P < 0.01
P < 0.01
Room light
Daylight
7 days
3 days
5 days
7 days
9 AM
C
Control
3 days
5 days
7 days
D
Room Light
Daylight
E
Room light
Daylight
P < 0.05
Distance [km]
F
Room light
Daylight
P < 0.05
Amplitude [fold change]
G
Daylight
Room light
Cardiac PER2 luciferase activity [arbitrary units]
12am
3am
6am
9am
12pm
3pm
6pm
9pm
H
P < 0.05
P < 0.05
P < 0.05
Room light
Daylight
Distance [km]
C57BL/6J
Per2-/-
I
P < 0.05
P < 0.05
P < 0.05
Room light
Daylight
Amplitude
C57BL/6J
Per2-/-
J
Room Light
Per2-/-
Daylight
Per2-/-
K
'seeing' mice
PER2
ACTB
'blind' mice
PER2
ACTB
Room Light
Day-light
L
'Blind Mice'
'Seeing mice'
P < 0.0001
Fold change in PER2 protein
Room light
Daylight
M
'Seeing mice'
'Blind Mice'
P < 0.05
Cardiac Troponin-I [ng/mL]
9AM
9AM
9PM
9PM
N
'Seeing' 9PM
'Blind' 9PM

Figure 2

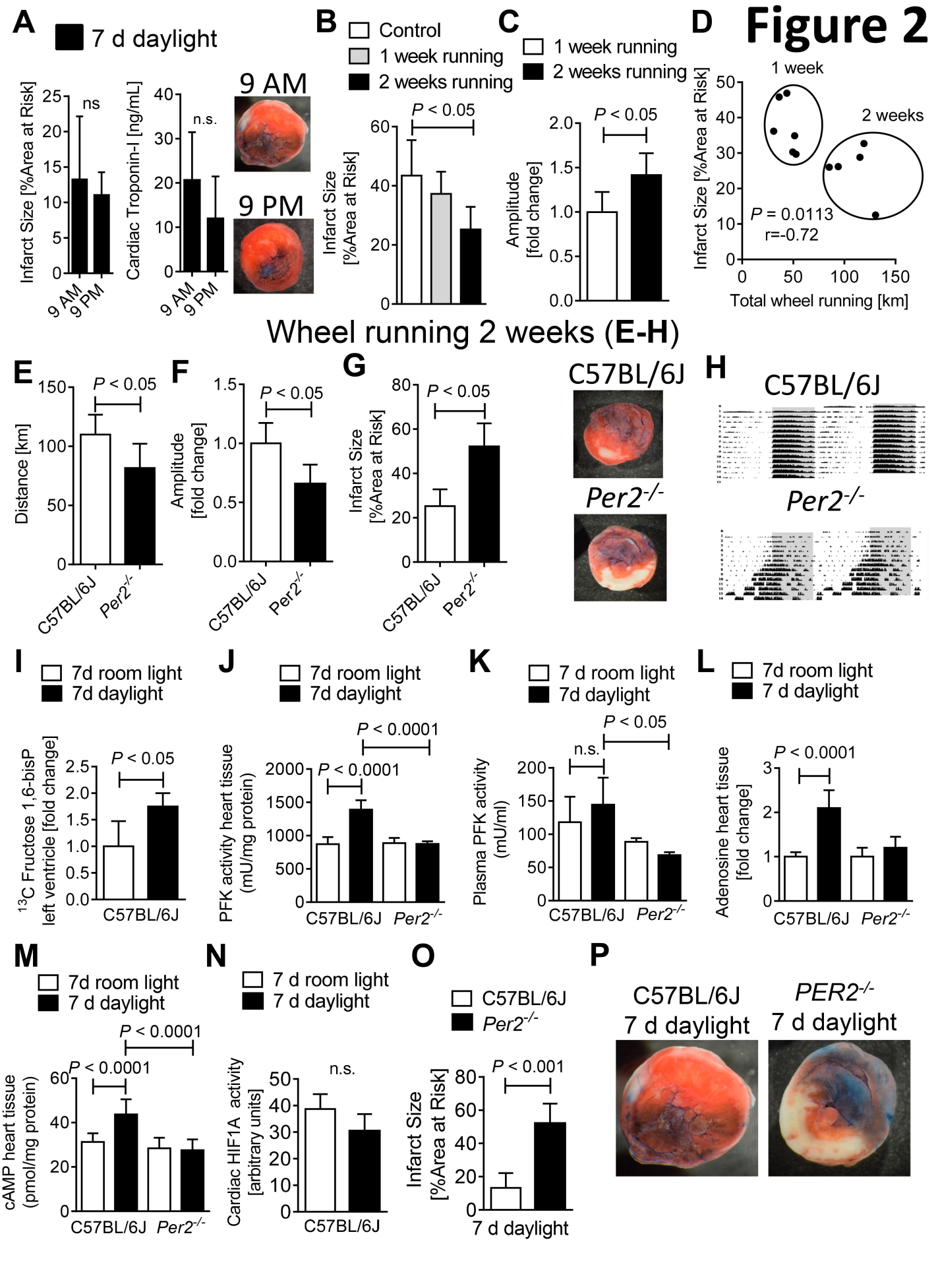
A
7 d daylight
Infarct Size [%Area at Risk]
ns
Cardiac Troponin-I [ng/mL]
n.s.
9 AM
9 PM
B
Control
1 week running
2 weeks running
P < 0.05
Infarct Size [%Area at Risk]
C
1 week running
2 weeks running
P < 0.05
Amplitude [fold change]
D
1 week
2 weeks
P = 0.0113
r=-0.72
Infarct Size [%Area at Risk]
Total wheel running [km]
Wheel running 2 weeks (E-H)
E
P < 0.05
Distance [km]
F
P < 0.05
Amplitude [fold change]
G
P < 0.05
Infarct Size [%Area at Risk]
C57BL/6J
Per2-/-
H
C57BL/6J
Per2-/-
I
7d room light
7d daylight
P < 0.05
13C Fructose 1,6-bisP left ventricle [fold change]
C57BL/6J
J
7d room light
7d daylight
P < 0.0001
P < 0.0001
PFK activity heart tissue (mU/mg protein)
C57BL/6J
Per2-/-
K
7 d room light
7d daylight
P < 0.05
n.s.
Plasma PFK activity (mU/ml)
C57BL/6J
Per2-/-
L
7d room light
7 d daylight
P < 0.0001
Adenosine heart tissue [fold change]
C57BL/6J
Per2-/-
M
7d room light
7 d daylight
P < 0.0001
P < 0.0001
cAMP heart tissue (pmol/mg protein)
C57BL/6J
Per2-/-
N
7 d room light
7 d daylight
n.s.
Cardiac HIF1A activity [arbitrary units]
C57BL/6J
O
C57BL/6J
Per2-/-
P < 0.001
Infarct Size [%Area at Risk]
7 d daylight
P
C57BL/6J
7 d daylight
PER2-/-
7 d daylight

Figure 3

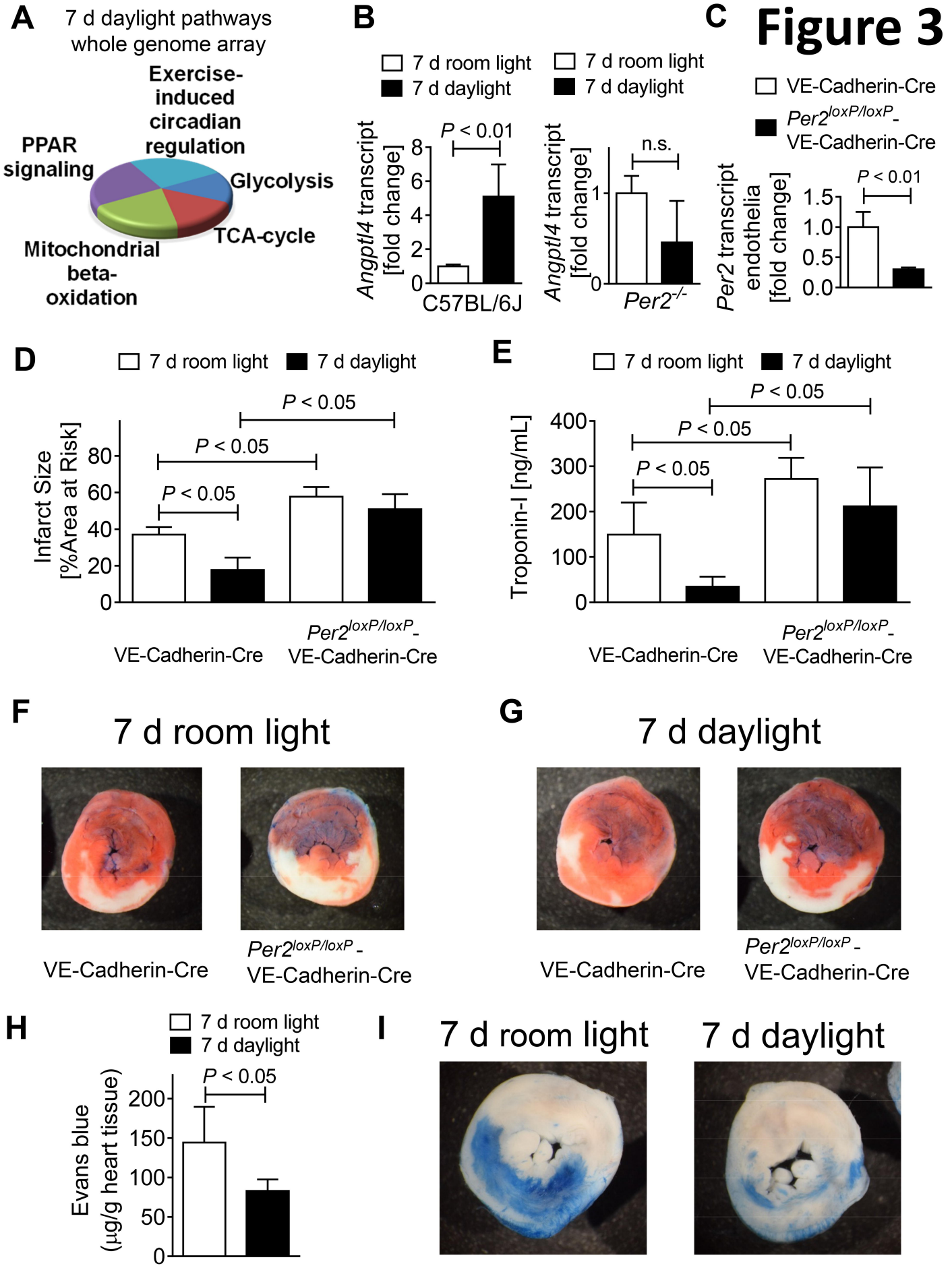
A
7 d daylight pathways
whole genome array
Exercise-induced circadian regulation
PPAR signaling
Glycolysis
TCA-cycle
Mitochondrial beta-oxidation
B
7 d room light
7 d daylight
Angptl4 transcript [fold change]
P < 0.01
C57BL/6J
n.s.
Per2-/-
C
VE-Cadherin-Cre
Per2loxP/loxP-VE-Cadherin-Cre
Per2 transcript endothelia [fold change]
P < 0.01
D
Infarct Size [%Area at Risk]
P < 0.05
P < 0.05
P < 0.05
VE-Cadherin-Cre
Per2loxP/loxP-VE-Cadherin-Cre
E
Troponin-I [ng/mL]
P < 0.05
P < 0.05
P < 0.05
VE-Cadherin-Cre
Per2loxP/loxP-VE-Cadherin-Cre
F
7 d room light
VE-Cadherin-Cre
Per2loxP/loxP-VE-Cadherin-Cre
G
7 d daylight
VE-Cadherin-Cre
Per2loxP/loxP-VE-Cadherin-Cre
H
7 d room light
7 d daylight
Evans blue (µg/g heart tissue)
P < 0.05
I
7 d room light
7 d daylight

Figure 4

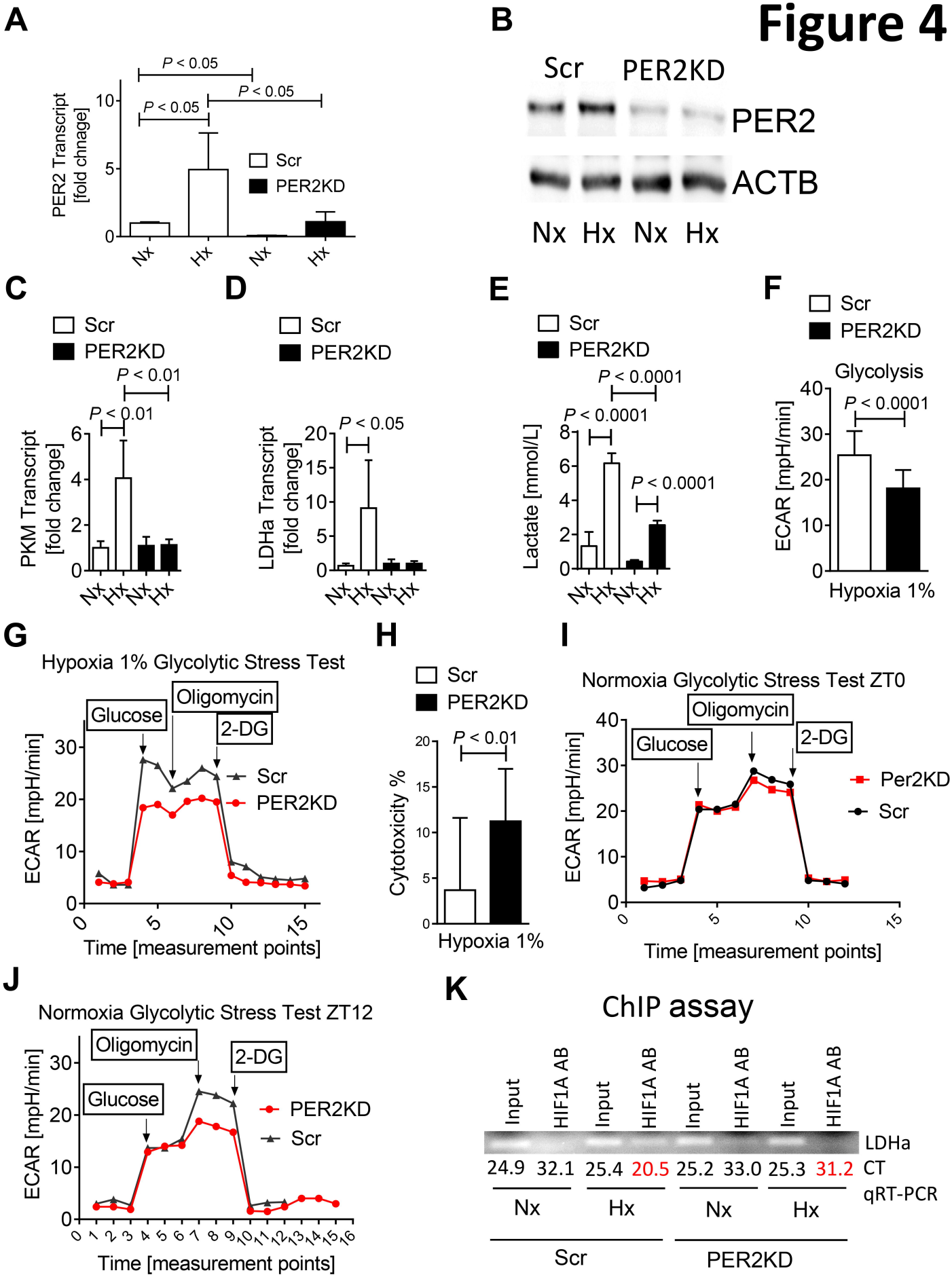
A
P < 0.05
P < 0.05
P < 0.05
PER2 Transcript [fold chnage]
Scr
PER2KD
Nx
Hx
Nx
Hx
B
Scr
PER2KD
PER2
ACTB
Nx Hx Nx Hx
C
Scr
PER2KD
P < 0.01
P < 0.01
PKM Transcript [fold change]
D
Scr
PER2KD
P < 0.05
LDHa Transcript [fold change]
E
Scr
PER2KD
P < 0.0001
P < 0.0001
P < 0.0001
Lactate [mmol/L]
F
Scr
PER2KD
Glycolysis
P < 0.0001
ECAR [mpH/min]
Hypoxia 1%
G
Hypoxia 1% Glycolytic Stress Test
Glucose
Oligomycin
2-DG
Scr
PER2KD
ECAR [mpH/min]
Time [measurement points]
H
Scr
PER2KD
P < 0.01
Cytotoxicity %
Hypoxia 1%
I
Normoxia Glycolytic Stress Test ZT0
Oligomycin
Glucose
2-DG
Per2KD
Scr
ECAR [mpH/min]
Time [measurement points]
J
Normoxia Glycolytic Stress Test ZT12
Oligomycin
Glucose
2-DG
PER2KD
Scr
ECAR [mpH/min]
Time [measurement points]
K
ChIP assay
Input
HIF1A AB
Input
HIF1A AB
Input
HIF1A AB
Input
HIF1A AB
LDHa
24.9 32.1 25.4 20.5 25.2 33.0 25.3 31.2
CT
qRT-PCR
Nx
Hx
Nx
Hx
Scr
PER2KD

Figure 5

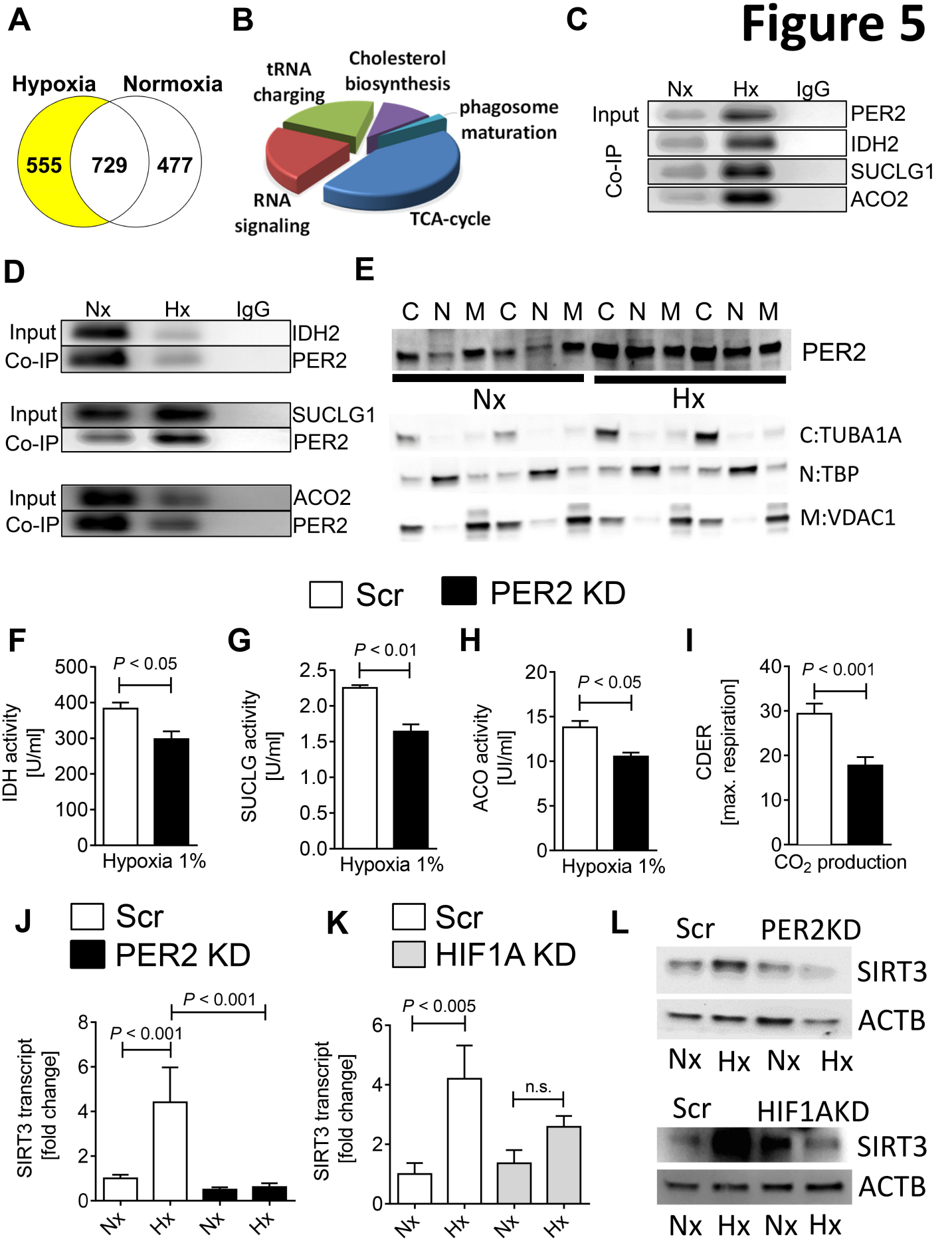
A
Hypoxia
Normoxia
555
729
477
B
tRNA charging
Cholesterol biosynthesis
phagosome maturation
RNA signaling
TCA-cycle
C
Nx
Hx
IgG
Input
Co-IP
PER2
IDH2
SUCLG1
ACO2
D
Nx
Hx
IgG
Input
Co-IP
IDH2
PER2
SUCLG1
PER2
ACO2
PER2
E
C N M C N M C N M C N M
PER2
Nx
Hx
C:TUBA1A
N:TBP
M:VDAC1
Scr
PER2 KD
F
IDH activity [U/ml]
P < 0.05
Hypoxia 1%
G
SUCLG activity [U/ml]
P < 0.01
Hypoxia 1%
H
ACO activity [UI/ml]
P < 0.05
Hypoxia 1%
I
CDER [max. respiration]
P < 0.001
CO2 production
J
Scr
PER2 KD
SIRT3 transcript [fold change]
P < 0.001
P < 0.001
Nx
Hx
Nx
Hx
K
Scr
HIF1A KD
SIRT3 transcript [fold change]
P < 0.005
n.s.
Nx
Hx
Nx
Hx
L
Scr
PER2KD
SIRT3
ACTB
Nx Hx Nx Hx
Scr
HIF1AKD
SIRT3
ACTB
Nx Hx Nx Hx

Figure 6

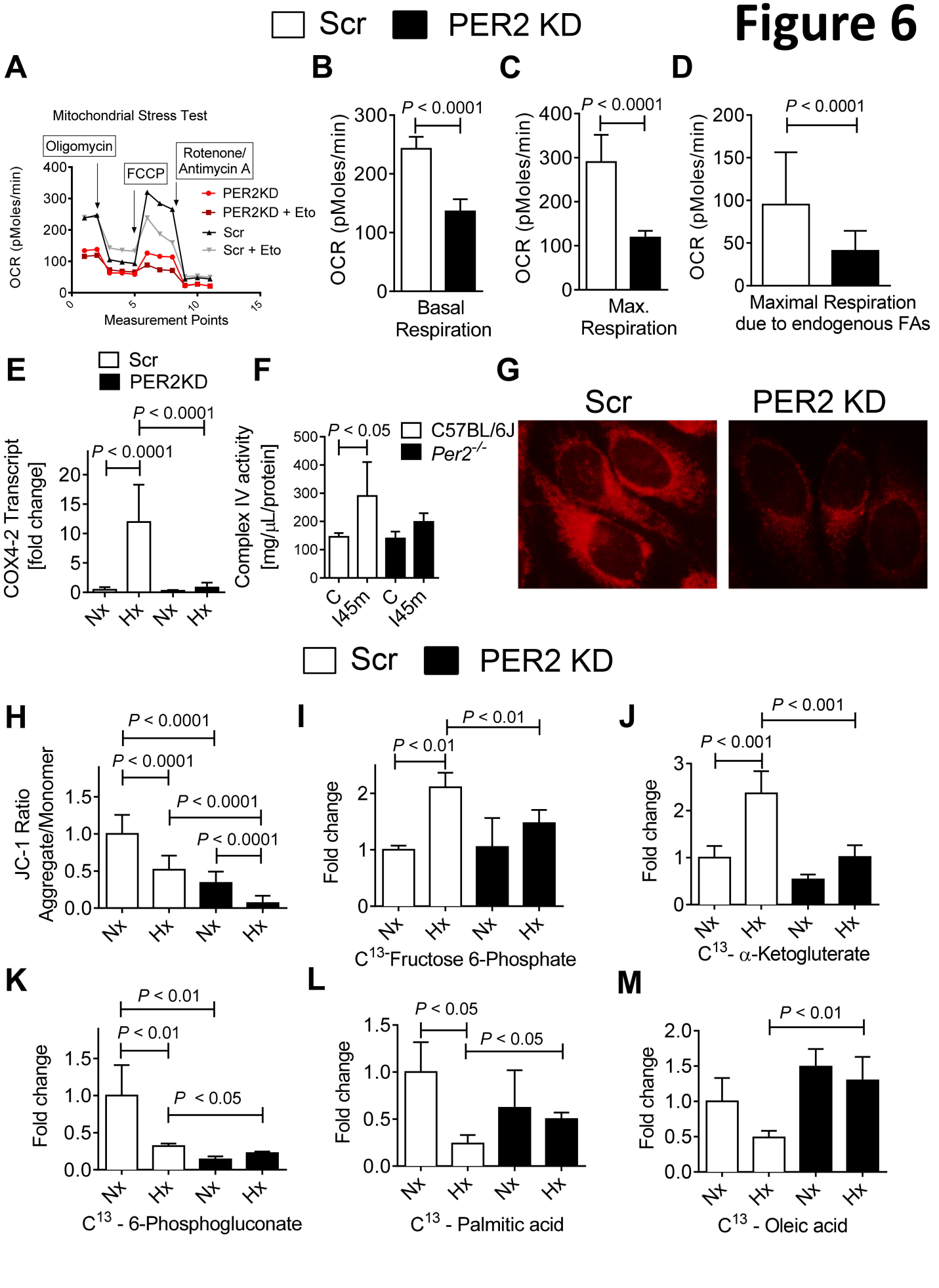
Scr
PER2 KD
A
Mitochondrial Stress Test
Oligomycin
FCCP
Rotenone/
Antimycin A
PER2KD
PER2KD + Eto
Scr
Scr + Eto
OCR (pMoles/min)
Measurement Points
B
P < 0.0001
OCR (pMoles/min)
Basal
Respiration
C
P < 0.0001
OCR (pMoles/min)
Max.
Respiration
D
P < 0.0001
OCR (pMoles/min)
Maximal Respiration
due to endogenous FAs
E
Scr
PER2KD
P < 0.0001
P < 0.0001
COX4-2 Transcript
[fold change]
Nx
Hx
Nx
Hx
F
P < 0.05
C57BL/6J
Per2-/-
Complex IV activity
[mg/μL/protein]
C
I45m
C
I45m
G
Scr
PER2 KD
Scr
PER2 KD
H
P < 0.0001
P < 0.0001
P < 0.0001
P < 0.0001
JC-1 Ratio
Aggregate/Monomer
Nx
Hx
Nx
Hx
I
P < 0.01
P < 0.01
Fold change
C13-Fructose 6-Phosphate
J
P < 0.001
P < 0.001
Fold change
C13- α-Ketogluterate
K
P < 0.01
P < 0.01
P < 0.05
Fold change
C13 - 6-Phosphogluconate
L
P < 0.05
P < 0.05
Fold change
C13 - Palmitic acid
M
P < 0.01
Fold change
C13 - Oleic acid

Figure 7

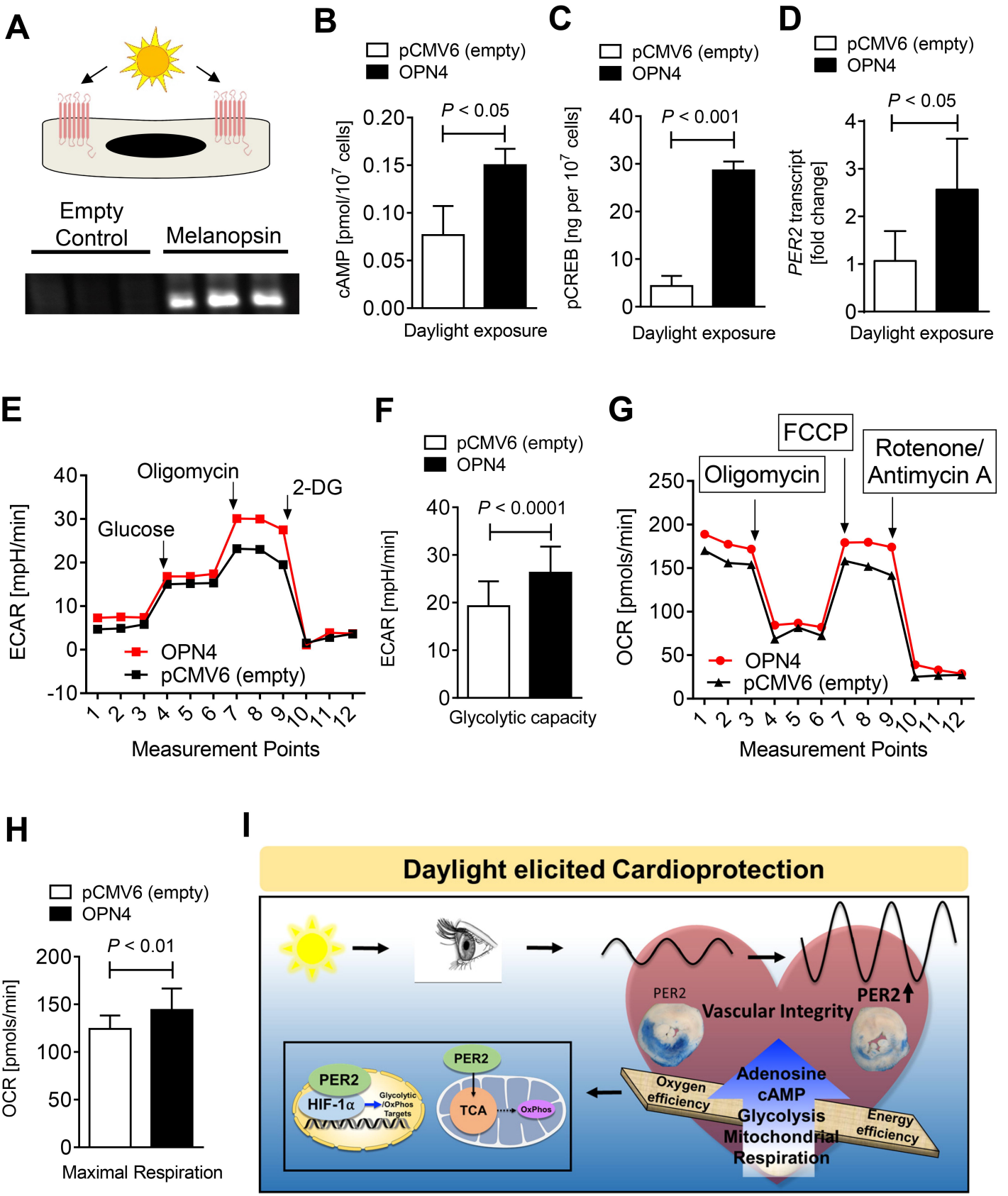
A
Empty
Control
Melanopsin
B
pCMV6 (empty)
OPN4
P < 0.05
cAMP [pmol/10^7 cells]
Daylight exposure
C
pCMV6 (empty)
OPN4
P < 0.001
pCREB [ng per 10^7 cells]
Daylight exposure
D
pCMV6 (empty)
OPN4
P < 0.05
PER2 transcript [fold change]
Daylight exposure
E
Oligomycin
2-DG
Glucose
ECAR [mpH/min]
OPN4
pCMV6 (empty)
Measurement Points
F
pCMV6 (empty)
OPN4
P < 0.0001
ECAR [mpH/min]
Glycolytic capacity
G
FCCP
Oligomycin
Rotenone/ Antimycin A
OCR [pmols/min]
OPN4
pCMV6 (empty)
Measurement Points
H
pCMV6 (empty)
OPN4
P < 0.01
OCR [pmols/min]
Maximal Respiration
I
Daylight elicited Cardioprotection
PER2
Vascular Integrity
PER2↑
PER2
HIF-1α
Glycolytic /OxPhos Targets
PER2
TCA
OxPhos
Oxygen efficiency
Adenosine
cAMP
Glycolysis
Mitochondrial Respiration
Energy efficiency

Figure 8

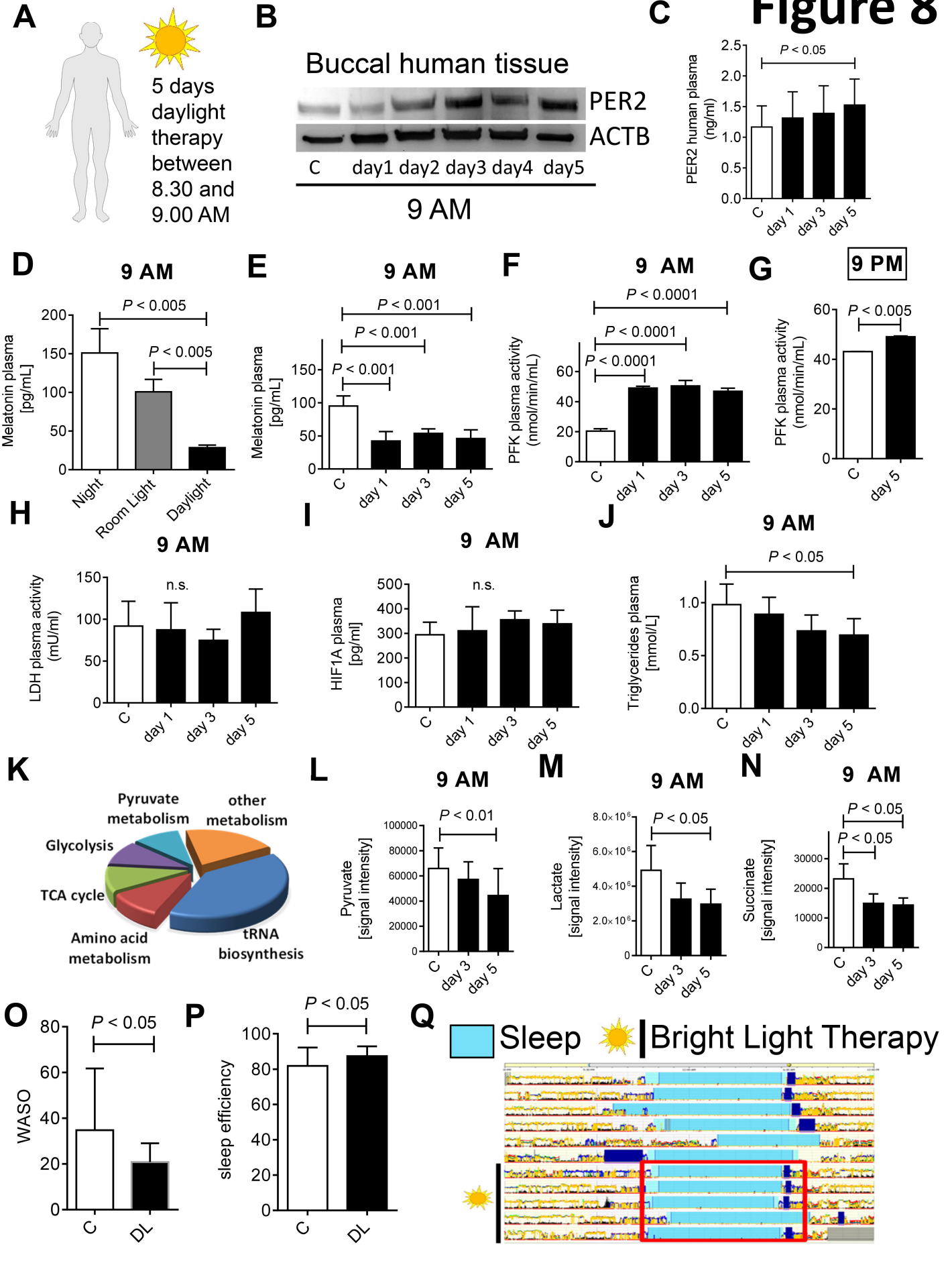
A
5 days daylight therapy between 8.30 and 9.00 AM
B
Buccal human tissue
PER2
ACTB
C day1 day2 day3 day4 day5
9 AM
C
PER2 human plasma (ng/ml)
P < 0.05
C day 1 day 3 day 5
D
9 AM
Melatonin plasma [pg/mL]
P < 0.005
P < 0.005
Night
Room Light
Daylight
E
9 AM
Melatonin plasma [pg/mL]
P < 0.001
P < 0.001
P < 0.001
C day 1 day 3 day 5
F
9 AM
PFK plasma activity (nmol/min/mL)
P < 0.0001
P < 0.0001
P < 0.0001
C day 1 day 3 day 5
G
9 PM
PFK plasma activity (nmol/min/mL)
P < 0.005
C day 5
H
9 AM
LDH plasma activity (mU/ml)
n.s.
C day 1 day 3 day 5
I
9 AM
HIF1A plasma [pg/ml]
n.s.
C day 1 day 3 day 5
J
9 AM
Triglycerides plasma [mmol/L]
P < 0.05
C day 1 day 3 day 5
K
Pyruvate metabolism
other metabolism
Glycolysis
TCA cycle
Amino acid metabolism
tRNA biosynthesis
L
9 AM
Pyruvate [signal intensity]
P < 0.01
C day 3 day 5
M
9 AM
Lactate [signal intensity]
P < 0.05
C day 3 day 5
N
9 AM
Succinate [signal intensity]
P < 0.05
P < 0.05
C day 3 day 5
O
WASO
P < 0.05
C DL
P
sleep efficiency
P < 0.05
C DL
Q
Sleep
Bright Light Therapy